
# NAVAL POSTGRADUATE SCHOOL

**MONTEREY, CALIFORNIA**

# THESIS

**EFFECT OF DUAL NANOPARTICLES REINFORCEMENT AND HEAT TREATMENT ON THE MECHANICAL AND TRIBOLOGICAL PROPERTIES OF COLD SPRAYED ALUMINUM COATINGS**

by

Kia Min Phua

September 2022

Thesis Advisor: Troy Ansell
Second Reader: Erick S. Alley

THIS PAGE INTENTIONALLY LEFT BLANK

| REPORT DOCUMENTATION PAGE | *Form Approved OMB No. 0704-0188* |
|---|---|



| **1. AGENCY USE ONLY** *(Leave blank)* | **2. REPORT DATE** September 2022 | **3. REPORT TYPE AND DATES COVERED** Master's thesis |
|---|---|---|

**4. TITLE AND SUBTITLE**
EFFECT OF DUAL NANOPARTICLES REINFORCEMENT AND HEAT TREATMENT ON THE MECHANICAL AND TRIBOLOGICAL PROPERTIES OF COLD SPRAYED ALUMINUM COATINGS

**5. FUNDING NUMBERS**
RMKT1

**6. AUTHOR(S)** Kia Min Phua

**7. PERFORMING ORGANIZATION NAME(S) AND ADDRESS(ES)**
Naval Postgraduate School
Monterey, CA 93943-5000

**8. PERFORMING ORGANIZATION REPORT NUMBER**

**9. SPONSORING / MONITORING AGENCY NAME(S) AND ADDRESS(ES)**
Office of Naval Research

**10. SPONSORING / MONITORING AGENCY REPORT NUMBER**

**11. SUPPLEMENTARY NOTES** The views expressed in this thesis are those of the author and do not reflect the official policy or position of the Department of Defense or the U.S. Government.

**12a. DISTRIBUTION / AVAILABILITY STATEMENT**
Approved for public release. Distribution is unlimited.

**12b. DISTRIBUTION CODE**
A

**13. ABSTRACT (maximum 200 words)**

Aluminum-based metal matrix composites (Al-MMCs) have shown enhanced strength, hardness, and wear properties. Hence, Al-MMCs are gaining momentum in the aerospace, automotive, defense and marine industries as a protective wear layer and for battlefield repairs. Recently, Al-MMC coatings were fabricated through cold spray (CS), a form of additive manufacturing (AM). The CS process has shown advantages of minimal oxidation, no phase transformation, and good metallurgical bonding when applied to a substrate. However, drawbacks such as porosity and low ductility limits its practical application. Heat treatments to CS coatings were successful in overcoming the drawbacks but sacrificed hardness for ductility. In a recent study, four variations of Al-MMCs CS coatings were fabricated using nano-sized aluminum and dual ceramic nanoparticle (NP) reinforcements, where the CS feedstock was synthesized through cryo-milling and high-energy ball milling. The study showed that the use of ceramic reinforcements of nano-boron carbide and boron nitride nanoplatelets at various combinations up to 2 vol% showed improvements in the hardness of the coating. Further research into controlling the properties of NP-reinforced Al-MMC CS coatings can further its application. This study examines the effect of heat treatments and the addition of up to two ceramic nanoparticles on the mechanical and tribological properties of an Al-MMCs coating fabricated by CS.

**14. SUBJECT TERMS**
material science, cold spray, coating, microstructure, heat treatment, aluminum, nanoparticles, wear testing, metal matrix composite

**15. NUMBER OF PAGES**
113

**16. PRICE CODE**

| **17. SECURITY CLASSIFICATION OF REPORT** | **18. SECURITY CLASSIFICATION OF THIS PAGE** | **19. SECURITY CLASSIFICATION OF ABSTRACT** | **20. LIMITATION OF ABSTRACT** |
|---|---|---|---|
| Unclassified | Unclassified | Unclassified | UU |

NSN 7540-01-280-5500

Standard Form 298 (Rev. 2-89)
Prescribed by ANSI Std. 239-18

THIS PAGE INTENTIONALLY LEFT BLANK

**Approved for public release. Distribution is unlimited.**

# EFFECT OF DUAL NANOPARTICLES REINFORCEMENT AND HEAT TREATMENT ON THE MECHANICAL AND TRIBOLOGICAL PROPERTIES OF COLD SPRAYED ALUMINUM COATINGS

Kia Min Phua
Major, Singapore Army
B.Eng (Hons) Materials Science & Engineering, National University of Singapore, 2012
M.Sc Mechanical Engineering, National University of Singapore, 2015

Submitted in partial fulfillment of the
requirements for the degree of

**MASTER OF SCIENCE IN MECHANICAL ENGINEERING**

from the

**NAVAL POSTGRADUATE SCHOOL**
**September 2022**

Approved by: Troy Ansell
Advisor

Erick S. Alley
Second Reader

Brian S. Bingham
Chair, Department of Mechanical and Aerospace Engineering

THIS PAGE INTENTIONALLY LEFT BLANK

# ABSTRACT

Aluminum-based metal matrix composites (Al-MMCs) have shown enhanced strength, hardness, and wear properties. Hence, Al-MMCs are gaining momentum in the aerospace, automotive, defense and marine industries as a protective wear layer and for battlefield repairs. Recently, Al-MMC coatings were fabricated through cold spray (CS), a form of additive manufacturing (AM). The CS process has shown advantages of minimal oxidation, no phase transformation, and good metallurgical bonding when applied to a substrate. However, drawbacks such as porosity and low ductility limits its practical application. Heat treatments to CS coatings were successful in overcoming the drawbacks but sacrificed hardness for ductility. In a recent study, four variations of Al-MMCs CS coatings were fabricated using nano-sized aluminum and dual ceramic nanoparticle (NP) reinforcements, where the CS feedstock was synthesized through cryo-milling and high-energy ball milling. The study showed that the use of ceramic reinforcements of nano-boron carbide and boron nitride nanoplatelets at various combinations up to 2 vol% showed improvements in the hardness of the coating. Further research into controlling the properties of NP-reinforced Al-MMC CS coatings can further its application. This study examines the effect of heat treatments and the addition of up to two ceramic nanoparticles on the mechanical and tribological properties of an Al-MMCs coating fabricated by CS.

THIS PAGE INTENTIONALLY LEFT BLANK

# TABLE OF CONTENTS

# LIST OF FIGURES

# LIST OF TABLES

THIS PAGE INTENTIONALLY LEFT BLANK

# LIST OF ACRONYMS AND ABBREVIATIONS

| | |
|---|---|
| Al | Aluminum |
| Al-MMC | Aluminum Metal Matrix Composite |
| AM | Additive Manufacturing |
| BDAR | Battlefield Damage and Repair |
| COF | Coefficient of Friction |
| CS | Cold Spray |
| CTE | Coefficient of Thermal Expansion |
| DOD | Department of Defense |
| EBSD | Electron Backscatter Diffraction |
| EDX | Energy-dispersive X-ray Spectroscopy |
| He | Helium |
| MMC | Metal Matrix Composite |
| $N_2$ | Nitrogen (Gas) |
| STEM | Scanning Tunneling Electron Microscope |
| UFG | Ultra-fine Grain |
| WOI | Work of Indentation |

THIS PAGE INTENTIONALLY LEFT BLANK

# ACKNOWLEDGMENTS

First, I would like to thank my thesis advisors, Dr. Ansell and Dr. Alley, for the guidance and mentorship for the thesis. I enjoyed the meetings and discussions we had, and I hope your stay in NPS will see more useful materials being applied onto military systems. To the late Dr. Nieto, you are a special individual who left an indelible mark on your students, and we hope that we are able to carry your good work. A special mention to Mr. Thomas Stapel and his help in the Physics NanoMEMS laboratory to get the optical profilometry done.

To my fellow material science friends who work and study in WA-204: LCDR Nicolas Twisselman, LT David Tauber, LT Collin Vorbroker and LT Maggie Ruud—a big thank you for the fun times we had, and I hope that we will meet one another very soon!

To my parents, a big thank you for instilling the need for exploration, innovating and enjoying the process of doing so. Your advice and support were something that I always could turn to when things got tough.

Most importantly, to my wife, Pin Fang: You mean the world to me. It was a difficult decision to make this 27,362 km round trip between Singapore and NPS, but it was definitely worth it, and I'm so glad you did it. I couldn't have done this without you and can't wait to spend our future together.

THIS PAGE INTENTIONALLY LEFT BLANK

# I. INTRODUCTION

## A. MOTIVATION

The DOD reported that military equipment continues to be over-utilized due to combat and contingency operations [1]. Over-utilization of military equipment results in degradation of its components and leads to failure being more commonplace. To meet operational requirements, repairs or replacement of degraded components are essential actions performed on failed equipment to restore it. However, these maintenance activities are limited by the obsolescence of repair tools or spare parts, which hamstrings any technical crew's ability to restore failed equipment for usage.

Militaries around the world are looking for innovative technologies to overcome this issue. One such technology is additive manufacturing (AM), and it is quickly gaining traction in the around the world as a maintenance capability for the military. In 2015, Freeman and Paoli [2] described AM as a potential method to overcome obsolescence for military equipment by being able to produce mechanical parts quickly, accurately and on demand. Since then, militaries have adopted AM successfully to manufacture obsolete parts to replace damaged components out in the field [3]. Cold Spray (CS) technologies, a subset of AM, had recently gained traction and was implemented by the U.S. Army and Navy as a maintenance capability to quickly repair damaged parts. CS repairs have shown improved performance against traditional repair techniques [4], [5].

Thus, CS can be exploited by a military repair crew to repair mechanical damage due to its portability and ease of setup. However, inherent drawbacks of CS like poor tensile properties and low ductility limits its practical utility. Strategies to improve the utility of CS include studies into powder feed-stock design and process optimization. Powder feedstock that are manufactured from Metal Matrix Composites (MMCs) have shown promise in improvements of mechanical and tribological properties but have not overcome its inherent drawbacks [6]. Hence, the primary objective of this thesis focuses on understanding the effects of using an annealing process on nano-sized to micron-sized ceramic particulates reinforcing aluminum metal matrix composite's (Al-MMC)

microstructure. In turn, this would change its mechanical and tribological properties, and can be used to improve the feasibility of using a CS process with composite Al-MMCs powders on the repair of components.

## B. REVIEW OF THE STATE OF THE ART

### 1. Cold Spray Technology

Cold spray can be seen as a subcategory of additive manufacturing technologies and have recently gained traction in the material processing area. The techniques and processes for CS filed as a patent that set the basis for other CS procedures [7], [8]. CS is given its "cold" name because of the much lower temperature of the jet-stream consisting of the depositing material and carrier gas as compared to the depositing material's melting point. The mechanism for the deposition of materials using CS depends mainly on three steps: (i) propulsion of the depositing material towards the substrate, (ii) the adhesion of the depositing material onto a substrate and, (iii) the layered build-up of the depositing material.

The depositing material is propelled with a carrier gas at the substrate, using a de-Laval nozzle to achieve a jet-stream with particle velocities reaching 300–1200 m/s [9]. Raoelison et. al. reported that important parameters to consider for the depositing material jet-stream are: (1) the types of carrier gas used and (2) velocity of the stream [10]. Amongst the three main types of carrier gas Helium (He), Nitrogen ($N_2$) and air, Raoelison et. al. reported that He gas is capable from producing efficient jet−streams with high velocities owing to a higher specific gas constant and comparatively lower molecular weight [10].

Figure 1 shows the generalized schematic for the bonding mechanisms that occurs in CS process. Stage I occurs mainly through the CS material adhering onto a substrate. To understand this, the mechanisms that characterize this phenomenon between a CS-material/ substrate system were found to undergo adhesion either by (i) metallurgical bonding or (ii) mechanical interlocking [11].

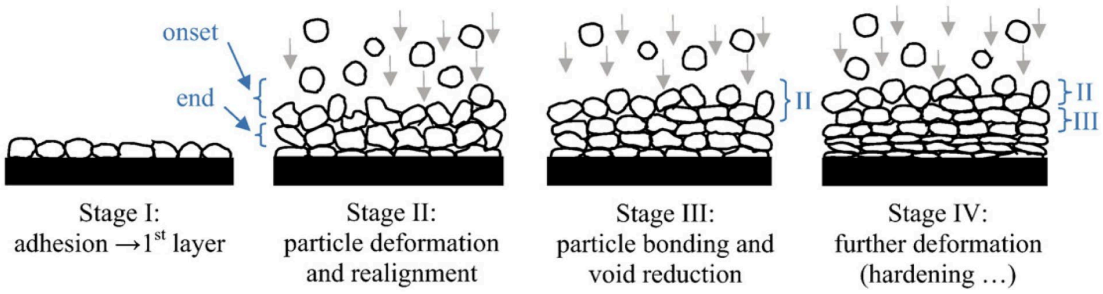


Figure 1. A Diagram of Cold Spray Coatings on its Substrate and Bonding Mechanisms. Source: [12].

Adhesion by metallurgical bonding was characterized by analyzing the collision interface between the CS material and the substrate where newly recrystallized nano-sized fine grains [13], [14] were found. This observation can be rationalized by the high plastic deformation rate that the CS material experiences when it impacts the substrate. The high plastic deformation rate causes an adiabatic shear and produces heat that is localized at the impact zone. This zone may undergo fast melting and cooling, forming an amorphous, adiabatic shear band-like zone, which also represents a form of metallurgical bond. Adhesion by mechanical interlocking can be classified as interfacial mixing and embedment onto substrate. The interfacial mixing phenomenon can be characterized by a swirling or roll-up feature morphology [15] and the embedment feature was found for various CS-material/substrate systems where the substrate is indented by CS materials to create a mechanical interlock [16]. Figure 2 shows an example of mechanical interlocking in CS processes.

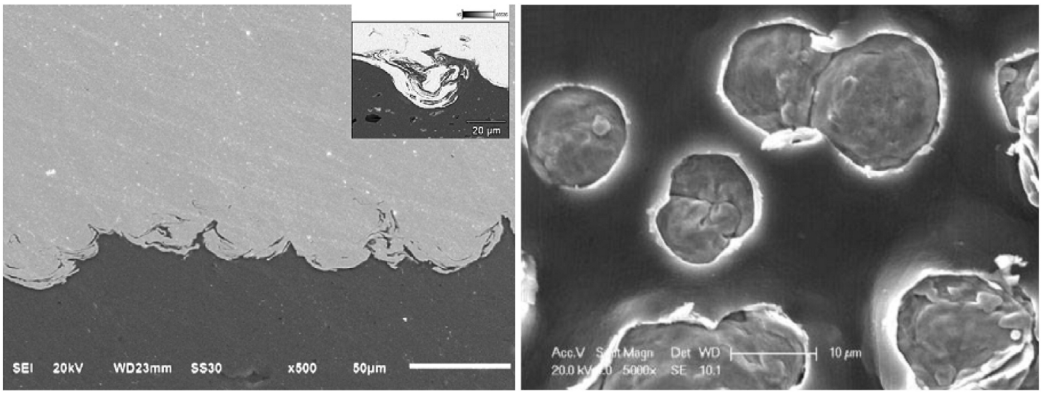


(a) (b)

Figure 2. (a) Swirled or Roll-Up Feature Morphology due to Interfacial Mixing, (b) Mechanical Embedment of Copper Particles on Aluminum Substrate. Sources: [14], [17].

After the successful adhesion of the initial layer, Stage II represents the build-up of the CS coating where the CS particles are colliding onto the substrate, causing deformation of the particulates and the start of densification of the CS deposit. Stage III represents the further densification of the CS deposit layer that decrease the porosity of the layer and the start of interparticle bonding. Stage IV marks the last stage where of the CS coating build-up, where the densification of the CS is followed by hardening of the particles.

In order to achieve a well-engineered MMC coating, the mechanisms behind the coating's deposition and tuning of its mechanical properties should be understood. As shown by Spencer et. al., MMCs have also shown their potential as a deposit material and the resulting composite coating could be engineered by tuning the volume percentage of the reinforcing phase to achieve the required mechanical properties [18]. Taking a more microscopic look in terms of how the dispersed phase and the matrix interact to produce the desired mechanical properties, Nieto et. al. [19] postulated possible strengthening mechanisms for MMCs such as: (1) grain refinement, (2) Orowan strengthening, (3) an improvement in the stress transfer from the composite matrix to a harder reinforcing phase and (4) an increase in dislocation density due to the strain generated by coefficient of thermal expansion mismatch and strain hardening during fabrication.

The microstructure of CS coatings also plays a large role in the outcome of its mechanical properties. Rokni et. al. characterized a CS Al-MMC and identified three

distinctive microstructures that correspond to different areas of the particles that make up the coating [13]. Referencing Figure 3(a), a scanning transmission electron micrograph taken from the work of Rokni et. al. [13], the first unique microstructural feature is found in the inner core of a CS particle "splat" was found with larger micron-sized grains. In between CS particles or "splats," two other microstructural features were found. The second unique microstructural feature was a stretched and banded grain that were about 100 nm in width and micro-sized in length. The last unique microstructural feature is fine nano-sized grains that were also found in between CS particle splats.

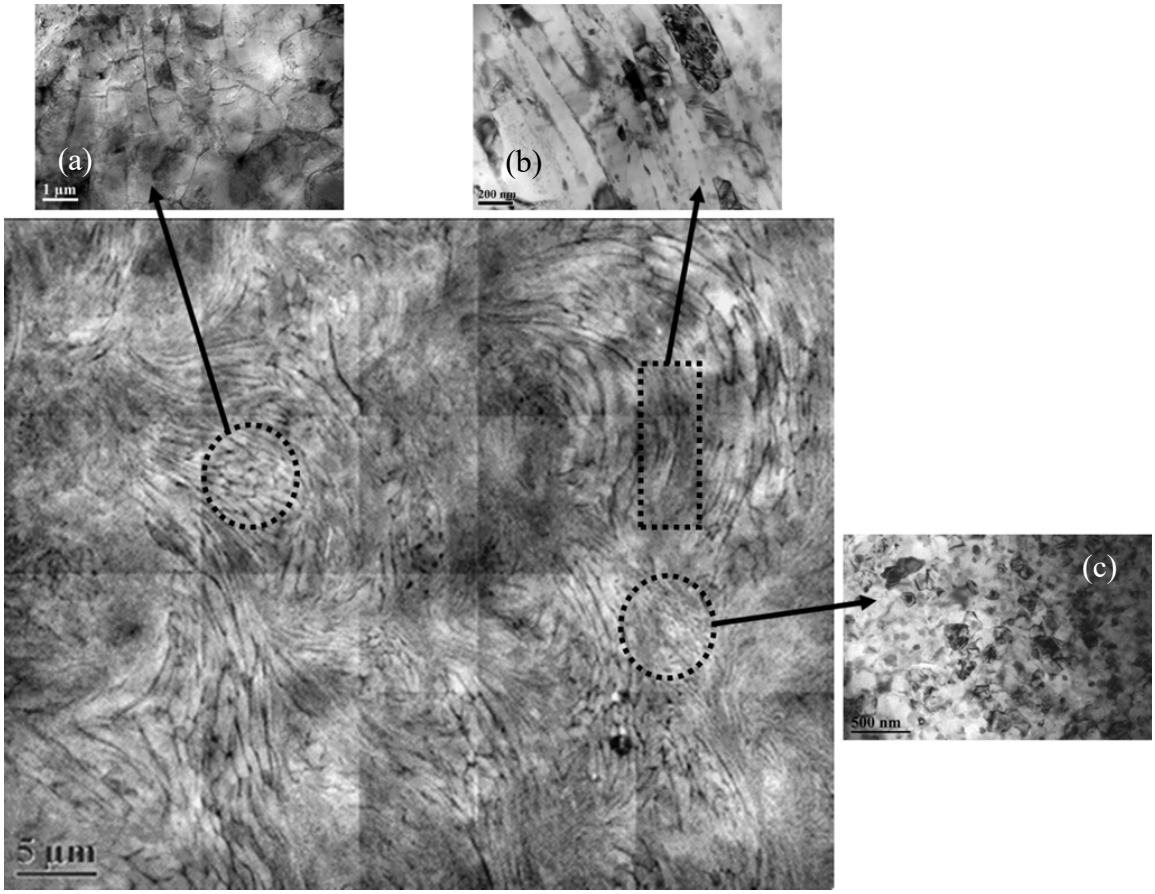


Figure 3. A STEM Image Showing the Microstructure of an As-deposited Al-7075 CS Coating. (a) Micron-sized Grain Structure in a CS Particle "Splat," (b) Stretched Banded Grain Structure between CS Particle "Splats" and (c) Fine Nanosized Grain Structure between CS Particle "Splats." Source: [13].

## 2. Al-MMC

Al-MMCs have attracted increased attention in research as a composite material. Due to aluminum's performance-to-weight ratio, more military, aerospace and automotive manufacturers are using it for their parts. Al-MMCs are being utilized in both aerospace and automotive industries for their high specific strength and high specific stiffness [20], and good wear resistance [21]. Depending on the reinforcing phase's aspect ratio, Al-MMCs can be spilt into three major categories: (1) continuous fiber reinforced Al-MMCs, (2) short-fiber reinforced Al-MMCs and (3) particulate-reinforced Al-MMCs (see Figure 4 for a schematic representation of the types of composites).

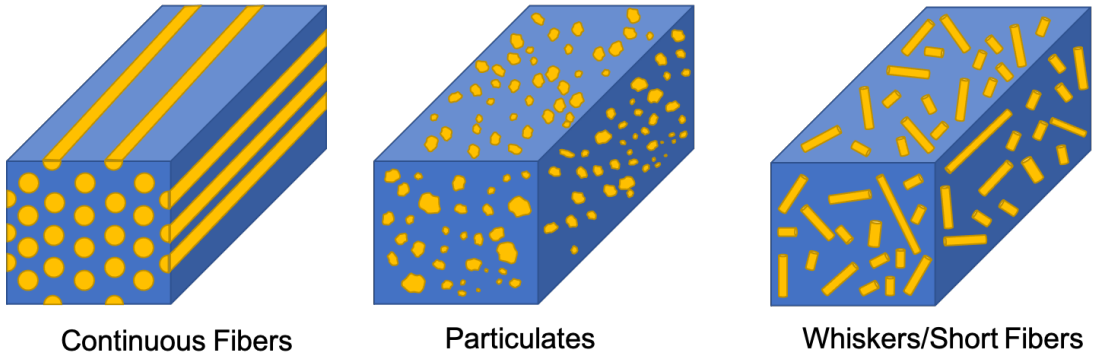


Figure 4. Schematic of the Categories of a Metal Matrix Composite, Based on the Reinforcing Phase's Aspect Ratio.

Particulate-reinforced Al-MMCs have attractive isotropic properties that is used extensively in the industry [22]. In addition, the ability to tailor material properties through the use of Al-MMCs by varying the reinforcing phases are gaining traction. Popular particulate reinforcements include alumina, silicon carbide, graphite and have been used extensively in engine blocks, brake pads and lubricating pistons [23].

In terms of the chemical and phase stability of the CS Al-MMC, it is inert and does not change as much as other traditional processes. As observed by Moridi et. al., common chemical features of build-up and adhesion of MMC materials by the CS process are: (1) negligible alloying of its constituents, (2) no phase transformation of the matrix or

reinforcing phases, and (3) no exothermic reactions between the metal matrix and metallic oxides [24].

While the attractiveness of using composite materials like particulate-reinforced Al-MMCs are largely due to exploiting their vastly different chemical, mechanical and thermal properties of aluminum and its reinforcing particulates, issues still exist in them. These issues are [25]:

- The homogeneity of the reinforcing phase is still difficult to achieve through advanced manufacturing techniques such as liquid metallurgy or stir casting.
- The hardness of the composite material improved by increasing the volume fraction or by decreasing the particulate size of the reinforcing phase. Hardness is adversely affected by the presence of porosity. The hardness can also be improved by appropriate heat treatments.
- Mechanical properties such as yield stress, tensile stress and Young's modulus of Al-MMCs increased as compared to their alloys. The tensile properties also increased with the reinforcement fraction but ductility suffered.
- Compression strength of Al-MMCs increased with reinforcement fraction and with increased compressive strains.
- Flexural strength of the Al-MMCs increased in general with reinforcement fraction and reduces after a certain point.
- Impact strength of Al-MMCs were increased by reinforcement fraction or by aging treatment to a certain point.
- Fractography of tensile tested Al-MMCs show that tensile failure is mainly due to a combination of ductile failure of the aluminum matrix, pull out of the reinforcement particulates from the matrix and also brittle fracture failure of the reinforcement particulates itself.

## 3. Strategies for Improving Mechanical Properties of Al-MMCs

In order to tune the mechanical properties of Al-MMCs, engineering its micro-structural features would be key. In general, to control the microstructure of a material, processes that lead to its formation are very important. In this study, we would focus on using methods that (i) improve the mechanical properties of the aluminum matrix and (ii) introduce reinforcing phases that improve mechanical properties of the composite. Therefore, a short introduction to some of these strengthening mechanisms are given.

### *a. Effects of Heat Treatment on CS Coatings*

The Hall-Petch relationship is one of the well-known strengthening mechanisms for polycrystalline metals, where it was shown that the strength of the metallic material is inversely related to the square root of the grain size, to a certain extent [26]. The yield strength, $\sigma_{Hall-Petch}$ is given by:

$$\sigma_{Hall-Petch} = \sigma_0 + \frac{k_{Hall-Petch}}{\sqrt{d}}, \quad (1)$$

where $\sigma_0$ is the frictional stress for dislocation motion of a single crystal, $k_{Hall-Petch}$ is the Hall-Petch constant that varies with the material, and $d$ is the average grain size of a polycrystalline material.

In order to control the interplay between maintaining material strength with the right amount of ductility, heat treatments such as annealing are usually employed to change the grain size of metallic materials. From various studies by Huang et. al. and Rokni et. al., annealing was shown to be a promising approach to improve an aluminum CS coating's hardness, ductility, and strength [27], [28]. However, it is of interest to study whether heat treatments can help with the density of grain boundaries or achieve certain grain sizes to optimize the mechanical performance of a CS coating. It is of interest to note that Rokni et. al. showed that for Al-7075, annealing above 370°C increased the CS coating hardness due to recrystallization of the grain structure from one that is stretched and banded to a finer equiaxed grain structure [28].

### *b. Al-MMCs reinforced by Nanoparticles*

With the introduction of nanoparticles, they can act as smaller strengthening phases or Orowan strengthening as explained by Zener pinning [29]. Zener pinning occurs when the strengthening phases create a dragging force and retards grain boundary movement, which limits the average diameter of the grain size to $D_{limit}$ given by:

$$D_{limit} = \frac{4r}{3f_v\alpha}, \tag{2}$$

where $r$ is the radius of the strengthening phase, $f_v$ is the volume fraction of the strengthening phase and $\alpha$ is a material dependent constant [30].

The strengthening phases can also impede dislocations and cause dislocations lines to loop around the strengthening phases that has a higher shear stress as compared to its matrix phase. As suggested by Hertzberg et. al. [31], the stress $\tau$ required for a dislocation loop to bow is:

$$\tau = \frac{Gb}{l}, \tag{3}$$

where $G$ is the shear modulus, $b$ is the Burger vector and $l$ is the distance between particles of the strengthening phase. Figure 5 shows a schematic of the Orowan strengthening mechanism.

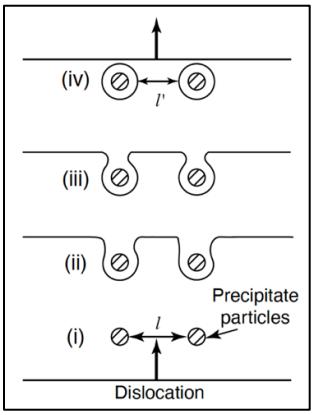


Figure 5. Schematic of Dislocation Loops Around a Strengthening Phase Particle. Source: [31].

### *c. Load Transfer Effect Between Matrix and Reinforcement Phase*

In a revised Shear Lag model, it was it can better estimate the strength of an aluminum composite, given the shape and the volume fraction of its particulate reinforcement phase [32]. In the composite material model proposed by Nardone and Prewo [32], the estimate of the strength of the composite material $\sigma_{LT}$ is calculated by:

$$\sigma_{LT} = \sigma_m[\frac{1}{2} v_p(S+2) + v_m], \quad (4)$$

where $v_p$ and $v_m$ are volume fraction of the reinforcement phase and the matrix phase respectively, $\sigma_m$ is the yield strength of the matrix phase and $S$ is the aspect ratio of the reinforcement phase.

## C. THESIS OBJECTIVES

The literature showing the influence of one or more homogenously dispersed nanoparticles in a CS composite coating to its mechanical and tribological properties and its response to heat treatment is lacking. It would be this study's objective to take a closer look at heat treatments on the coatings. To further the study on dual nanoparticles in a composite material, we aim to create one composition with distinct dispersions of singly-reinforced particles through a two-step mixing process of its precursors. Figure 6 shows the schematic of the various composite materials synthesized for the study.

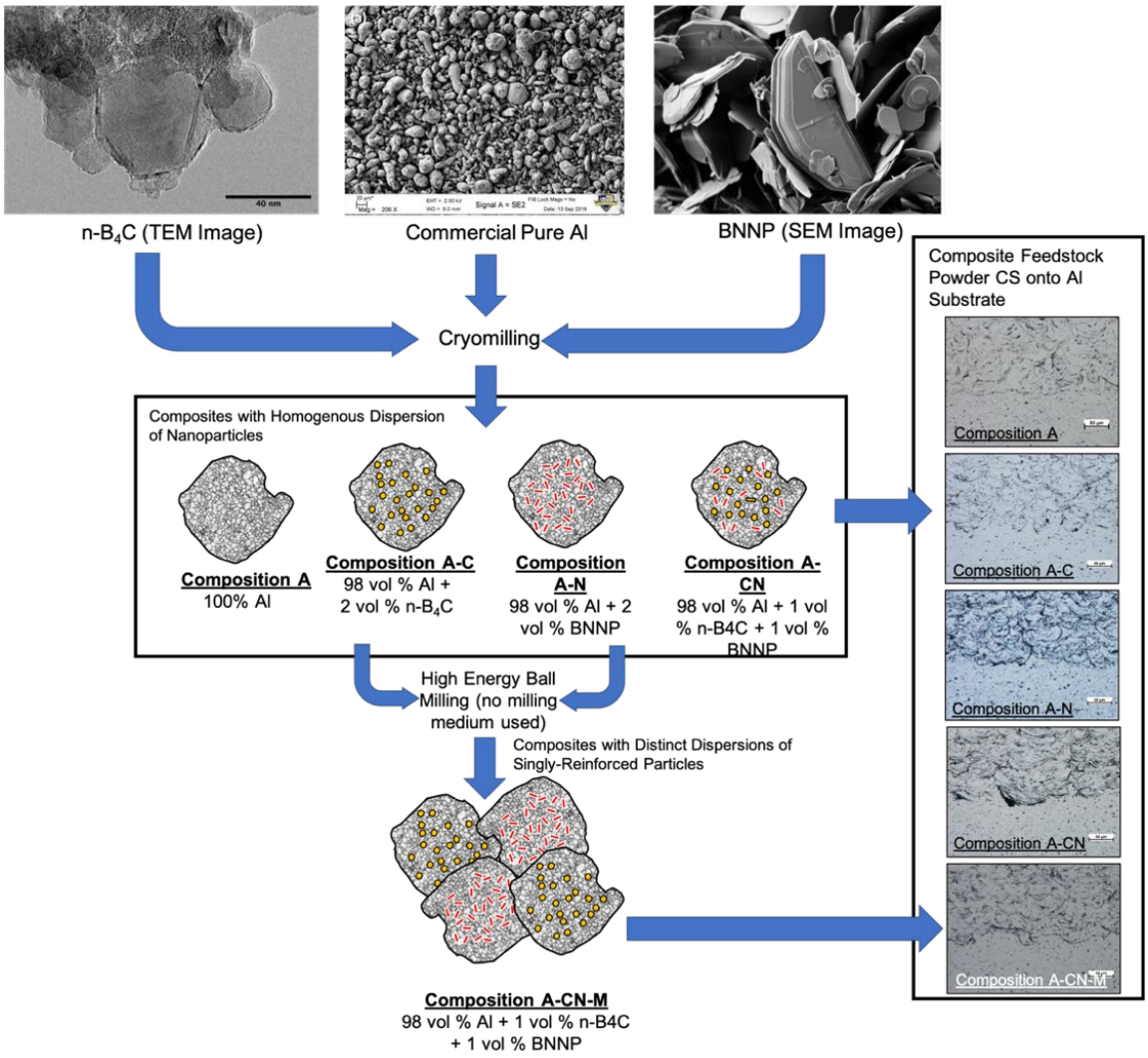


Figure 6. Schematic of the Synthesis of the Single or Dual Reinforced Composites Used in the CS Powder Feedstock.

This study aims to provide a way for military engineers to control the desired properties of aluminum CS composites that can potentially be applied as a technique in Battlefield Damage and Repair (BDAR). BDAR is commonly used by soldiers to perform expedient repairs on failed equipment to return them into the battlefield. Currently, in situations where component replacement is unavailable, BDAR can be performed on defects such as holes or join two surfaces together, techniques such as welding, epoxy filling or fabrication are employed.

Welding is a fabrication technique where parts are fused together using heat and/or pressure, typically with the use of a filler material. Drawbacks still exist for aluminum welding, such as: the use of incorrect welding fillers, porosity in welds, cracks and poor management of welding geometries. Additional requirements for post-process heat treatments are also required to prevent excessive precipitation of alloying elements and to relieve residual stresses that affect the integrity of the aluminum weld.

Repairing with epoxy is another method that can be easily executed by military personnel. They can be mixed and applied to a damaged component with the help of molds or retainers. There are still drawbacks to using an epoxy filler as shown by a study by Zhang et. al. [33], epoxy fillers have much lower tensile strength and bonding strength as compared to an aluminum (Al) 6061-T5 weld joint and an Al CS coating respectively. It can be seen that an epoxy filler is not a permanent method, but a temporary stop-gap measure where personnel can have enough functionality in their equipment to reach a well-stocked maintenance depot for part replacement or full repairs. Fabrication is another repair method but its execution requires materiel to be readily available. Successful fabrication of a replacement component through traditional metalworking also requires extensive personnel training, availability of tools and the available time allocated for the repair task.

CS does have its drawbacks but it circumvents the problems of current BDAR techniques. Therefore, we can see the potential of using CS in BDAR in the near future with the use of highly tunable composite materials such as an Al-MMCs, in order to extend the useful life of our military equipment.

# II. MATERIALS AND EXPERIMENTAL PROCEDURE

## A. MATERIALS

For the materials used in this thesis, the base powder was prepared from a previous study [34]. The matrix phase of the coatings was made with 99.5% purity (min.) Al sourced from Centerline Limited, SST5001, Windsor, ON, Canada. The Al powders were characterized with SEM and were mostly spherically shaped and had an average particle diameter of 27.4 μm [34]. One of the reinforcing phases used in this study was a nano-sized Boron Carbide (n-$B_4C$) with > 99% purity procured from U.S. Research Nanomaterials Inc., US2140, Houston, TX, USA. SEM imaging revealed that the n-$B_4C$ particulates ranged from 10 to 50 nm in diameter [34]. The other reinforcing phase used was boron nitride nanoplatelets (BNNP) with 99.5% purity, produced by SkySpring Nanomaterials, 1523DX, Houston, TX, USA. SEM imaging revealed that the BNNP had an average length of 2.1 μm and few tens of nm thick [34].

In order to study the reinforcement effects of nanoparticles to an Al matrix, five compositions for the cold spray base powder were made. The first composition (Composition A[1]) is the control, where the base powder consists only of commercial pure Al. The second and third compositions were synthesized to provide the performance baseline for singly-reinforced Al by nanoparticles. Composition A-C consists of 2 vol.% of n-$B_4C$ added to Al and was cryomilled for five cycles in a two-minute on/off manner. Composition A-N consists of 2 vol.% of BNNP added to Al and was cryomilled in similar fashion. This cryomilling method formulated by Norell et. al. was shown to have minimized the loss of the spherical shape of the Al powder and the growth or agglomeration of the reinforcing phases added to it.

The fourth and fifth compositions were synthesized to provide the results of dual-reinforced Al by nanoparticles. Composition A-CN consists of 1 vol.% of BNNP and 1 vol.% of n-$B_4C$ added to Al and was cryomilled similarly to achieve dual-reinforced

[1] Using shortened forms for Aluminum (A), Carbide (C), Nitride (N), milling (M) to name the compositions for clarity.

aluminum particles. Composition A-CN-M has the exact composition as Composition A-CN, and utilizes a two-step mixing procedure. In order to achieve a mixture of two single-reinforced aluminum particles, Al particles were cryomilled with 2 vol.% n-$B_4C$ and with 2 vol.% BNNP separately, and then HEBM (SPEX 8000, without milling medium) together for five minutes. All five compositions were sieved (100 μm) to filter larger particles out that could have been formed during the mixing process to maintain the flowability during the coating synthesis. A summary of the different compositions and their processing methods is in Table 1.

Table 1. Summary of CS Coating Compositions with Processing Methods. Source: [34].

| Nomenclature | Composition | Processing Method |
|---|---|---|
| Composition A | 100% Al | Cryomilled |
| Composition A-C | 98 vol % Al + 2 vol % n-$B_4C$ | Cryomilled |
| Composition A-N | 98 vol % Al + 2 vol % BNNP | Cryomilled |
| Composition A-CN | 98 vol % Al + 1 vol % n-$B_4C$ + 1 vol % BNNP | Cryomilled (all 3 constituents) |
| Composition A-CN-M | 98 vol % Al + 1 vol % n-$B_4C$ + 1 vol % BNNP | Two separate composites were cryomilled.<br>(1) Al with BNNP<br>(2) Al with n-$B_4C$<br>Both composites are then HEBM together to form Composition A-CN-M |

## B. SYNTHESIS OF COATINGS

Continuing the work from Norrell et. al. [34], AA6061 grade substrates were grit blasted with 40μm alumina particulates for enhanced adhesion for the cold sprayed coating. The powders were desiccated in a pre-heating oven and were shaken to loosen lightly aggregated particles to improve the flowability of the powders in the CS feeder.

The cold spray feedstocks were applied onto the substrate at Army Research Lab (ARL), Aberdeen Proving Grounds, Maryland. The cold spray parameters are recorded in

Table 2. It should be noted that the pressure parameter used in this experiment is slighter higher than the accepted definition of high-pressure cold spray at > 2.0 MPa.

Table 2. Summary of Cold Spray Parameters Used. Source: [34].

| | |
|---|---|
| **Gas Propellant** | Helium |
| **Pressure** | 3.447 MPa |
| **Temperature** | 425°C |
| **Raster Velocity** | 200 mm/s |
| **Target Thickness of Coating** | 250 μm |

## C. EXPERIMENTAL METHODS

### 1. Heat Treatment

Each composition is subjected to four annealing conditions. A 0.5 mm thick section of the cold sprayed substrate was sectioned from the *z* direction, exposing the cross section of the coating with the substrate it was sprayed onto. The samples were then heat treated by annealing. They were placed into a clamshell furnace (MTI Corporation, OTF-1200X). The specimens were heated to its annealing temperature at a heating rate of 5°C/min and held for 1 or 4 h (see Table 3 for the different annealing conditions). The sample was then cooled to room temperature. This heat treatment process was done in 0.03 MPa argon environment.

Condition 1 is used as a control that also reflects the current state where CS coatings are usually not heat treated. Temperatures used in Conditions 2 – 5 reflect a range to which aluminum alloys are annealed at and with a time difference to ensure that there is a uniform distribution of heat and to understand whether annealing times had an impact on the properties of a composite CS Al-MMC.

Table 3. Summary of the 4 Annealing Conditions with 1 Control

| Condition 1 | Condition 2 | Condition 3 | Condition 4 | Condition 5 |
|---|---|---|---|---|
| As Received (Control) | Annealed at 300°C for 1 hour | Annealed at 300°C for 4 hours | Annealed at 500°C for 1 hour | Annealed at 500°C for 4 hours |

## 2. Hardness Testing

Hardness Testing was performed on the coating using nanoindentation and microindentation methods, using an AGILENT Nanoindenter G200 and Struers DuraScan Hardness tester, respectively. Nanoindentation testing was performed in load control mode with a maximum load of 3 gram-force (gf) (29.42 mN) held for 3 seconds. An array of 50 (5 rows of 10 indentations) Berkovich indentations were made with 20 μm spacing in both *x* and *y* directions to obtain hardness and modulus of the coating with the Oliver-Pharr method [35]. Additionally, the work of indentation (WOI) is also obtained from the load-displacement curves of the nanoindentation tests.

Microindentation testing was performed in load control mode with a maximum load of 0.05kg held for 10 seconds. An array of 15 (3 rows of 5 indentations) Vickers indentations were made with 30 μm spacing in both *x* and *y* directions to obtain hardness readings for the CS coatings. Figure 7 shows where the indentations were made.

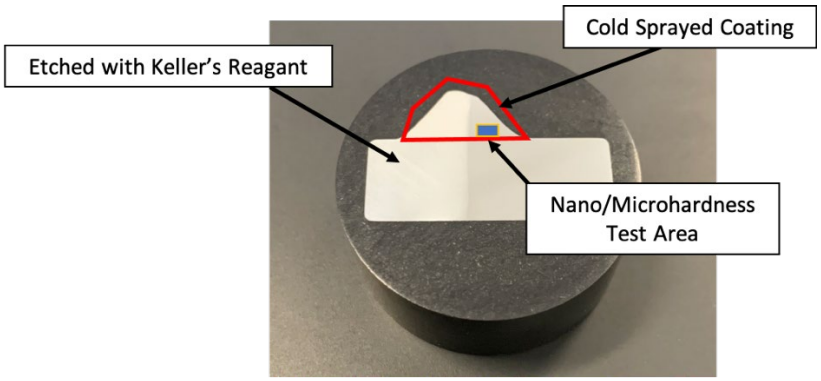


Figure 7. Schematic of Positions of Nano and Microindentations on the Coating Section.

### 3. Wear Tests

A Nanovea T50 tribometer was used to conduct ball-on-disk abrasive wear testing on the five compositions. A 1" x 1" sample with a CS coating of each composition, with their average thickness detailed in Table 4, was heat-treated with the annealing condition that gave the best improvements in mechanical properties.[2] A 5N load normal to the CS coating surface was applied to the samples with a 3mm diameter alumina contact ball in dry conditions. The wear track diameter was 3mm and the wear test was conducted at 100 RPM for 30 mins. For each sample, 5 wear tests were completed and the mass loss and average Coefficient of Friction (COF) was recorded. The wear debris were collected after each test for further analysis.

Table 4. Wear Testing Sample Conditions and Coating Thickness

| Composition | Heat Treatment | Average Coating Thickness |
|---|---|---|
| A | Annealed at 500°C for 1 hour | 271.33 mm ± 24.58 mm |
| A-C | | 324.17 mm ± 15.84 mm |
| A-N | | 163.70 mm ± 10.07 mm |
| A-CN | | 391.92 mm ± 16.55 mm |
| A-CN-M | | 412.29 mm ± 38.64 mm |

## D. CHARACTERIZATION METHODS

### 1. Metallographic and Microstructural Characterization

The as-sprayed and heat-treated samples were hot mounted into a Struers DuroFast epoxy with a Struers CitoPress Mounter. Mounted samples were then ground using 320, 800, 1200-grit SiC paper, then polished with a polishing cloth applied with 3 and 1μm

[2] Refer to Section III.C for the detailed discussion for the underlying reasons for Condition 4 to be selected as the ideal annealing condition.

monocrystalline diamond suspension and a 0.06 μm colloidal $SiO_2$ suspension. The polished samples were then etched using Keller's reagent (1% HF, 1.5% HCl, 2.5% $HNO_3$, rest $H_2O$) for 30 seconds to reveal the metallographic details. Optical microscopy (OM) was performed on the samples using a Nikon Epiphot 200 optical microscope to record the metallographic features of the samples.

### 2. Analysis of Wear Debris

Wear debris analysis was performed using a Zeiss Neon 40 dual beam FIB-SEM (White Plains, NY, USA). with an accelerating voltage ranging of 20 kV at a working distance of 5 mm. The debris size was determined by using Feret's diameter where the most significant distance between two points of the debris particle was recorded. An image processing software, ImageJ, was used to analyze the distribution of the particle sizes of the wear debris collected.

### 3. Wear Volume Profiling

A depth profile was performed to characterize the wear volume of the wear tracks. Using a Zygo NewView 7100 optical profilometer (Middlefield, CT, USA), 10 wear profile measurements were taken per wear track to calculate the average wear depth as a function of wear track width. In turn, the wear profile is used to approximate the wear volume and used to calculate the average density of the coating.

### 4. Wear Track Characterization

The wear track features were characterized with the SEM Scanning electron microscopy (SEM) using a Zeiss Neon 40 dual beam FIB-SEM (White Plains, NY, USA). with an accelerating voltage ranging of 20 kV at a working distance of 5 mm to identify the unique features of the wear tracks.

# III. RESULTS AND DISCUSSION

## A. MICROSTRUCTURE

### 1. Optical Microscopy

After mechanical polishing, etched surfaces of each coating were recorded with an optical microscope to examine the splat interfaces, coating-substrate interfaces, and the effects of heat treatment on the splats themselves. Figure 8 shows the side-by-side comparison of the effects of heat treatment on the macrostructure of the coating. From Figure 8, we can observe that splat sizes are relatively the same and the interfaces between the coating and substrate remain unchanged. Figure 8 also showed that the splat sizes from all the compositions ranged between 40 to 70 μm.

From the microscopy images, we can deduce that the high-pressure CS process had a positive effect on reducing porosity at the inter-splat and at the coating-substrate interfaces. From the left most column of Figure 8, the as-sprayed compositions show little porosity. After heat treatments, the coatings did not show any formation of pores in splat interiors or in between the CS coatings and substrates.

Similar to a study done by Hall et. al. [36], there was no grain growth observed across the heat-treated coatings for all compositions. We can infer from these observations that the heat treatment had resulted in recrystallisation of aluminum grains within the splats itself only. For detailed images of the microscopy, refer to Appendix A.

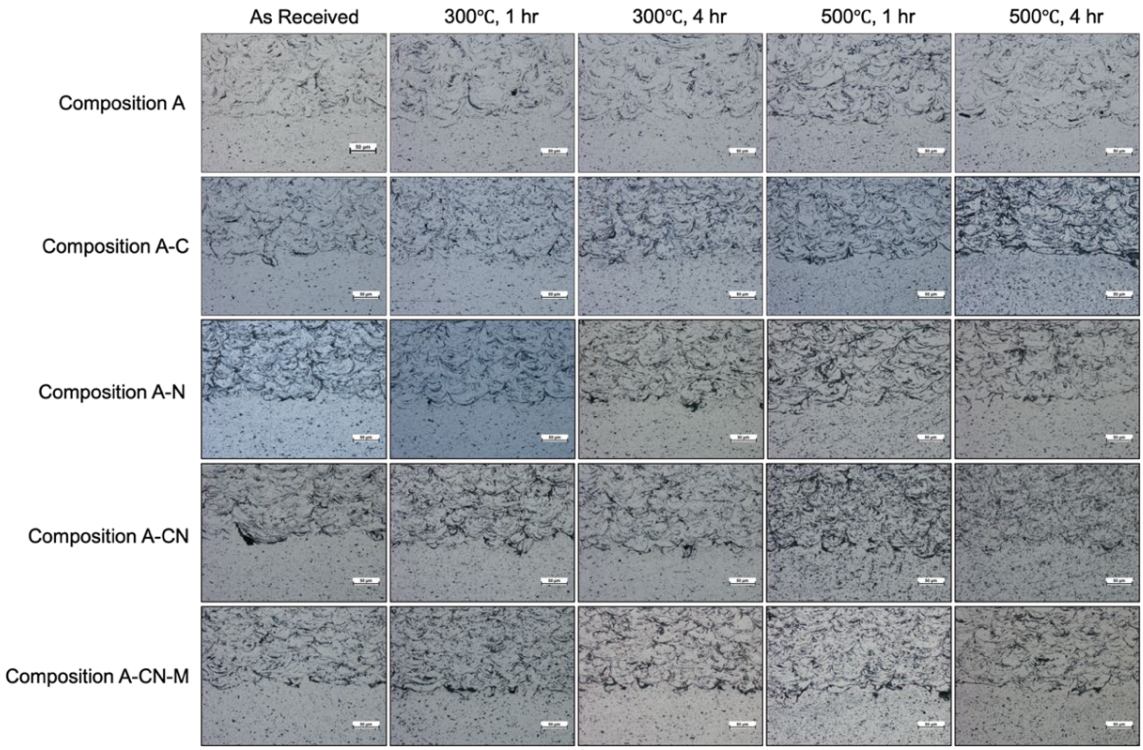


Figure 8. Comparison of Splat Sizes of Compositions and Heat Treatments.

## B. MECHANICAL PROPERTIES

### 1. Nanohardness, Elastic Modulus and Work of Indentation

50 nanoindentations were performed for each composition and their corresponding heat treatment. The dataset for each composition/heat treatment was assumed to be normally distributed and a Grubb's test[3] was performed iteratively to remove outliers. Figure 9, 10 and 11 summarizes the results for the nanohardness, modulus (using Oliver-Pharr method) and WOI results (See Appendix A, B and C for details for each parameter respectively) for each composition/heat treatment. Table 5 lists the WOI averages for each composition.

From Figure 9 and 10, we can observe that as a general trend, increasing the temperature and annealing times lowered the hardness and the modulus of the coating.

[3] Grubb's Test is used to test the presence of an outlier in a dataset that is assumed to have a normal distribution.

However, from Figure 11, the WOI increased over increased temperatures and annealing times, but only up to 1 hour. Beyond 500°C and 1 hour, the WOI of the coating reduces.

With nanohardness, modulus and WOI results, we can conclude that with heat treatment, the coating is able to regain some of its ability to absorb energy against indentations. Since the nanohardness test indentation is smaller than micro-sized splat, we can also infer that there are likely grain size changes within each splat that led to the increase in WOI, lowered hardness and modulus.

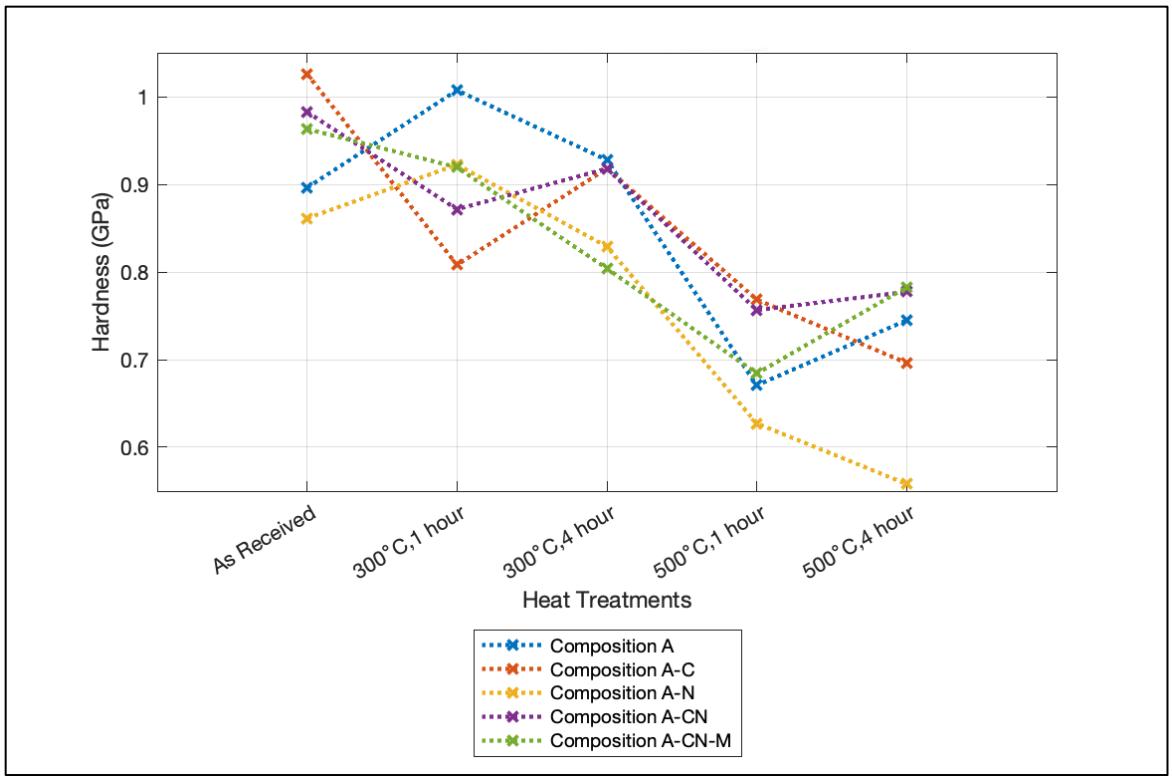


Figure 9. Results of Mean Coating Nanohardness for Each Composition / Heat Treatment.

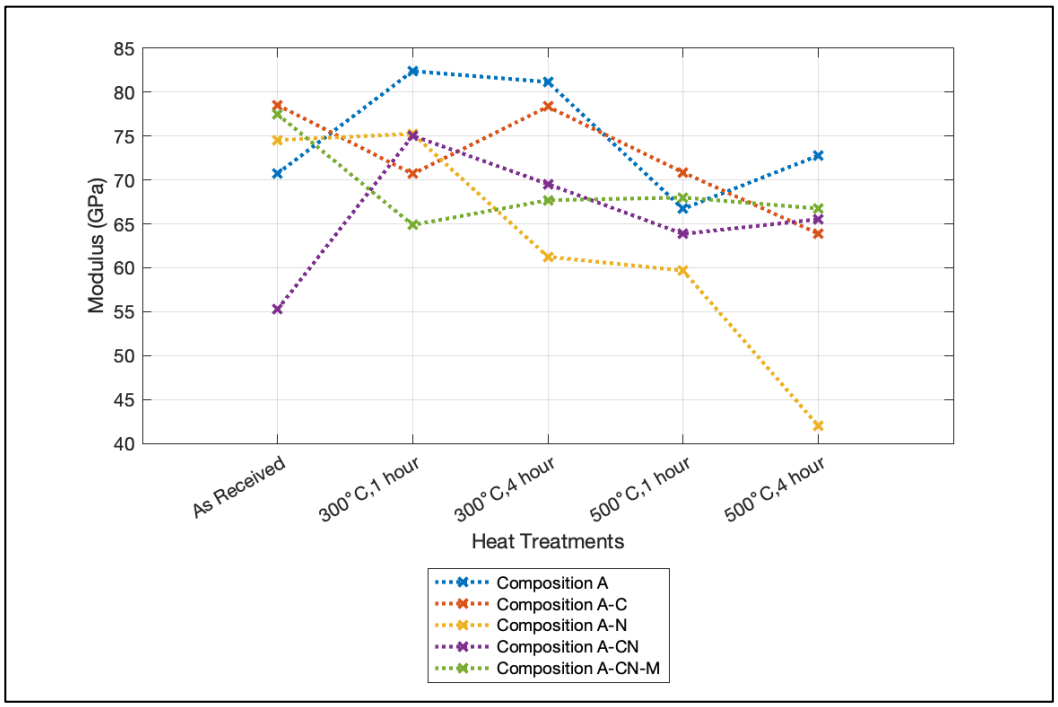


Figure 10. Results of Mean Coating Modulus for Each Composition / Heat Treatment.

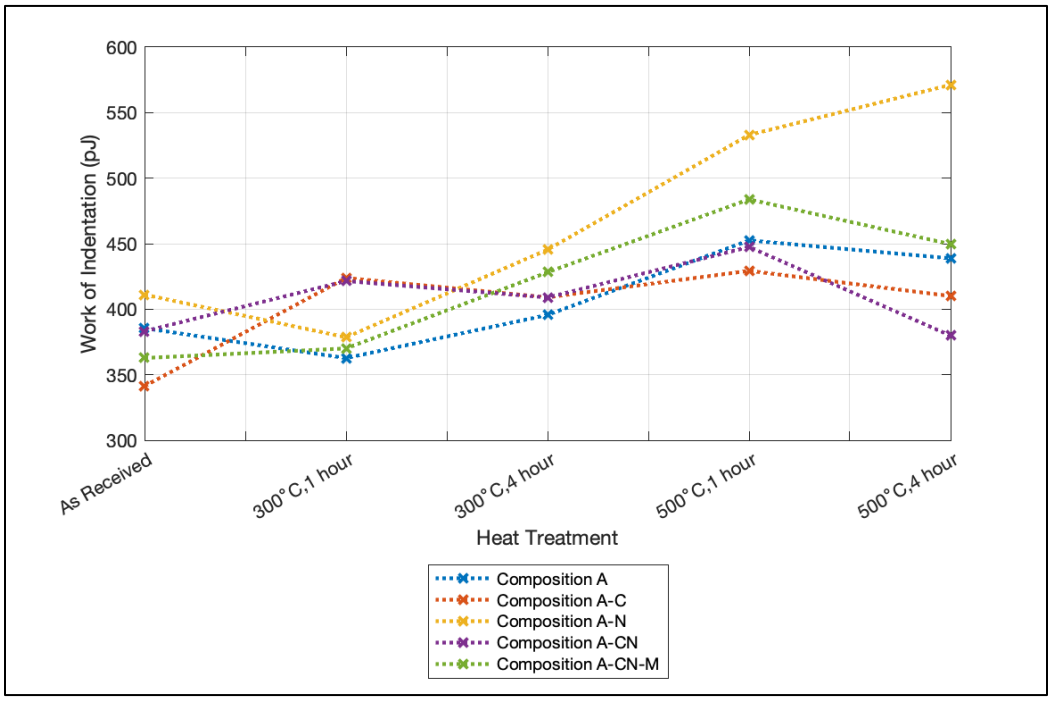


Figure 11. Results of Mean WOI for Each Composition / Heat Treatment.

Table 5. Average WOI for Each Composition / Heat Treatment.

| | Work of Indentation (pJ) | | | | |
|---|---|---|---|---|---|
| **Composition** | **Condition 1** | **Condition 2** | **Condition 3** | **Condition 4** | **Condition 5** |
| A | 385.49 | 362.68 | 395.61 | 452.51 | 438.79 |
| A-C | 341.29 | 423.86 | 409.04 | 429.29 | 410.01 |
| A-N | 411.10 | 378.56 | 445.39 | 532.97 | 571.22 |
| A-CN | 383.18 | 421.49 | 408.94 | 447.51 | 379.79 |
| A-CN-M | 362.74 | 370.05 | 428.19 | 483.81 | 449.65 |

### 2. Microhardness

Figure 12 summarizes the trend and the averaged results of the microhardness tests for each composition and their corresponding heat treatment (See Appendix D for more details). Figure 13 shows the indentation surfaces for the compositions and heat treatments. We can see a similar trend for microhardness as compared to nanohardness. Microhardness for the coating drops as the heat treatment temperature increases but have kept relatively constant when annealing times increased. This can be attributed to the likely changes in grain size of the Al matrix leading to the drop in hardness measurements. From the changes in microhardness with heat treatment, we can infer that the hardness changes in the Al matrix is dominating the hardening effects from the harder reinforcement phases at 2 vol. %.

Within each heat treatment condition, the reinforcement effects are slightly different. At 500°C, we can see that Compositions A-C and A-CN performing better than A-N and A-CN-M, while the control was the lowest. At 300°C, we can see very little differences between the hardness results for all compositions.

From Figure 13, we can also see that with heat treatment, we see fewer brittle features around the indentations during the heat treatment at Condition 4 and 5 as compared to the control and other heat treatment conditions. In column 4 of Figure 13, we see very little plastic deformations (ripple-like creases) around the Vickers-type indentations as

compared to the other indentations on coating exposed to other heat treatment conditions and the control.

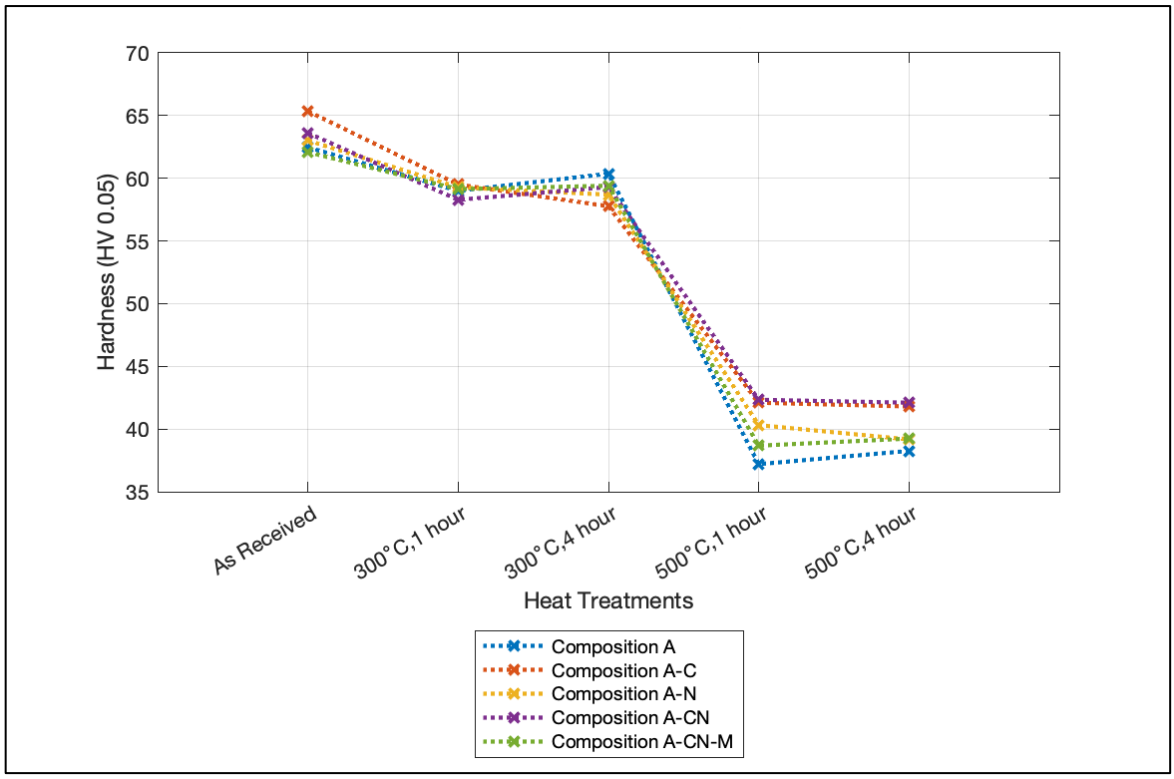


Figure 12. Results of Mean Microhardness for Each Composition / Heat Treatment.

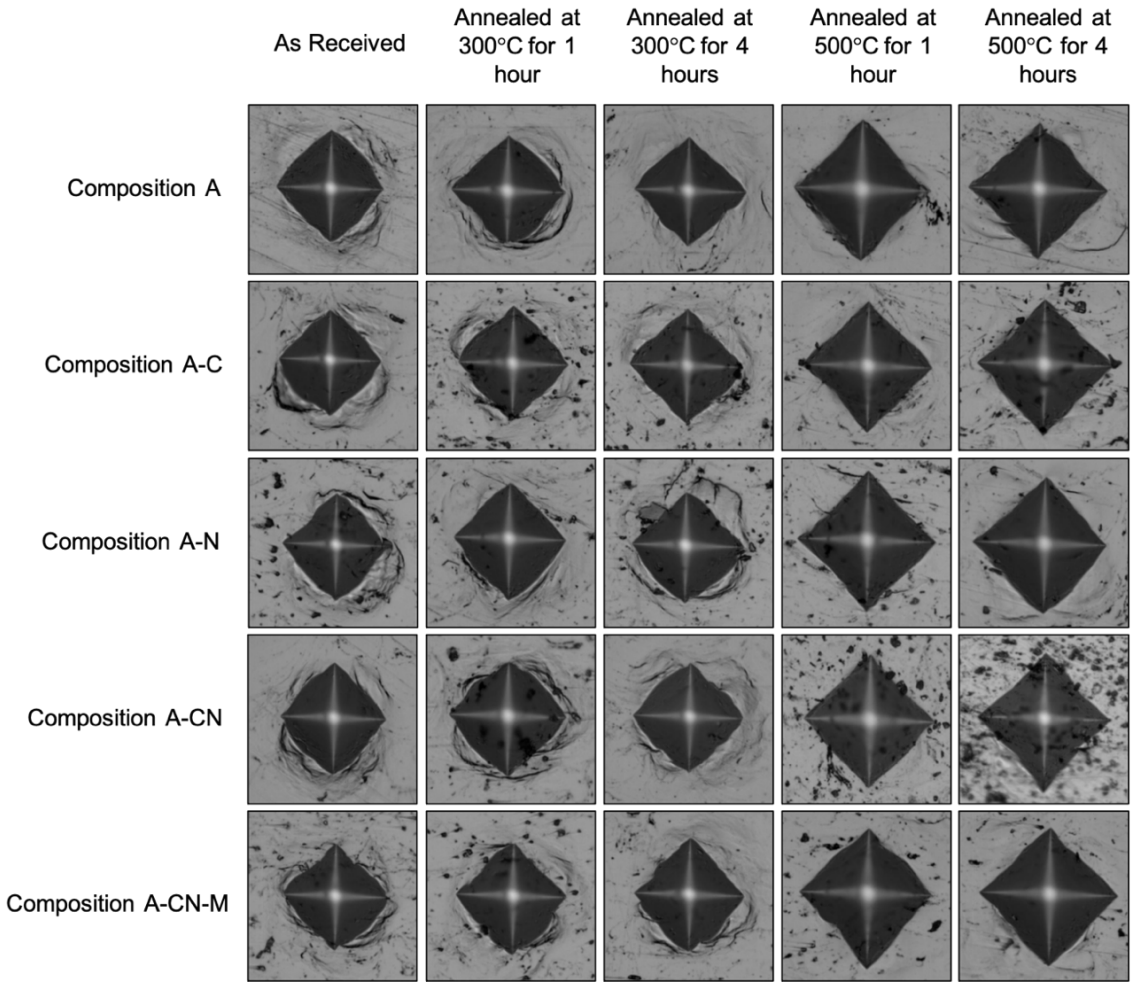


Figure 13. Results of Microhardness Test Surfaces for Each Composition / Heat Treatment.

## C. HEAT TREATMENT SELECTION

The mechanical tests revealed that by heat treating the coatings under Condition 4, the largest improvement in the compressive work was observed. All five compositions showed between 16% to 30% improvement in WOI (see Table 6) as compared to the control. From Figure 13, the indentation surfaces also presented qualitative data that under Condition 4, the coatings showed the least amount of cracking under compressive loads. Therefore, to understand the impact of heat treatments on tribological properties of reinforced CS coatings, condition 4 will be selected as the heat treatment of choice as it

presented the best results for withstanding compressive loads and improved ductility, without cracking.

Table 6. Percentage Improvement in WOI for Each Composition / Heat Treatment as Compared to Control.

| | % Increase in Work of Indentation Compared to Condition 1 | | | | |
|---|---|---|---|---|---|
| **Composition** | **Condition 1** | **Condition 2** | **Condition 3** | **Condition 4** | **Condition 5** |
| A | - | -5.92% | 2.63% | 17.39% | 13.83% |
| A-C | - | 24.19% | 19.85% | 25.78% | 20.14% |
| A-N | - | -7.92% | 8.34% | 29.64% | 38.95% |
| A-CN | - | 10.00% | 6.72% | 16.79% | -0.88% |
| A-CN-M | - | 2.02% | 18.04% | 33.38% | 23.96% |

## D. TRIBOLOGICAL PROPERTIES

The tribological properties of the reinforced coatings are characterized by the changes in COF over time, mass and volume loss of the coatings and wear track micrographs. As discussed in the previous section, the samples used for tribological testing underwent Condition 4 heat treatment in order to maximize its ability to withstand wear.

### 1. Coefficient of Friction as a Function of Time

Figure 14 summarizes the linear regression (least-squares) of the COF as a function of time for all five compositions after undergoing annealing Condition 4 (See Appendix E for the actual COF vs. time diagrams). From Figure 14, we can see that Composition A-CN had the lowest COF vs. time as compared to the rest of the composition. Composition A-N had a relatively stable COF after the wear tests, but the single or dual reinforced coatings with n-$B_4C$ showed a reduced COF over time. Composition A-CN-M, with distinct n-$B_4C$ / BNNP rich regions, showed a less steep decrease in COF as compared to the Al-MMCs added with n-$B_4C$. We can deduce that adding n-$B_4C$ reduces the COF of the coating while adding BNNP stabilizes the COF of the Al-MMC coating under abrasive wear.

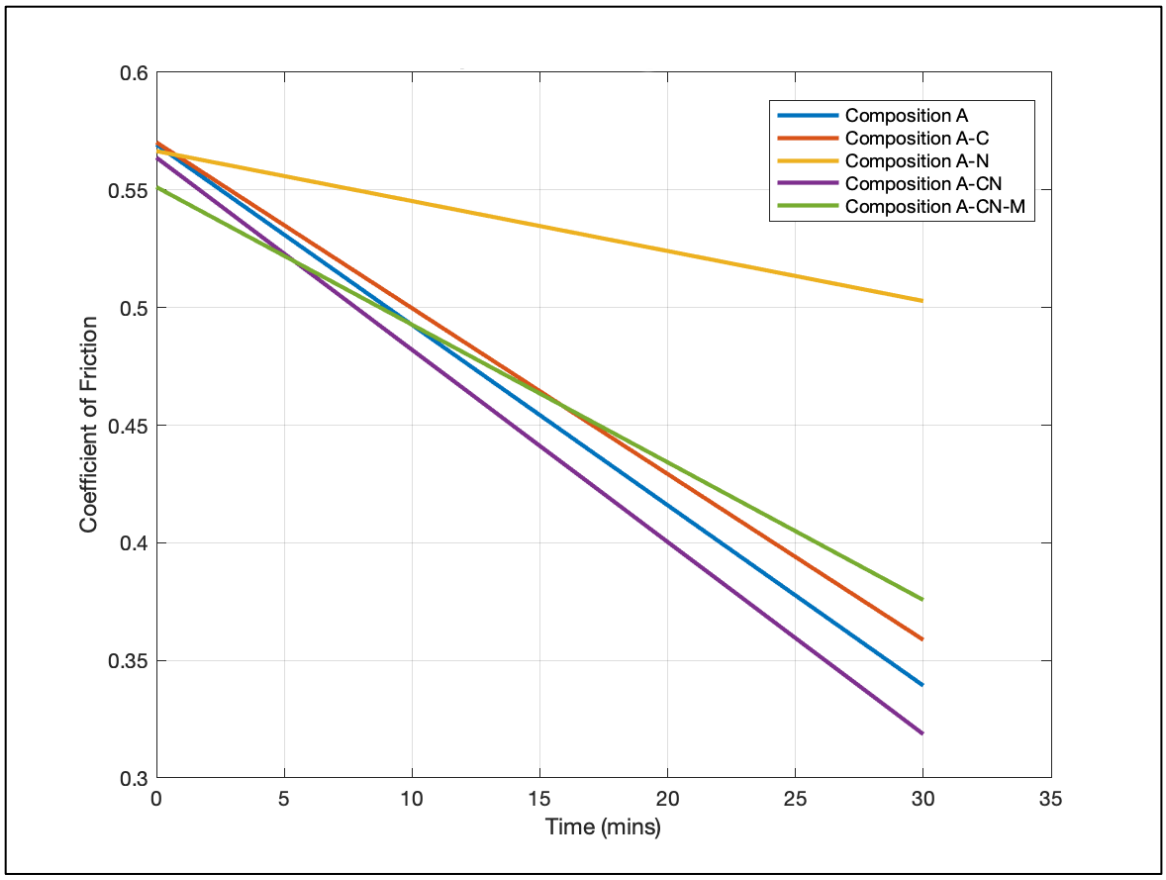


Figure 14. Results of Coefficient of Friction as a Function of Time for all Compositions Annealed at Condition 4.

### 2. Mass and Volume Loss

Figure 15 summarizes the average mass loss (of 5 wear tests) and COF for all five compositions after undergoing annealing Condition 4. The average volume loss for all compositions is summarized in Table 7, along with the average depth profile in Figure 16.

In terms of mass loss, we can see that Composition A-N showed the most mass loss, while Composition A-C showed the least mass loss amongst the reinforced compositions. The dual-reinforced Compositions A-CN and A-CN-M showed similar mass losses as A-C. Comparing Compositions A-CN and A-CN-M, A-CN-M showed a higher level of mass loss and this is likely linked to having distinct n-$B_4C$ / BNNP rich regions. It can be deduced that adding n-$B_4C$ to the Al-MMC coating helps with controlling the

amount of mass loss when added into the matrix while adding BNNP results in more mass loss.

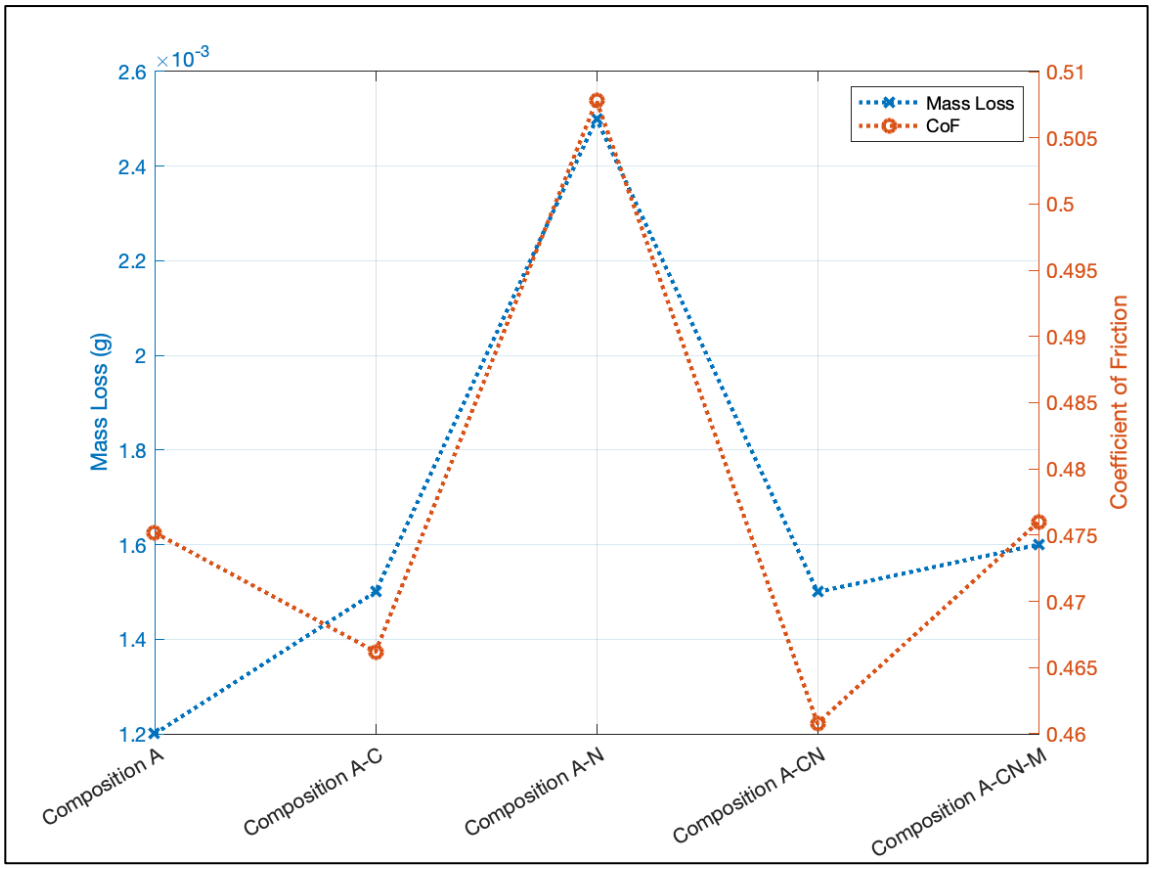


Figure 15. Results of Coefficient of Friction and COF for all Compositions Annealed at Condition 4

Figure 16 represents the depth mapping results from the optical profilometry performed on the compositions that underwent annealing under Condition 4. Ten depth profiles were taken for each composition and the average depth, width, estimated profile area, volume, and mass loss per unit volume are recorded in Table 7 (See Appendix E for details on mass loss). The average volume of the wear track was approximated by calculating the cross sectional area of a halved ellipse multiplied by $2\pi \times 1.5$mm (half of the wear track diameter). The specific wear rate was then calculated into Table 7, where the normal load was 0.05 N and the distance travelled by the wear ball is 29.258 m.

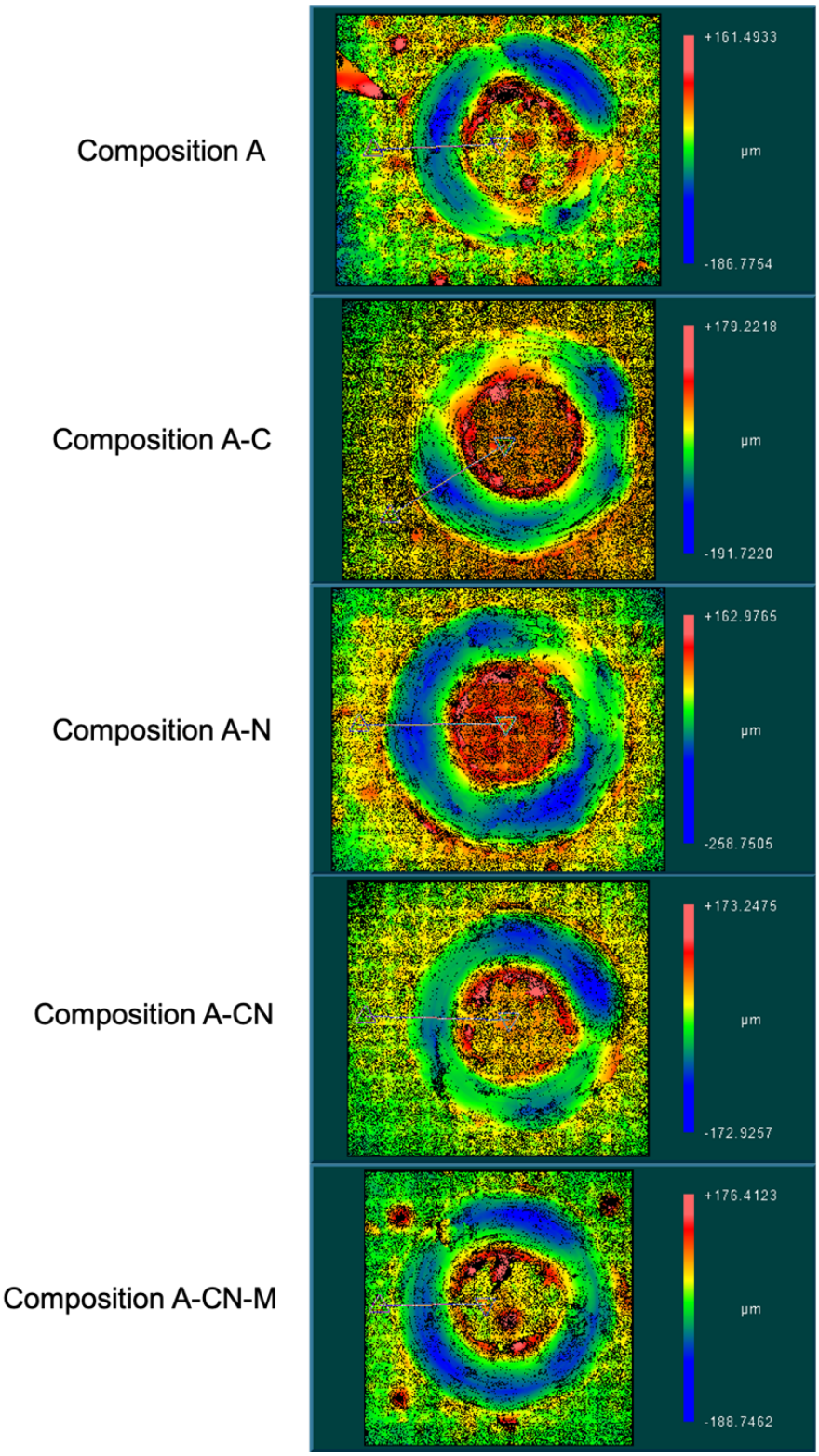


Figure 16. Depth Mapping Results for All Compositions After Annealing Condition 4

Table 7. Specific Wear Rate for all Compositions Annealed at Condition 4.

| Composition | Average Width (mm) | Average Depth (μm) | Volume ($nm^3$) | Specific Wear Rate[4] ($m^3$/Nm) |
|---|---|---|---|---|
| A | 0.9794 | 78.9640 | 0.5725 | 4.0519 x 10–$^{10}$ |
| A-C | 1.0888 | 101.5922 | 0.8188 | 5.7951 x 10–$^{10}$ |
| A-N | 1.0989 | 103.5406 | 0.8422 | 5.9608 x 10–$^{10}$ |
| A-CN | 0.9767 | 76.4467 | 0.5527 | 3.9118 x 10–$^{10}$ |
| A-CN-M | 0.9484 | 83.9462 | 0.5893 | 4.1708 x 10–$^{10}$ |

The wear test data shows that Composition A-CN showed an improved specific wear rate and Composition A-CN-M can be compared to Composition A. The single reinforced Compositions A-C and A-N showed higher specific wear rates as compared to A. From the depth maps, we can also see more significant wear depth created at the wear tracks for Compositions A-C and A-N and less on Compositions A-CN and A-CN-M. We can deduce that the dual reinforced coatings have a better effect on improving the specific wear rate of the Al-MMC coating under a compressive load, as compared to the singly reinforced Al-MMC coating.

### 3. Wear Track and Wear Debris Analysis

The reinforcement effects of the different nanoparticles can be understood by analyzing the SEM wear track micrographs. Wear scars were formed after running a 5N normal load to the coating surface for 30 minutes. From Figure 17, the lower magnification images show that the wear surfaces are relatively smooth in appearance. For Composition A-N, we can see that the wear surfaces are significantly rougher as compared to Composition A or A-C. This can explain its higher COF at the end of the wear tests. Composition A-CN showed smoother wear surfaces and did not have as much wear debris as compared to Compositions A-C and A-N and it explains its lowest COF during the wear

[4] Specific Wear Rate ($w_s$) is defined as the volume of removed material ($V$) divided by the product of the normal applied load ($P$) and the total sliding distance ($L$) of the wear ball. The equation is: $w_s = V/PL$.

test. Composition A-CN-M showed smoother surfaces than A-C and A-N, but presented rougher surfaces than Composition A-CN.

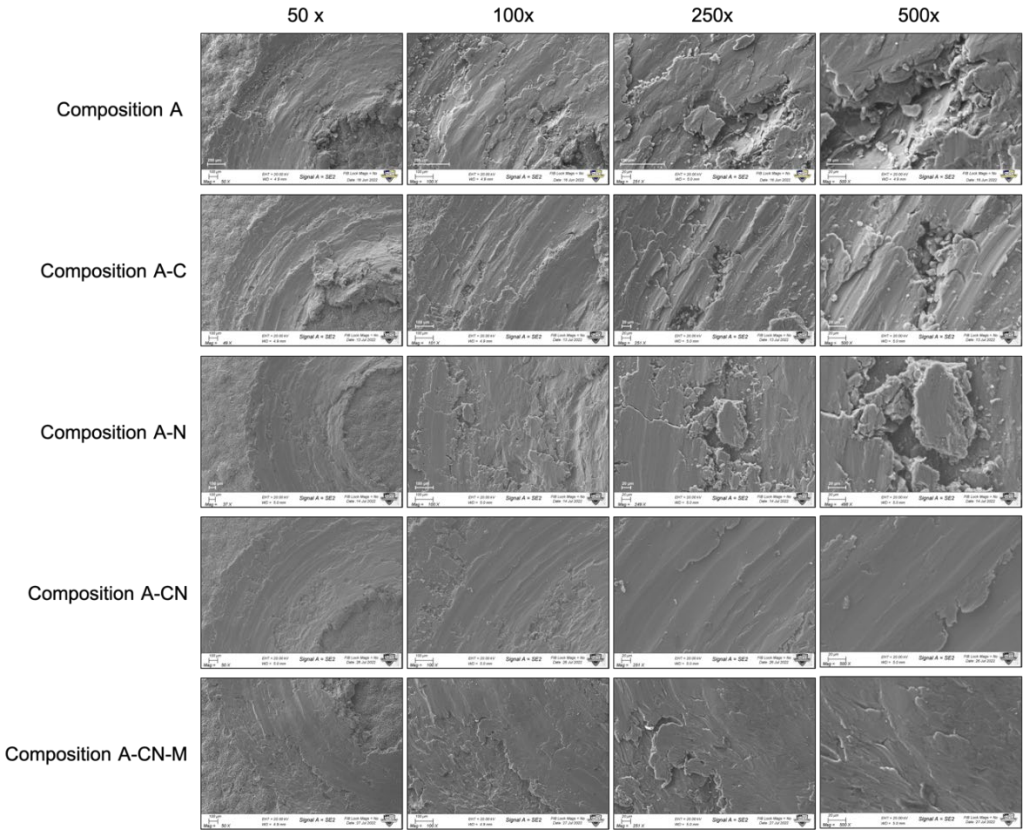


Figure 17. Comparative SEM Images for Single Reinforced Compositions at Condition 4, Between 50 to 500x.

From Figure 18, the formation of cracks and delaminated particles on the wear scars are seen. Delamination of the coatings are seen in Compositions A-C, A-C and A-N, but was rarely found in Composition A-CN and A-CN-M. Comparatively, Composition A-CN showed less delamination than A-CN-M and formed smoother wear tracks. Groove marks on A-C appear to be marked with deeper and finer cuts while groove marks on A-N are wider with more delaminated particles. Comparatively, Composition A-CN showed less delamination with smoother wear grooves. Composition A-CN-M showed slight deep cuts in the wear groove as compared to A-CN and also less delaminated particles as compared to the single reinforced compositions.

It can be deduced that adding BNNP to the coating results is a much smoother tribolayer as compared to the n-$B_4C$ reinforced coating but are marked with larger delaminated edges and particles. The n-$B_4C$ reinforced coatings show fine deeper cuts within their tribolayer and could be attributed to the delaminated particle causing third party wear. The homogenous mixture of n-$B_4C$ and BNNP into the Al-MMC coating makes it more resistant to abrasive wear and results in a smoother tribolayer. Composition A-CN-M formed slightly larger delaminated particles likely due to the distinct distributions of n-$B_4C$ rich and BNNP regions and also presented a smoother tribolayer as compared to the single reinforced coatings.

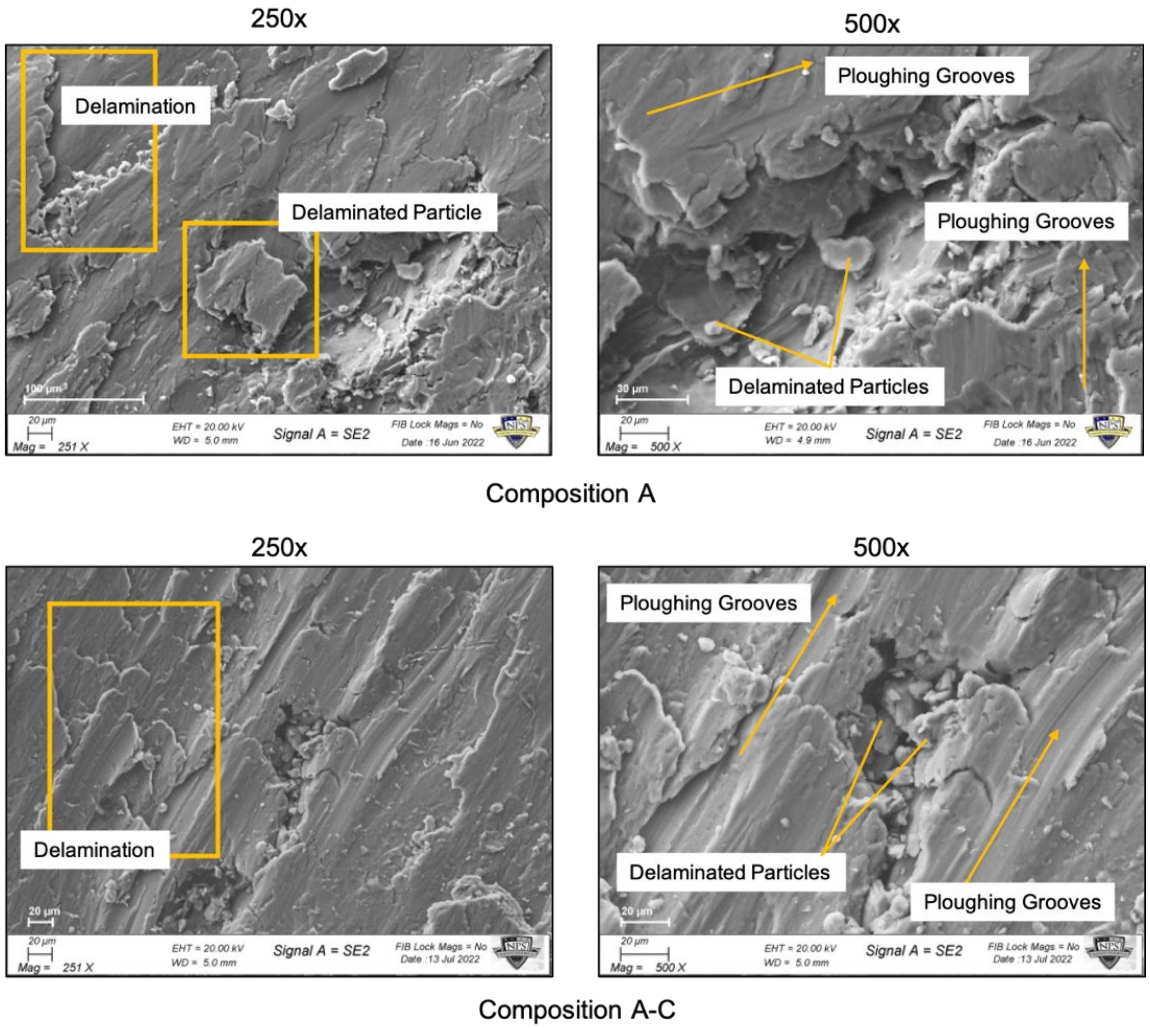


Figure 18. Wear Scar Feature Details for all Compositions

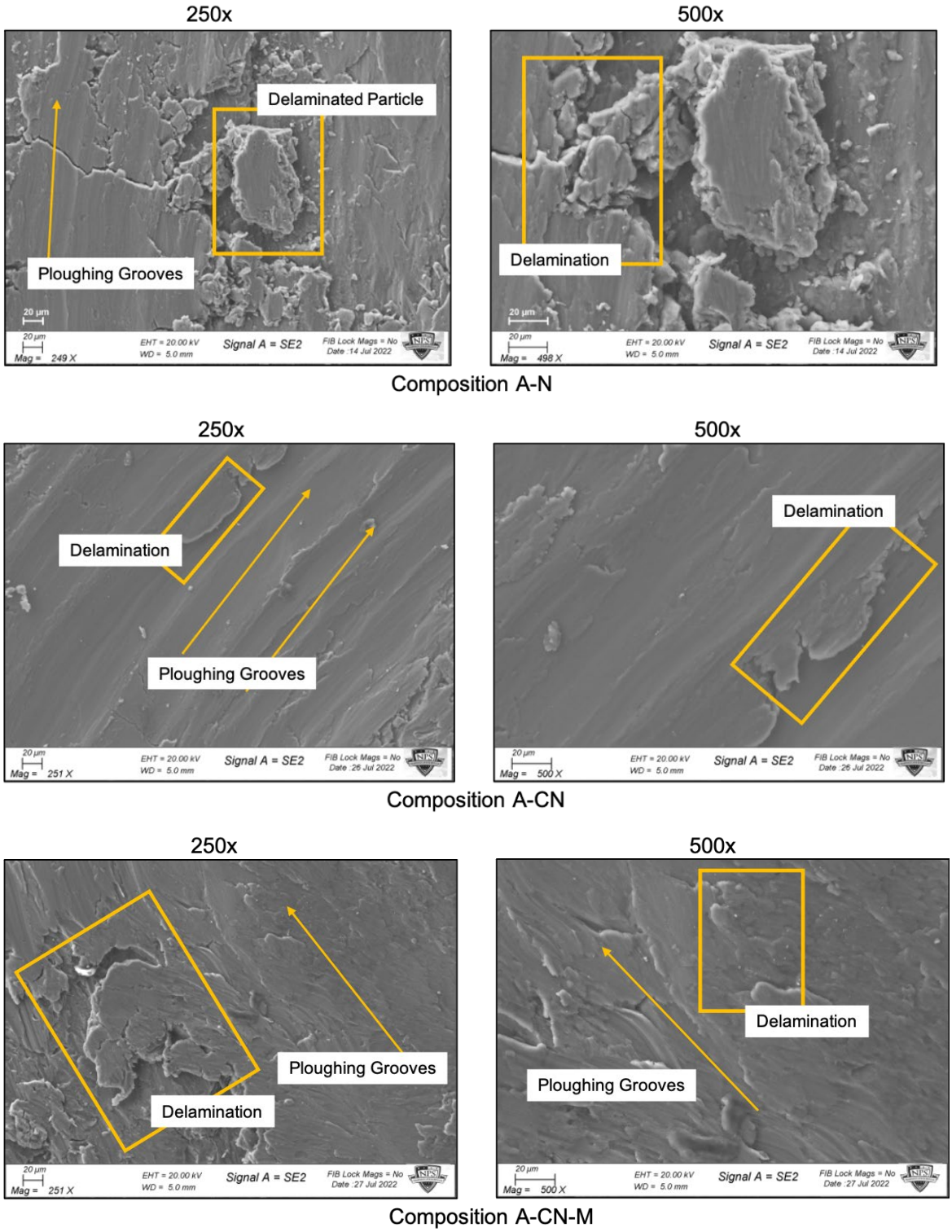


Figure 18 (continued)

The wear debris collected were imaged in the SEM to determine the average size of the delaminated particles. Table 8 below shows the average particle size for each Composition (see Appendix G for further details). Figure 19 shows the comparative sizes of the wear debris and some wear grooves can also be seen on some of the larger particles. The pure Al CS coating produced the largest sized particles. The effect of adding n-$B_4C$ to the Al-MMC coating created smaller wear debris which suggests that the coating was slightly more brittle and was less cohesive than the other coating compositions. Adding BNNP to the Al-MMC coatings resulted on larger wear debris as compared to other composition coatings. For Composition A-CN, the added BNNP had a more dominating effect and resulted in debris sizes similar to A-N. Composition A-CN-M produced slightly smaller wear debris than A-CN on average but was between A-C and A-N in size.

Table 8. Average Wear Debris Size for Each Composition

| | **Composition A** | **Composition A-C** | **Composition A-N** | **Composition A-CN** | **Composition A-CN-M** |
|---|---|---|---|---|---|
| Average Wear Debris Size (μm) | 106.559 | 49.489 | 78.735 | 73.686 | 68.923 |

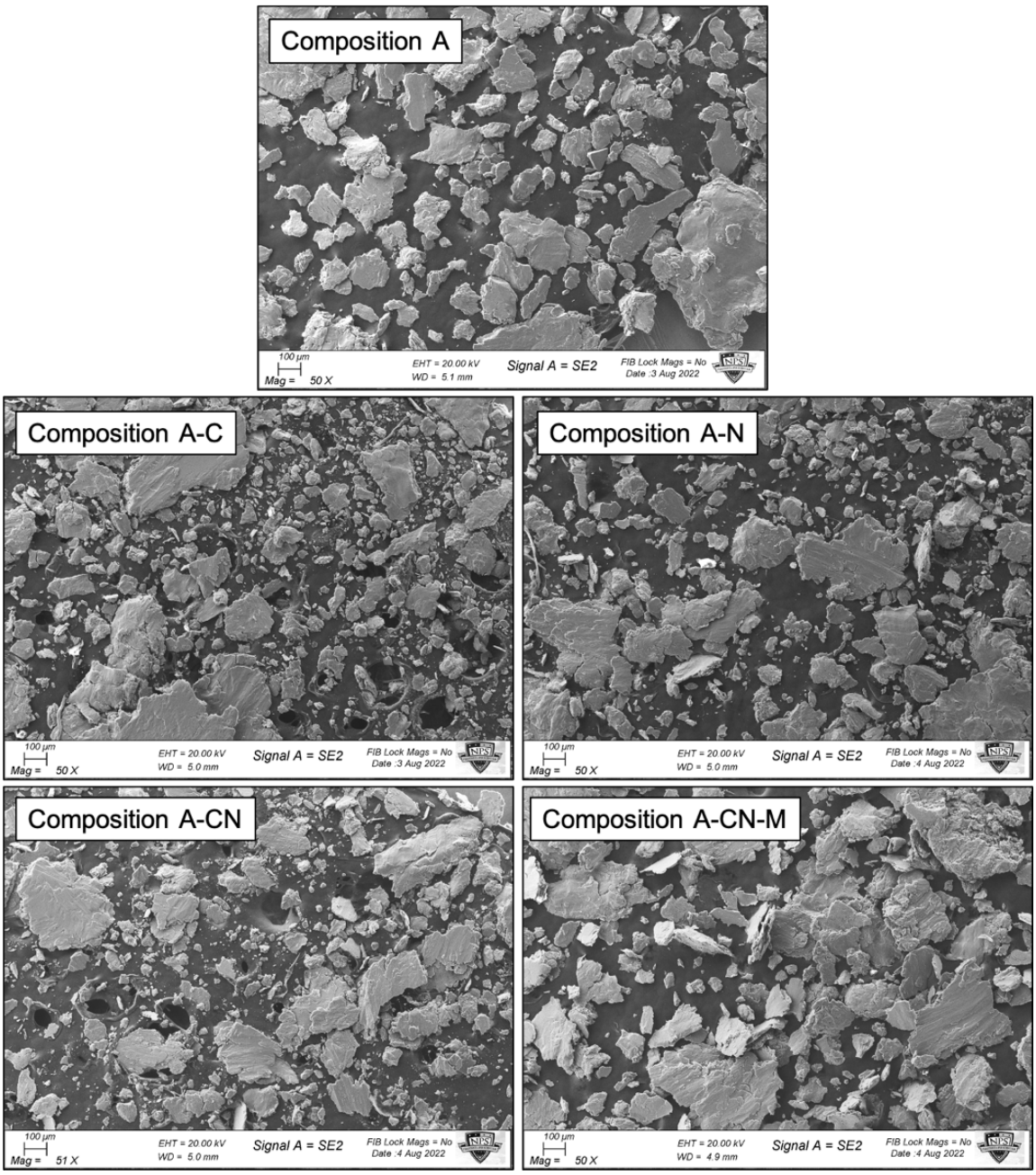


Figure 19. SEM Images of Wear Debris Particles for (a) Composition A, (b) Composition A-C, (c) Composition A-N, (d) Composition A-CN and (e) Composition A-CN-M

## E. EFFECTS OF REINFORCEMENT AND HEAT TREATMENT

In summary, the effects of reinforcing CS Al coatings with one or two nanoparticles have varying results on their microstructure, mechanical, and tribological properties.

### 1. Mechanical Properties

Table 9 shows the changes in mechanical properties, using their average value, for all five compositions and heat treatment conditions as compared to the baseline Al CS coating without heat treatment. In general, heat treatment of the pure or reinforced Al CS coating results in a reduction of nanohardness, microhardness, and stiffness but improved its WOI performance. The effects of adding n-$B_4C$, BNNP, both or in a dispersed mixture are discussed subsequently.

Table 9. Comparative Results of Mechanical Properties for all Compositions and Heat Treatments

| Condition 1: No Heat Treatment | | | | | | |
|---|---|---|---|---|---|---|
| Properties \ Composition | | Composition A | Composition A-C | Composition A-N | Composition A-CN | Composition A-CN-M |
| | | Average | Average | Average | Average | Average |
| Mechanical Properties | Nanohardness (GPa) | **0.896** | 1.026 | 0.861 | 0.982 | 0.963 |
| | Microhardness (HV0.05) | **62.470** | 65.350 | 63.010 | 63.610 | 62.080 |
| | Elastic Modulus (GPa) | **70.731** | 78.539 | 74.546 | 55.243 | 77.480 |
| | Work of Indentation (pJ) | **385.49** | 341.29 | 411.10 | 383.18 | 362.74 |

| Condition 2: 300°C, 1hr | | | | | | |
|---|---|---|---|---|---|---|
| Properties \ Composition | | Composition A | Composition A-C | Composition A-N | Composition A-CN | Composition A-CN-M |
| | | Average | Average | Average | Average | Average |
| Mechanical Properties | Nanohardness (GPa) | **1.007** | 0.808 | 0.922 | 0.872 | 0.919 |
| | Microhardness (HV0.05) | **58.990** | 59.500 | 59.280 | 58.280 | 59.130 |
| | Elastic Modulus (GPa) | **82.399** | 70.690 | 75.255 | 75.049 | 64.879 |
| | Work of Indentation (pJ) | **362.68** | 423.86 | 378.56 | 421.49 | 370.05 |

| Condition 3: 300°C, 4hr | | | | | | |
|---|---|---|---|---|---|---|
| Properties \ Composition | | Composition A | Composition A-C | Composition A-N | Composition A-CN | Composition A-CN-M |
| | | Average | Average | Average | Average | Average |
| Mechanical Properties | Nanohardness (GPa) | **0.9278** | 0.9181 | 0.8289 | 0.9179 | 0.8039 |
| | Microhardness (HV0.05) | **60.37** | 57.77 | 58.69 | 59.31 | 59.41 |
| | Elastic Modulus (GPa) | **81.1634** | 78.3539 | 61.2562 | 69.5326 | 67.6908 |
| | Work of Indentation (pJ) | **395.61** | 409.04 | 445.39 | 408.94 | 428.19 |

| Condition 4: 500°C, 1hr | | | | | | |
|---|---|---|---|---|---|---|
| Properties \ Composition | | Composition A | Composition A-C | Composition A-N | Composition A-CN | Composition A-CN-M |
| | | Average | Average | Average | Average | Average |
| Mechanical Properties | Nanohardness (GPa) | **0.6707** | 0.7685 | 0.6272 | 0.7565 | 0.6842 |
| | Microhardness (HV0.05) | **37.20** | 42.10 | 40.31 | 42.33 | 38.67 |
| | Elastic Modulus (GPa) | **66.7142** | 70.8595 | 59.6760 | 63.8569 | 67.9983 |
| | Work of Indentation (pJ) | **452.51** | 429.29 | 532.97 | 447.51 | 483.81 |

| Condition 5: 500°C, 4hr | | | | | | |
|---|---|---|---|---|---|---|
| Properties \ Composition | | Composition A | Composition A-C | Composition A-N | Composition A-CN | Composition A-CN-M |
| | | Average | Average | Average | Average | Average |
| Mechanical Properties | Nanohardness (GPa) | **0.7449** | 0.6962 | 0.5581 | 0.7774 | 0.7826 |
| | Microhardness (HV0.05) | **38.26** | 41.8 | 39.17 | 42.10 | 39.24 |
| | Elastic Modulus (GPa) | **72.7735** | 63.8943 | 42.0073 | 65.5182 | 66.7457 |
| | Work of Indentation (pJ) | **438.79** | 410.01 | 571.22 | 379.79 | 449.65 |

| Legend for Table 9: Percentage Change in Mechanical Property as Compared to Coating | | | | | | | | | |
|---|---|---|---|---|---|---|---|---|---|
| -40.001 to -50% | -30.001 to -40% | -20.001 to -30% | -10.001 to -20% | -0.001 to -10% | Same as Control | 0.001 to 10% | 10.001 to 20% | 20.001 to 30% | 30.001 to 40% |

The nanohardness test is a more localized hardness test and is likely to indent within a splat. In the single-reinforced cases, as compared to the baseline coating, the single reinforcement of n-$B_4C$ (Composition A-C) and the dual reinforcement of n-$B_4C$ and

BNNPs (Compositions A-CN and A-CN-M) improved the property in heat treatment Condition 4 onwards.

In the dual-reinforced case, it is interesting to note that the nanohardness property of both Compositions A-CN and A-CN-M behaved like a composite material with a rule of mixtures[5] between Composition A-C and A-N when the coating was formed as-sprayed. This behavior stayed true up to heat treatment Condition 1 (300°C, 1 hr). From Figure 20, with more aggressive heat treatment conditions, the performance of Compositions A-CN and A-CN-M changed (300°C, 4 hr and 500°C, 1 hr). Composition A-CN's properties moved towards the A-C (upper bound for nanohardness) while A-CN-M moved towards A-N (lower bound for nanohardness). At Condition 5, the performance of both A-CN-M and A-CN outperformed both A-C and A-N. We could infer that a dual reinforcement coating with different reinforcing particle morphologies improve the hardness better than single reinforcements.

Figure 21 shows the changes in elastic modulus for Compositions A-CN and A-CN-M as compared to the single reinforced and baseline compositions with increasingly aggressive heat treatment conditions. Composition A-CN-M's elastic modulus decreased upon heat treatment but stayed relatively constant around 67 GPa. Between heat treatment Conditions 3 and 4, the elastic modulus for A-CN-M behaved similarly to the rule of mixtures for Composition A-C and A-N. Similarly, Composition A-CN's elastic modulus decreased upon heat treatment. At heat treatment Condition 2, the elastic modulus for A-CN behaved similarly to the rule of mixtures for Composition A-C and A-N. Beyond that, between heat treatment Condition 3 and 4, the elastic modulus for A-CN behaved similarly to Composition A-C. Similarly at Condition 5, the elastic modulus performance of both A-CN-M and A-CN outperformed both A-C and A-N. We could infer that adding n-$B_4C$ had a stiffening effect while adding BNNPs softened the CS composite.

[5] Rule of Mixtures for composite materials is widely used predictor of its modulus and strength, based on the weighted mean of reinforcement material and its matrix material. For example, the density of a fibre-reinforced composite material can be calculated by $\rho_{composite} = \rho_{fibre}V_{fibre} + \rho_{matrix}V_{matrix}$

For microhardness, the effect of the reinforcing particles had little or no influence on changing the performance of the CS Al-MMC under heat treatments up to 300°C. From Figure 12, we can only see that adding n-$B_4C$ had a positive effect the microhardness of the coating at annealing temperatures of 500°C. At that same temperature, adding BNNP to a CS Al-MMC coating had a lesser positive effect but it still showed a slight improvement over the pure CS Al coating. This is likely due to better bonding between the reinforcing and matrix phases at the elevated heat treatment temperature and time, but it is seen that at 2 vol. % reinforcement, the changes matrix phase's hardness dominated the overall performance of the CS composite coating.

The effect of reinforcing particles on the WOI performance of the CS Al-MMC that underwent heat treatments was most improved when BNNP was added. We can see that both Compositions A-N and A-CN-M saw improvements in their WOI performance as the heat treatments got more aggressive. Adding n-$B_4C$ to Al-MMCs saw the best improvement in WOI at heat treatment Condition 2, however, beyond that the more aggressive heat treatments resulted in a minimal improvement in WOI.

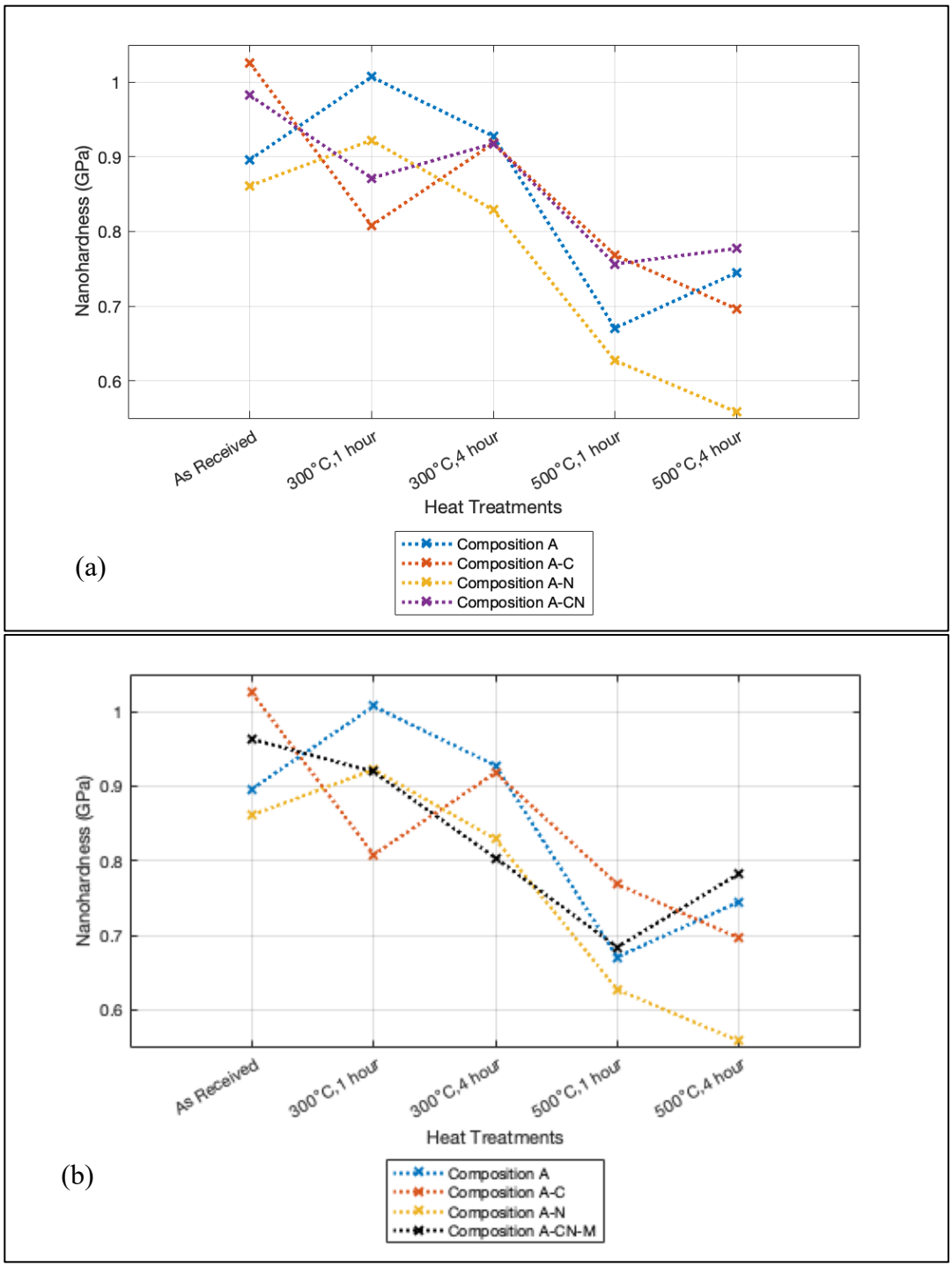


Figure 20. (a) Comparison of Nanohardness Between Composition A-C, A-N and A-CN. (b) Comparison of Nanohardness Between Composition A-C, A-N and A-CN-M. Composition A is Imposed onto Both Graphs as a Baseline Comparison.

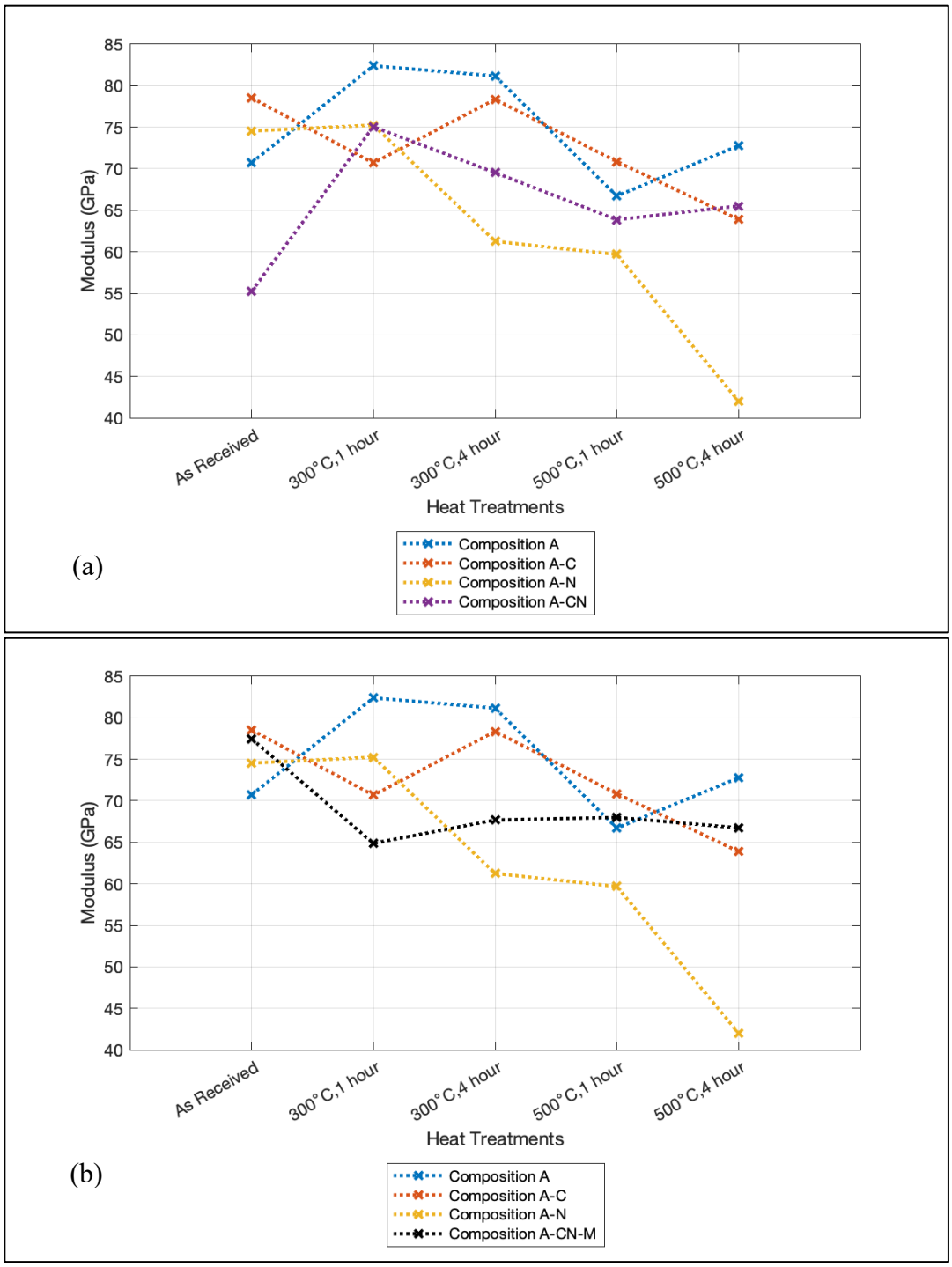


Figure 21. (a) Comparison of Elastic Modulus Between Composition A-C, A-N and A-CN. (b) Comparison of Elastic Modulus Between Composition A-C, A-N and A-CN-M. Composition A is Imposed onto Both Graphs as a Baseline Comparison.

### 2. Tribological Properties

Table 10 shows the changes in tribological properties, for the compositions that underwent heat treatment Condition 4. In comparison with CS Al coatings, the effect of adding n-$B_4C$ had reduced the friction of the coating, adversely effected its specific wear rate, and produced smaller wear debris. Adding BNNPs increased the friction of the coating, adversely effected its specific wear rate, and produced slightly larger wear debris compared to the n-$B_4C$ reinforced CS Al coating.

The homogenously reinforced Composition A-CN had reduced the friction of the coating, improved its specific wear rate and produced smaller wear debris similarly sized as the BNNP reinforced CS Al coating. Composition A-CN-M had similar COF as the baseline, similar specific wear rate as the baseline and produced smaller wear debris similarly sized as the BNNP reinforced CS Al coating.

In terms of the changes in COF over time, adding BNNPs had an effect maintaining the COF as the coating was being worn. Adding n-$B_4C$ had not changed the same property much and behaved similarly as the baseline case.

Table 10. Comparative Results of Tribological Properties for all Compositions at Heat Treatment Condition 4

| Condition 4: 500°C, 1hr | | | | | | |
|---|---|---|---|---|---|---|
| Properties \ Composition | | Composition A | Composition A-C | Composition A-N | Composition A-CN | Composition A-CN-M |
| | | Average | Average | Average | Average | Average |
| Tribological | Average COF | 0.4752 | 0.4662 | 0.5078 | 0.4608 | 0.4760 |
| | Reduction in COF over Time | High | High | Low | High | Lowest |
| | Specific Wear Rate ($m^3$/Nm) | 4.0519 x $10^{-10}$ | 5.7951 x $10^{-10}$ | 5.9608 x $10^{-10}$ | 3.9118 x $10^{-10}$ | 4.1708 x $10^{-10}$ |
| | Average Debris Size | 106.559 | 49.489 | 78.735 | 73.686 | 68.923 |

| | | | | | | | | | | |
|---|---|---|---|---|---|---|---|---|---|---|
| -40.001 to -50%+ | -30.001 to -40% | -20.001 to -30% | -10.001 to -20% | -0.001 to -10% | Same as Al CS Coating Baseline | 0.001 to 10% | 10.001 to 20% | 20.001 to 30% | 30.001 to 40% | 40.001 to 50% |

During wear tests, some delaminated particles would have acted as third-party wear particles, causing more abrasive action on the coating and delamination from the coating. The harder n-$B_4C$ particles could have also caused the deep and small cuts at the wear grooves seen on Figure 18. The average wear debris size is similar to the average splat size found from the optical microscope images, and suggests that adding n-$B_4C$ had little resistive effect on delaminating splats from the layer of cohesive coating. A suggested schematic of the effect of adding n-$B_4C$ on the tribological behavior is shown on Figure 22.

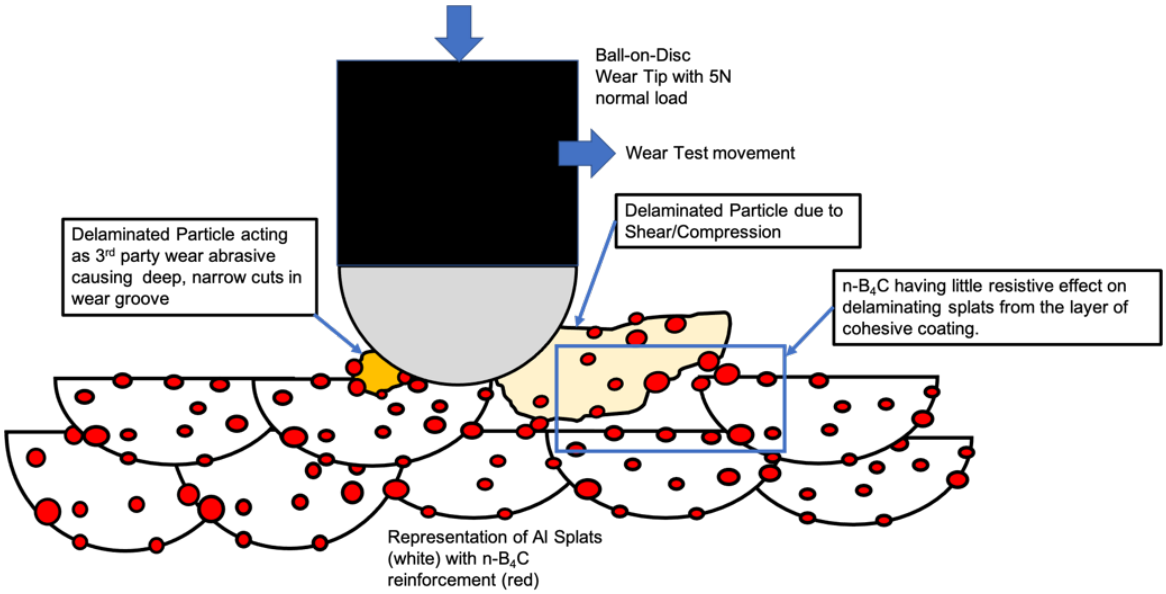


Figure 22. Schematic of the Effects of Adding n-$B_4$Cs on the Tribological Behavior of Al-MMC CS Coatings

Adding BNNPs increased the friction of the coating, adversely effected its specific wear rate, and produced slightly larger wear debris compared to the n-$B_4$C reinforced CS Al coating. Like with the $B_4$C, the harder BNNP particles also caused deep and small cuts at the wear grooves, again as seen in Figure 18, but to a smaller extent due to its plate morphology. In a study by Tanaji et. al. found that were variations in hardness in hexagonal boron nitride (hBN) reinforced cast aluminum are due to the random orientation of the 2D plate-like hBN that could be perpendicular or parallel to the indentation load [37]. Similarly, BNNPs could also be orientated in a manner that is angled or perpendicular to the wear surface adding more surface roughness, which resulted in a higher COF than the rest. However, for BNNPs that were oriented parallel to the wear surface acted as a lubricative phase and could have led to the low reduction in COF over time. The angled or perpendicular BNNPs could also added some resistance to the delamination of splats, causing larger wear debris to form during the wear tests. A suggested schematic of the effect of adding BNNP on the tribological behavior is shown on Figure 23.

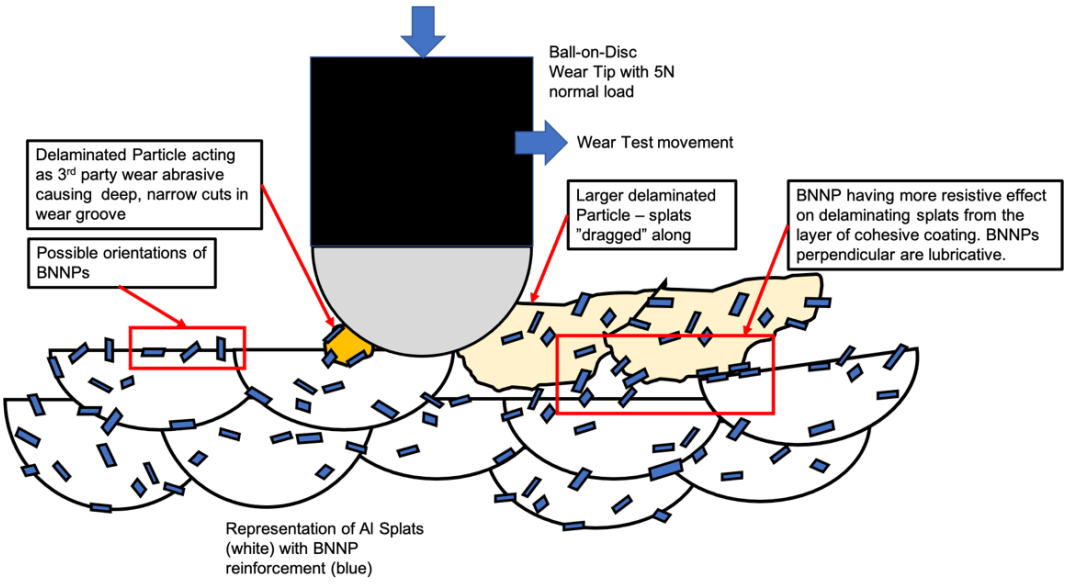


Figure 23. Schematic of the Effects of Adding BNNPs on the Tribological Behavior of Al-MMC CS Coatings

The dual homogenous reinforced Composition A-CN had reduced the friction of the coating, improved its specific wear rate and produced smaller wear debris similarly sized as the BNNP reinforced CS Al coating. When the dual homogenous reinforced Al-MMC underwent wear tests, some delaminated particles would have acted as third-party wear particles with both harder BNNP and n-$B_4C$ around its surface. Due to the morphology of the BNNP and n-$B_4C$ particles, the third-party wear debris would have caused more ploughing instead of finer cuts found on Composition A-C. Similar to Composition A-N, the angled or perpendicular BNNPs could also added some resistance to the delamination of splats, causing larger wear debris to form during the wear tests, but the spherically shaped n-$B_4Cs$ could have reduced that effect, resulting in the smaller wear debris formed. The average COF for Composition A-CN is almost between the performance for A-C and A-N and is likely due to the mixed performance of the slightly resistive BNNPs and smoother n-$B_4Cs$. The combined effects of having both BNNPs and n-$B_4Cs$ on the change of COF over time is likely dominated by the repetitive ploughing by BNNPs and also the finer cuts by n-$B_4Cs$. A suggested schematic of the effect of adding BNNP on the tribological behavior is shown on Figure 24.

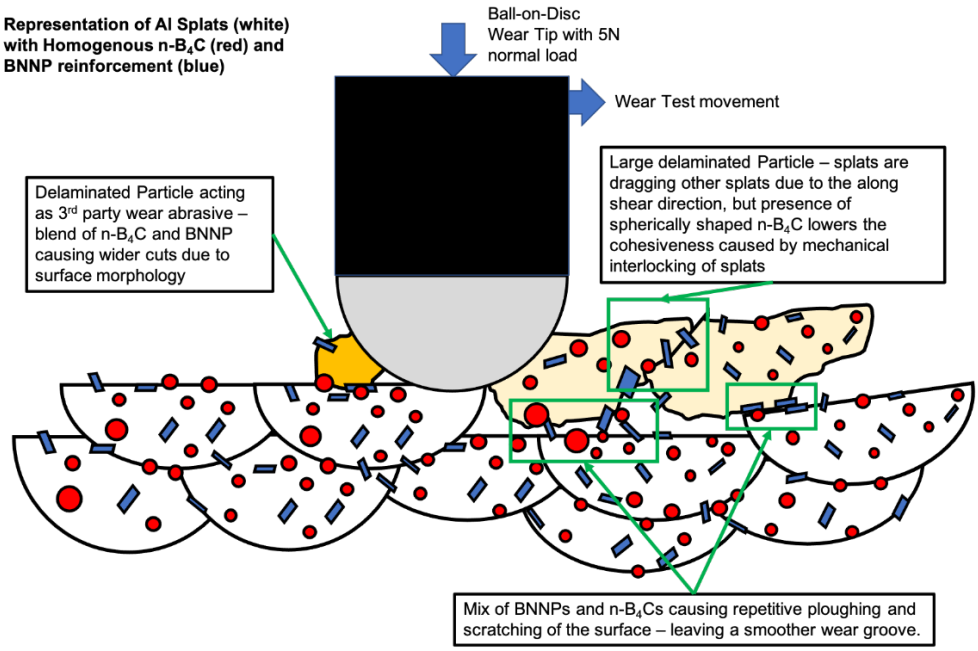


Figure 24. Schematic of the Effects of Adding n-$B_4C$ and BNNPs Homogenously on the Tribological Behavior of Al-MMC CS Coatings

The dual reinforced Composition A-CN-M with disperse distributions of BNNPs and n-$B_4Cs$ had similar COF as the baseline, similar specific wear rate as the baseline and produced wear debris similarly sized as the BNNP reinforced CS Al coating. The wear debris is this system is slightly different where it could be either coated with BNNP or n-$B_4C$. Due to the morphology of the BNNP or n-$B_4C$ particles, the third-party wear debris would have caused more ploughing with finer cuts; a combination between Compositions A-C and A-N. Similar to Composition A-CN, the angled or perpendicular BNNPs could also added some resistance to the delamination of splats, causing larger wear debris to form during the wear tests, but the spherically shaped n-$B_4Cs$ could have reduced that effect, resulting in the smaller wear debris formed. The mechanism resulting in the results for average COF is similar to Composition A-CN. The combined effects of having both BNNPs and n-$B_4Cs$ in a dispersed manner had caused a less aggressive drop in COF over time due to the increased likelihood of BNNP-rich regions shearing across other BNNP-rich regions with less frictional force, in a manner similar to Composition A-N. A suggested schematic of the effect of adding BNNP on the tribological behavior is shown on Figure 25.

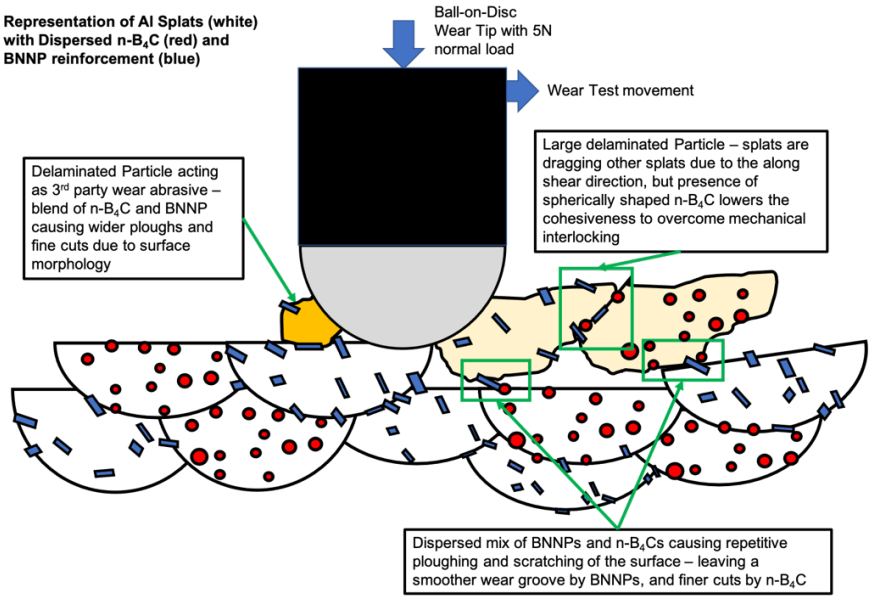


Figure 25. Schematic of the Effects of Adding Dispersed Distributions of n-B4C and BNNPs on the Tribological Behavior of Al-MMC CS Coatings

# IV. CONCLUSION

In conclusion, through the high-pressure CS process, fabrication of Al-MMCs with reinforcement concentrations of single n-$B_4C$ or BNNPs; dual homogenous or dispersed n-$B_4C$, and BNNPs of up to 2 vol. % was performed. The effects of heat treatments on such single or dual reinforced Al-MMCs were analyzed through the resulting mechanical, tribological and microstructural properties. The list of the effects is shown below:

- Minimal inter-splat porosity of CS Al-MMC coatings due to the higher velocity used in the deposition process. Subsequent heat treatments saw almost no changes in the inter splat porosity from optical microscope images.

- From the optical microscope images, changes in microstructures occurred mainly within the splats without diffusion across splat boundaries.

- From the nanohardness data, we could infer that a dual reinforcement coating with different reinforcing particle morphologies improved the hardness better than single reinforcements.

- From the microhardness test, we can see that the changes in the microstructure of the matrix phase of the Al-MMCs likely outstripped the contributive effects from the harder n-$B_4C$ and/or BNNPs. At 500°C heat treatments, the bonding between the phases improved and saw that the contributive effects on hardness from n-$B_4C$ is higher than BNNPs.

- WOI increased with heat treatments in general, with single or dual reinforcements. Adding BNNPs saw the largest increase in WOI at heat treatment Condition 5 (highest annealing temperature and time in this study) which can be attributed to the large increase in elastic modulus with heat treatment. Adding n-$B_4C$s to heat treated Al-MMCs had a stabilizing effect comparatively to elastic modulus and as a consequence saw smaller improvements to WOI.

- Heat treatment of single or dual reinforced Al-MMCs have different outcomes on their tribological behavior. A dual homogenous reinforcement of 1 vol. % each of n-$B_4C$s and BNNPs results in the lowest specific wear rate, average COF and lowest COF over time. This is likely due to the mixed effects from the increased likelihood of the plate face of BNNPs acting as lubricative portions against other hard BNNPs and n-$B_4C$s that are homogenously distributed in the Al matrix.

From this study, engineers would be able to use heat treatment on nanoparticle reinforced CS Al-MMCs and create coatings that are more ductile and improved tribological behavior. By adding dual nanoparticles with different morphologies and different attributes with varying degrees of heat treatments, we are able to control the performance required for the application of CS Al-MMCs.

# V. FUTURE WORK AND RECOMMENDATIONS

The compositions that were used in this study were of low reinforcement concentrations. There was some data from this study that the drop in the hardness of the Al matrix after heat treatments outstripped the reinforcement effects from the nanoparticles. It is recommended to study into increasing the reinforcement vol. %, up to even 10 vol. %, to further understand its effects on the mechanical and tribological properties.

Tensile or adhesion tests can be performed on the composite CS Al-MMC coatings in the near future to further characterize the interaction of the reinforcements with the Al matrix during pull out event.

Finally, an actual test of using this composition on damaged military parts can be performed in order to prove its utility as a BDAR technique. Being able to quickly repair parts and enhance the system's survivability would be valuable to any military outfit.

THIS PAGE INTENTIONALLY LEFT BLANK

# APPENDIX A. OPTICAL MICROSCOPY RESULTS

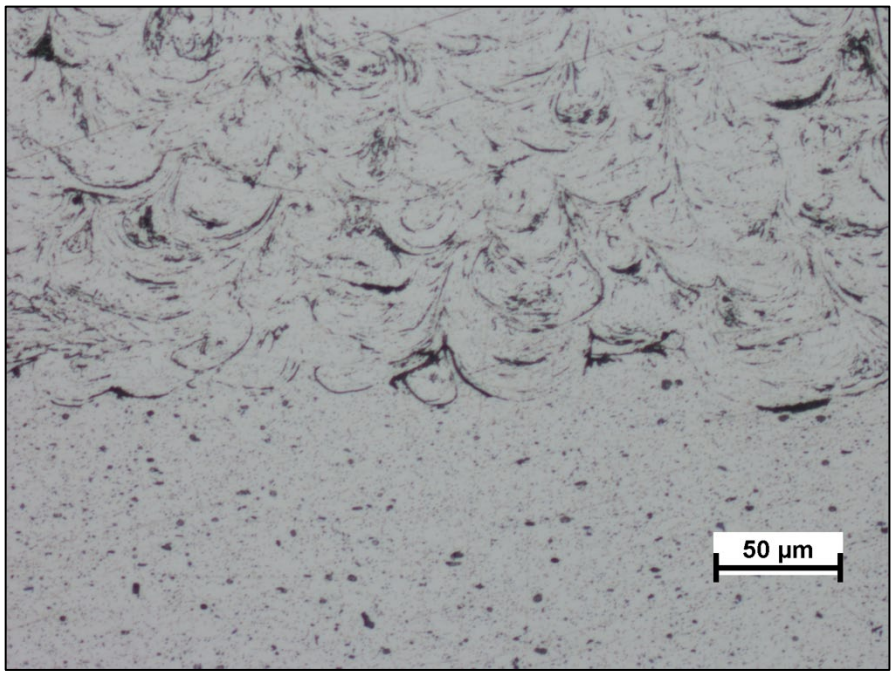


Optical Microscopy of Composition A at Condition 1

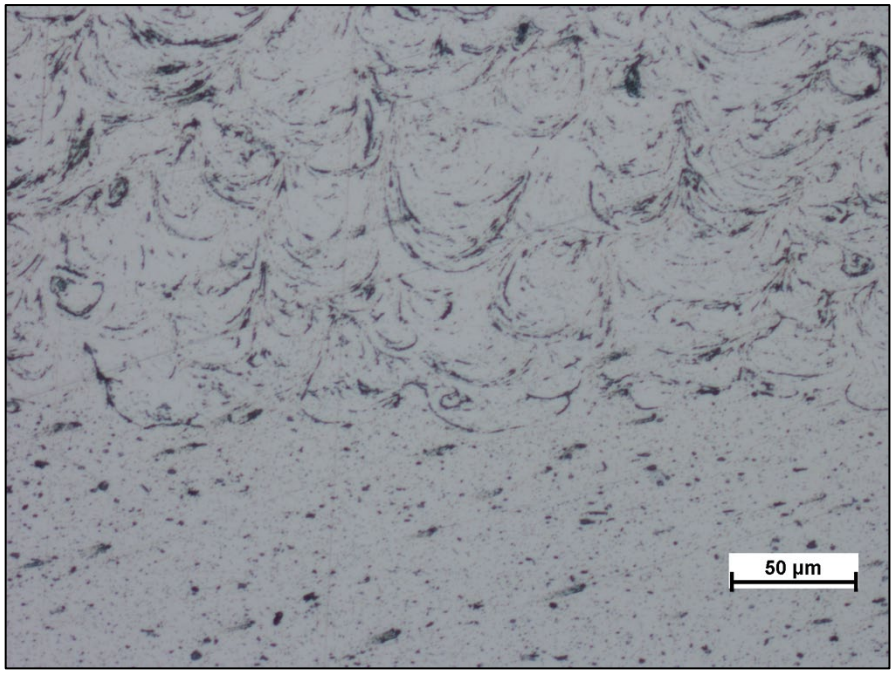


Optical Microscopy of Composition A at Condition 2

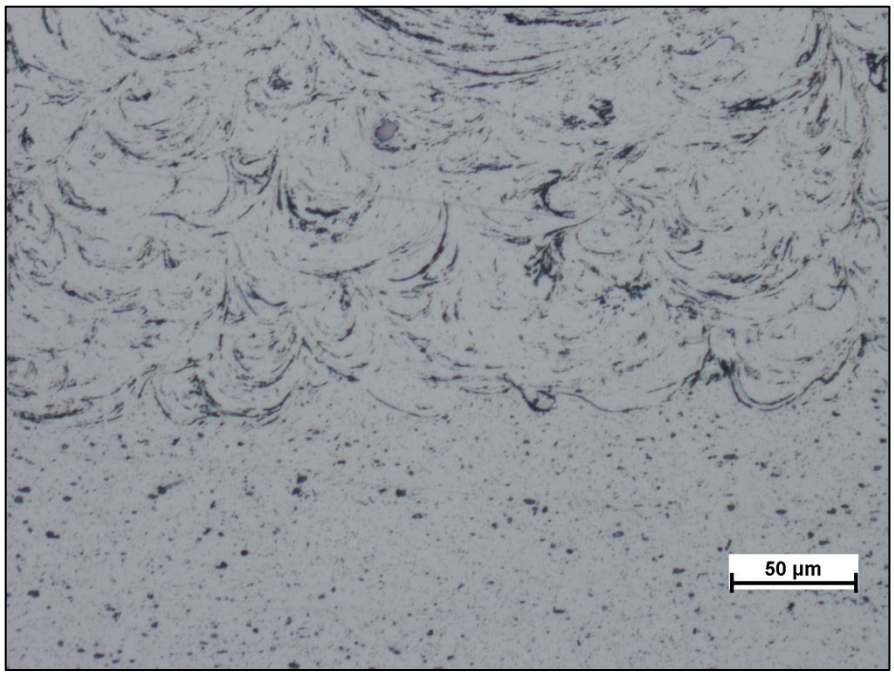


Optical Microscopy of Composition A at Condition 3

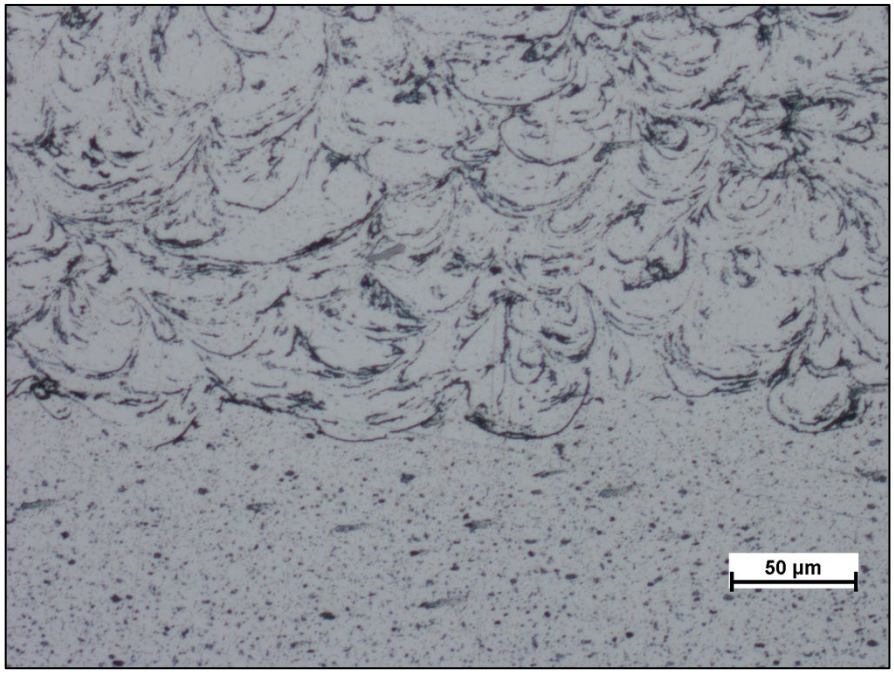


Optical Microscopy of Composition A at Condition 4

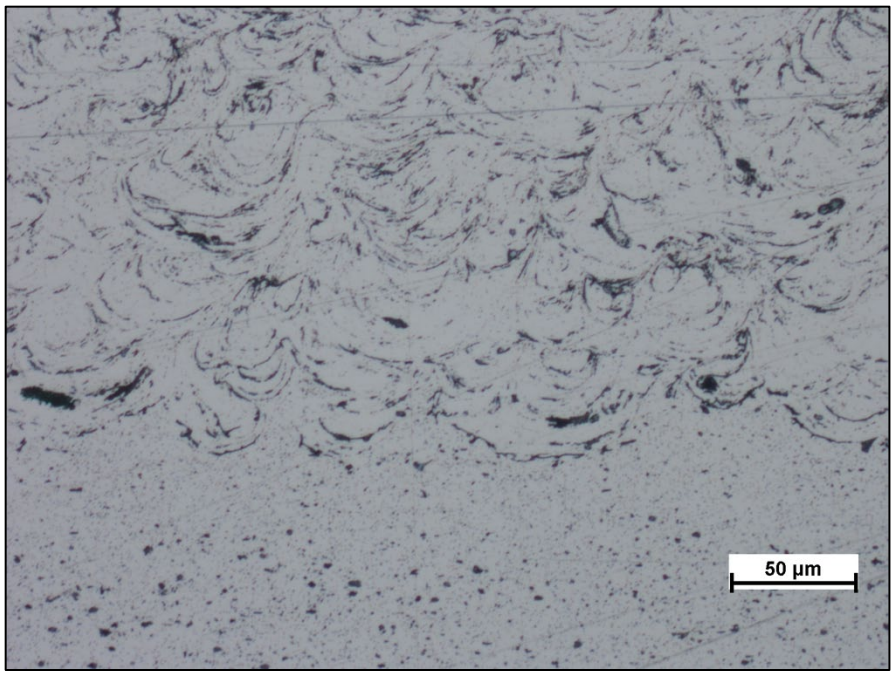


Optical Microscopy of Composition A at Condition 5

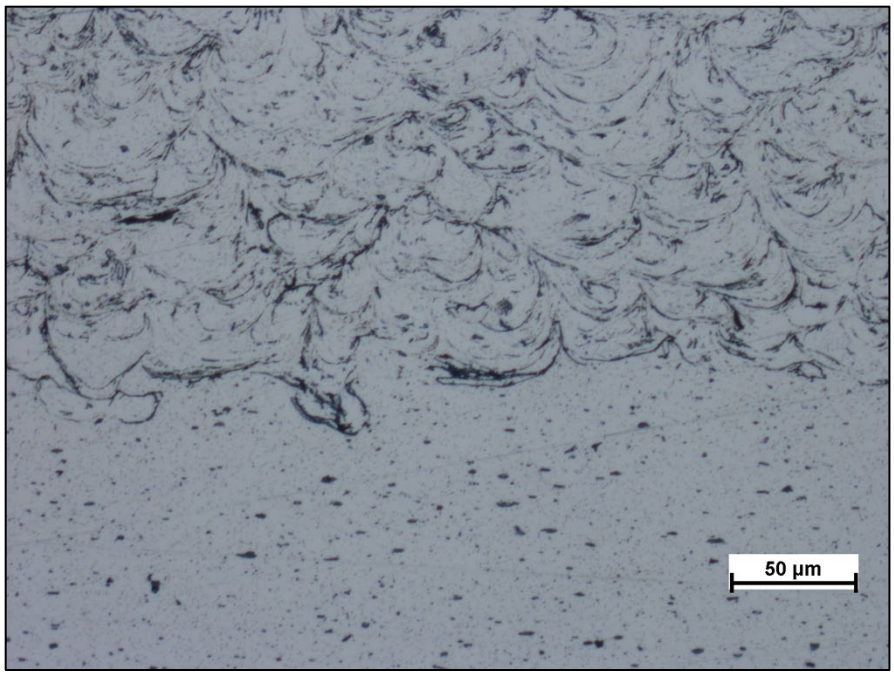


Optical Microscopy of Composition A-C at Condition 1

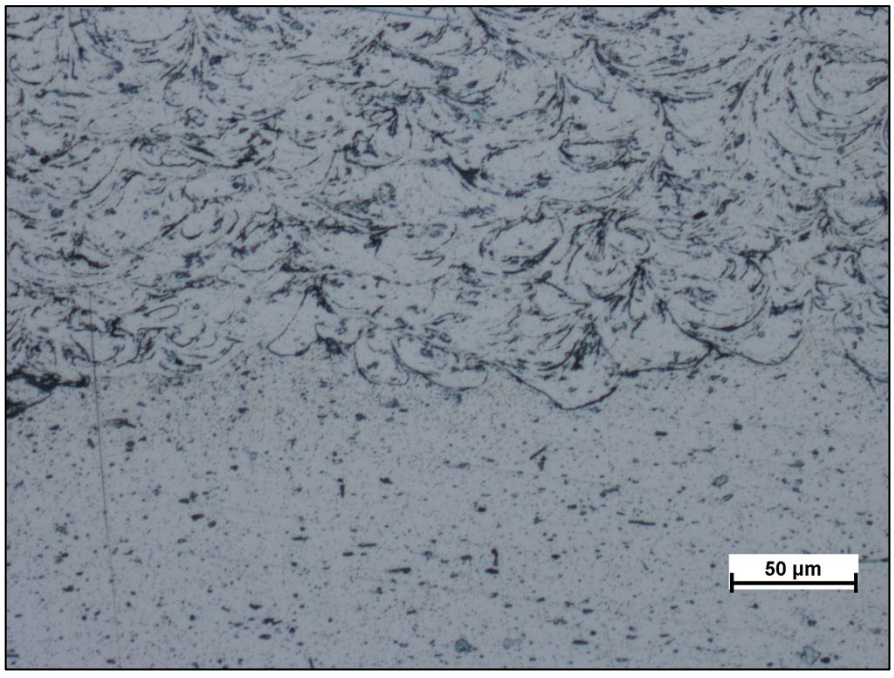


Optical Microscopy of Composition A-C at Condition 2

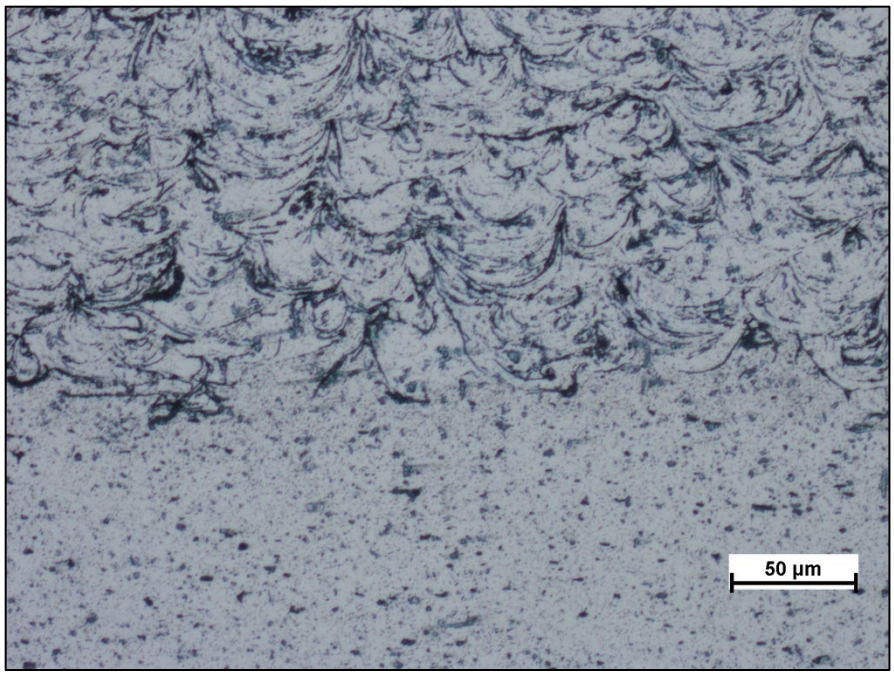


Optical Microscopy of Composition A-C at Condition 3

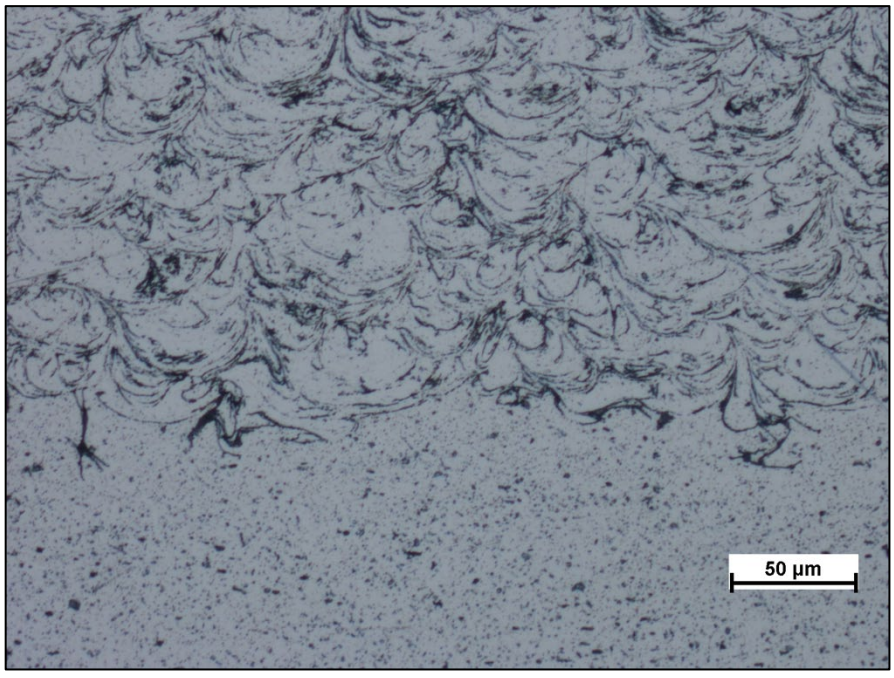


Optical Microscopy of Composition A-C at Condition 4

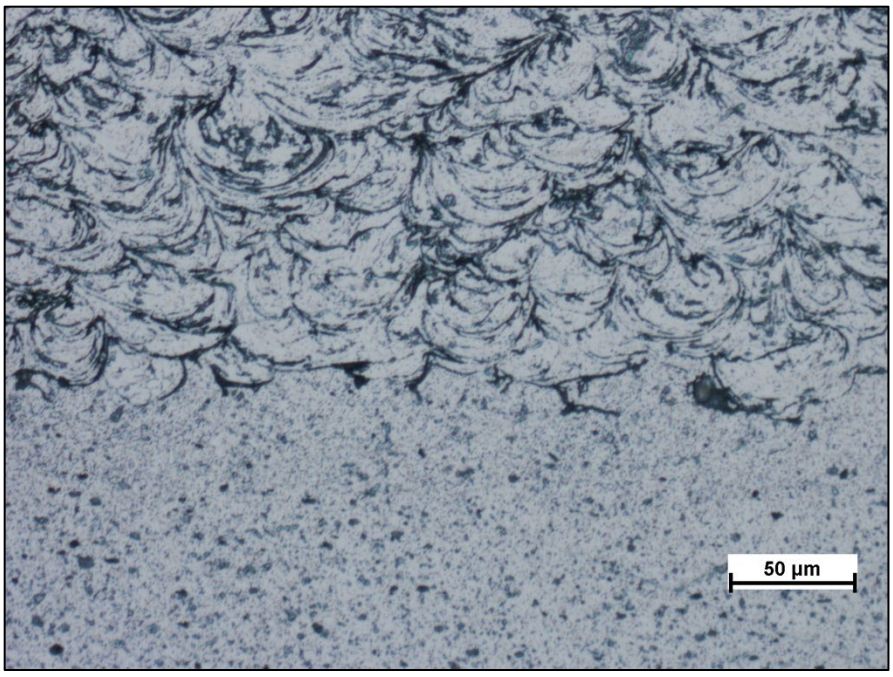


Optical Microscopy of Composition A-C at Condition 5

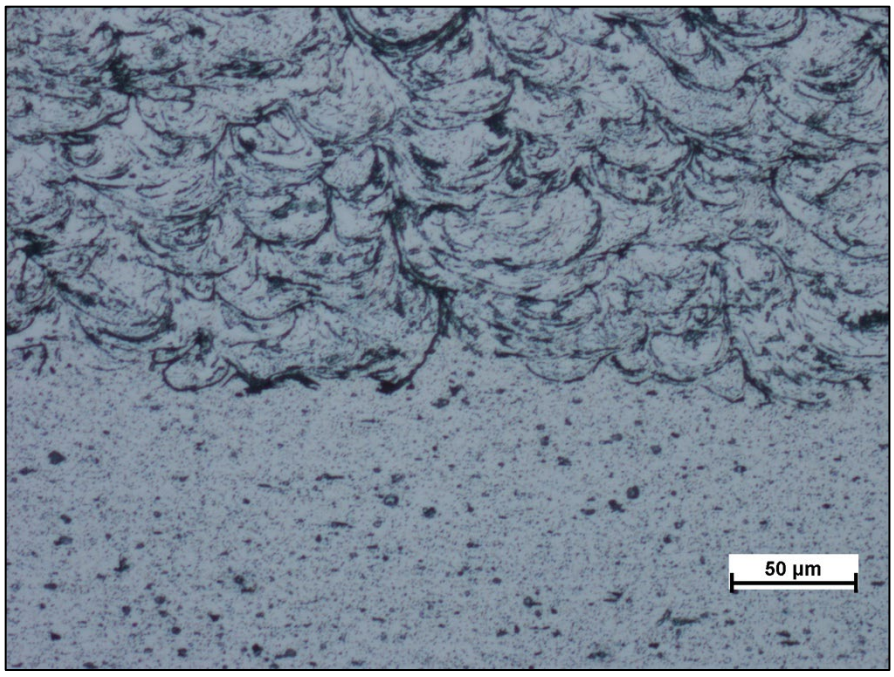


Optical Microscopy of Composition A-N at Condition 1

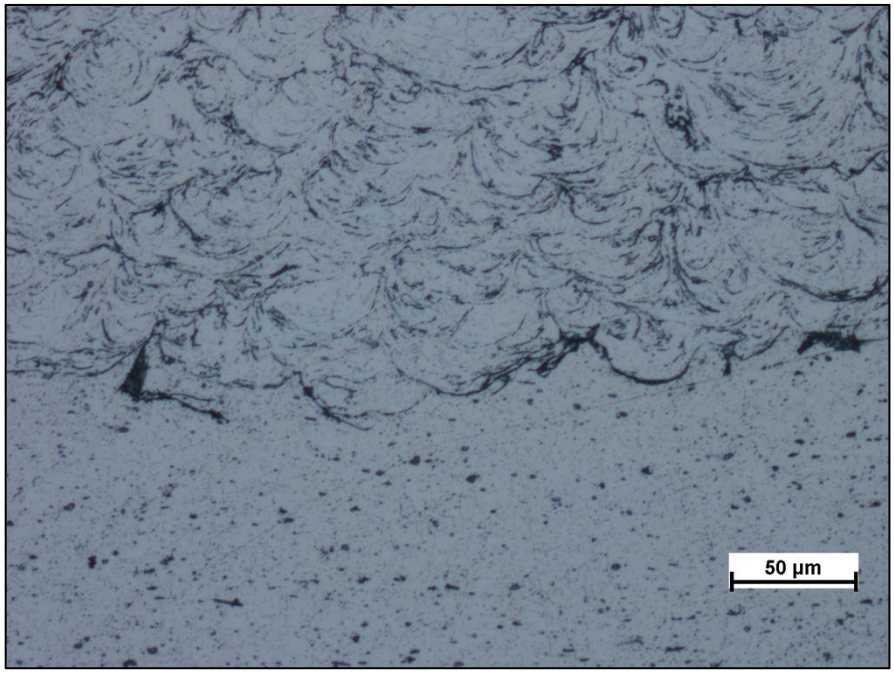


Optical Microscopy of Composition A-N at Condition 2

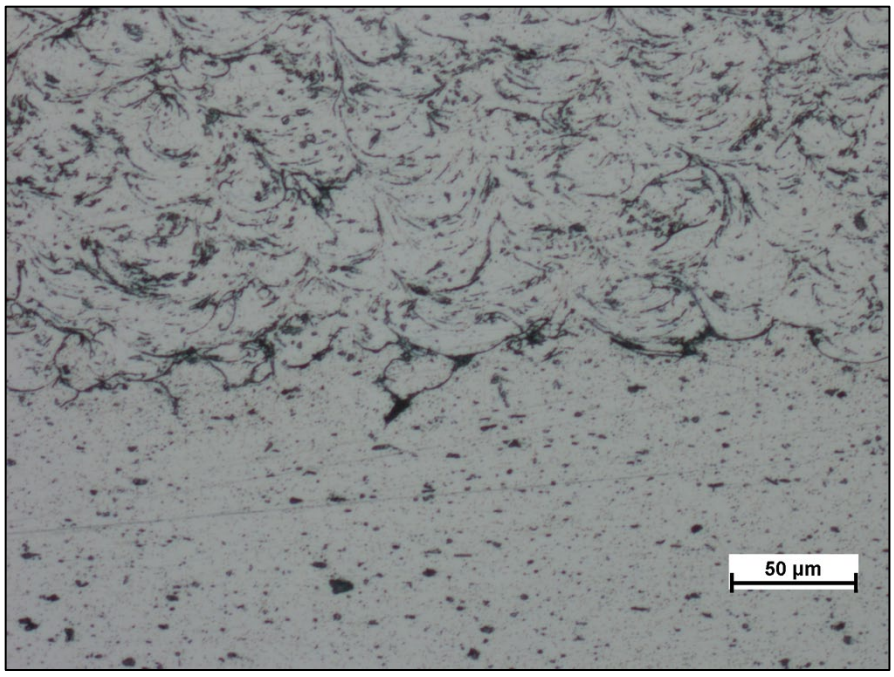


Optical Microscopy of Composition A-N at Condition 3

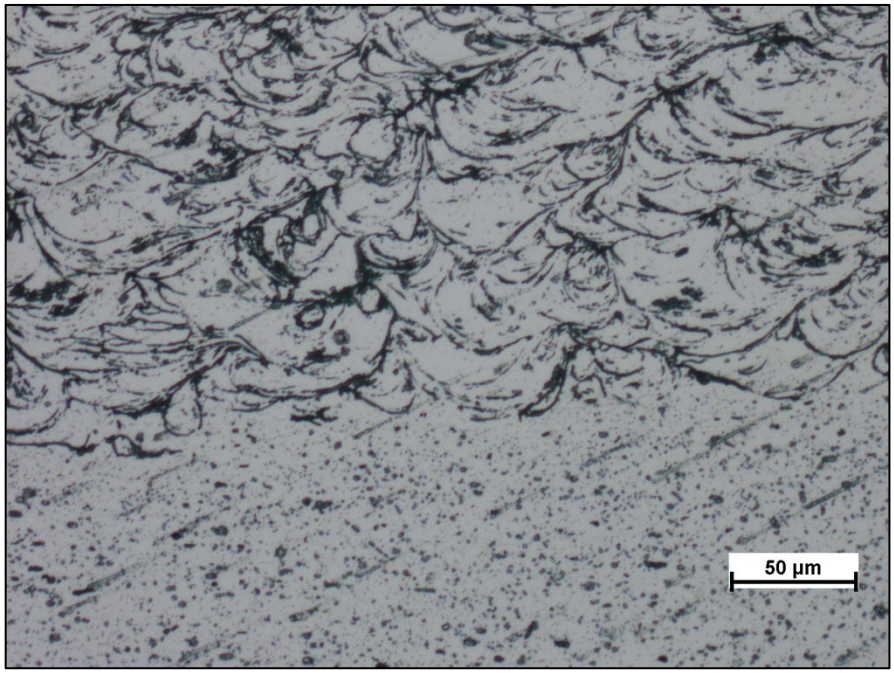


Optical Microscopy of Composition A-N at Condition 4

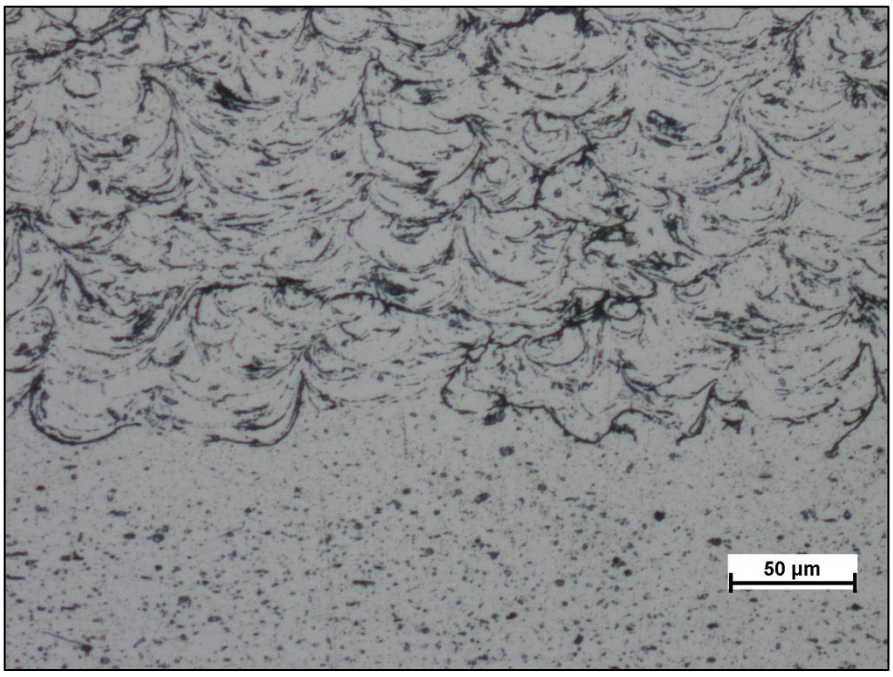


Optical Microscopy of Composition A-N at Condition 5

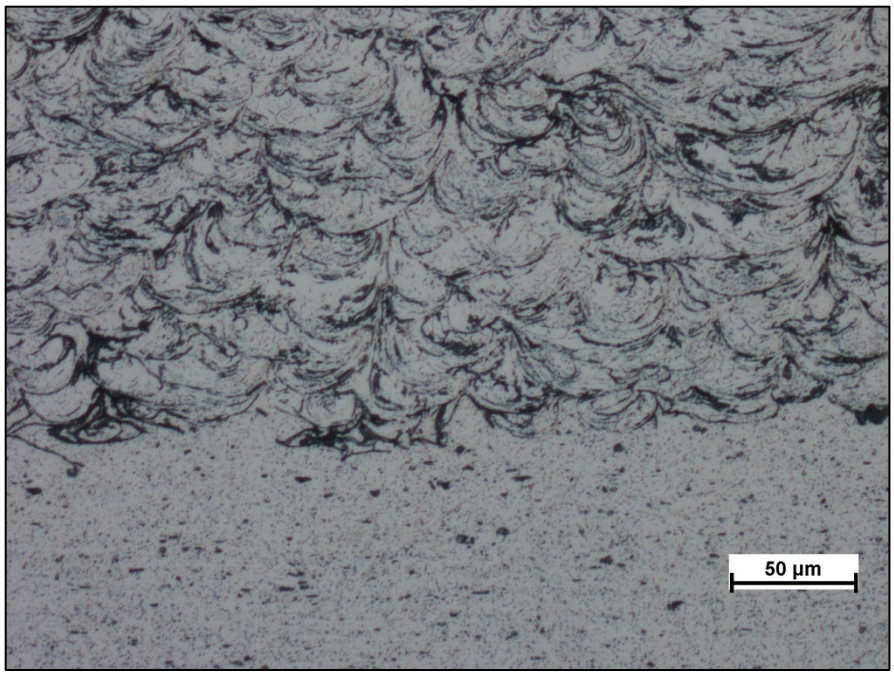


Optical Microscopy of Composition A-CN at Condition 1

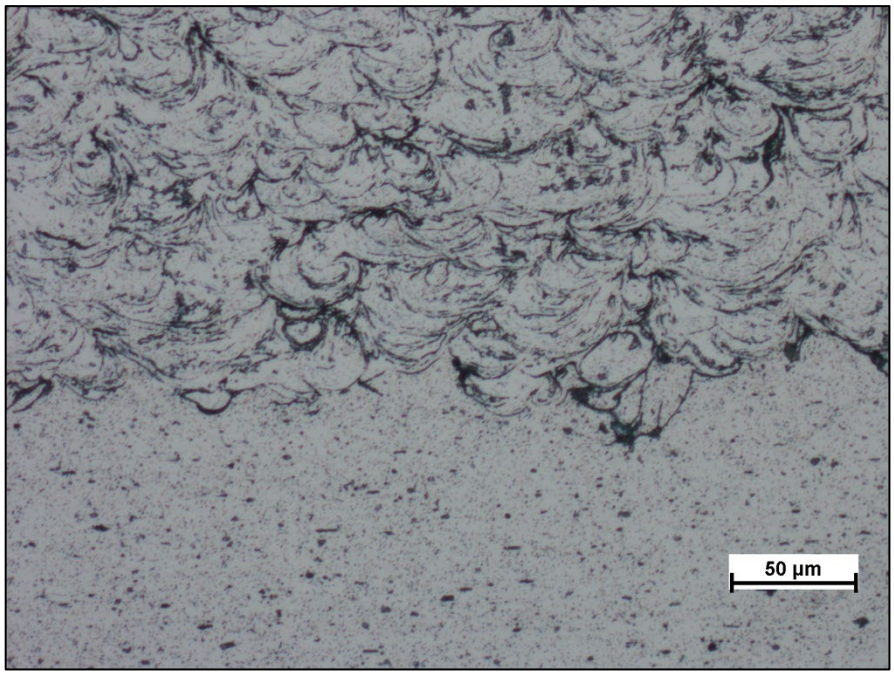


Optical Microscopy of Composition A-CN at Condition 2

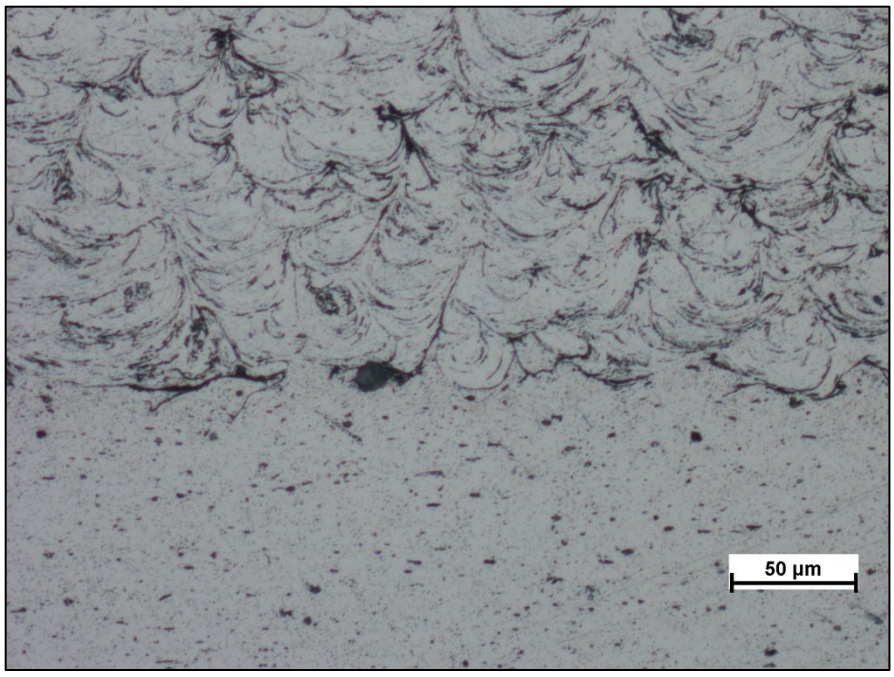


Optical Microscopy of Composition A-CN at Condition 3

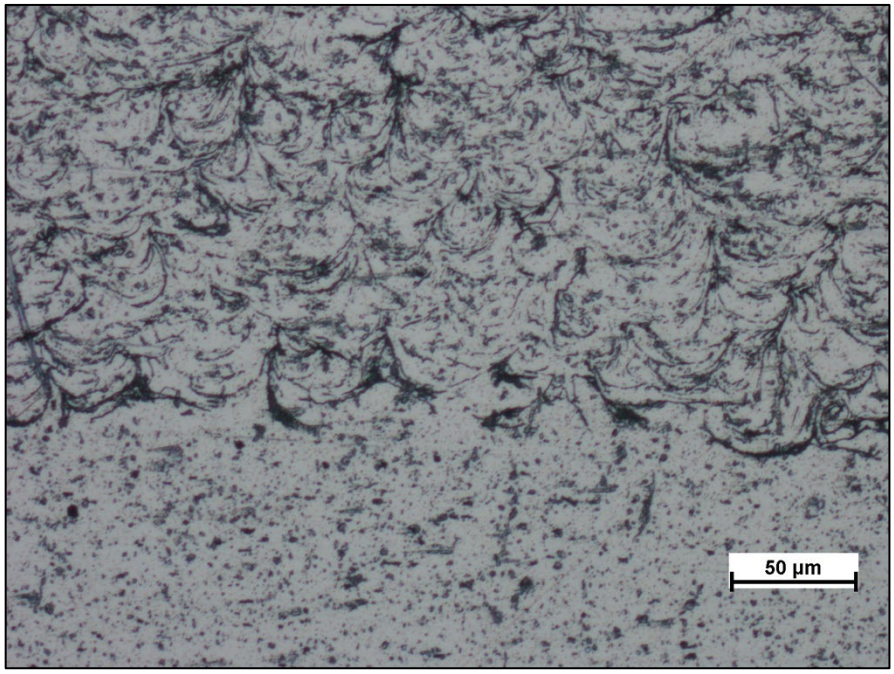


Optical Microscopy of Composition A-CN at Condition 4

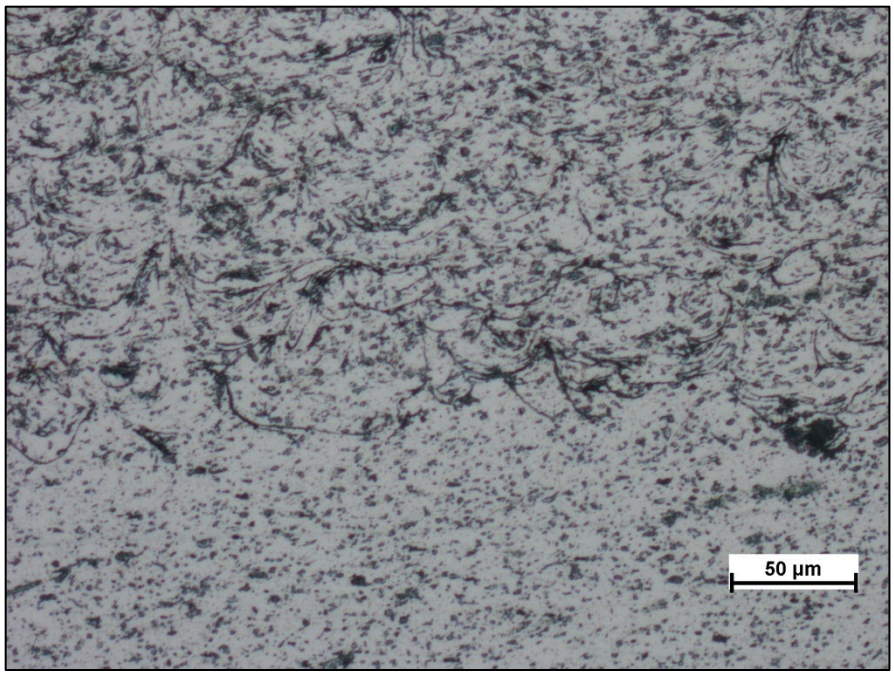


Optical Microscopy of Composition A-CN at Condition 5

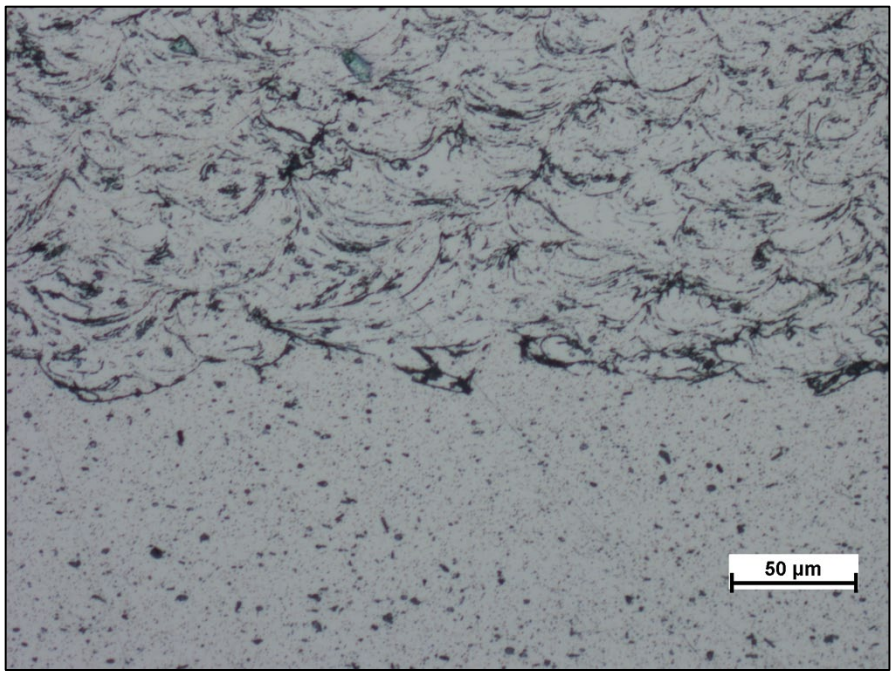


Optical Microscopy of Composition A-CN-M at Condition 1

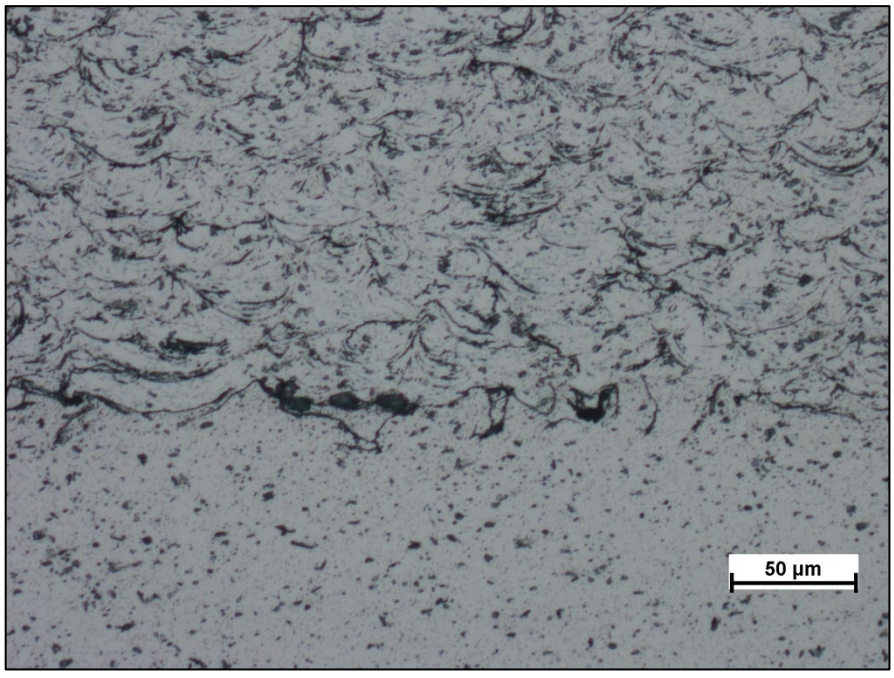


Optical Microscopy of Composition A-CN-M at Condition 2

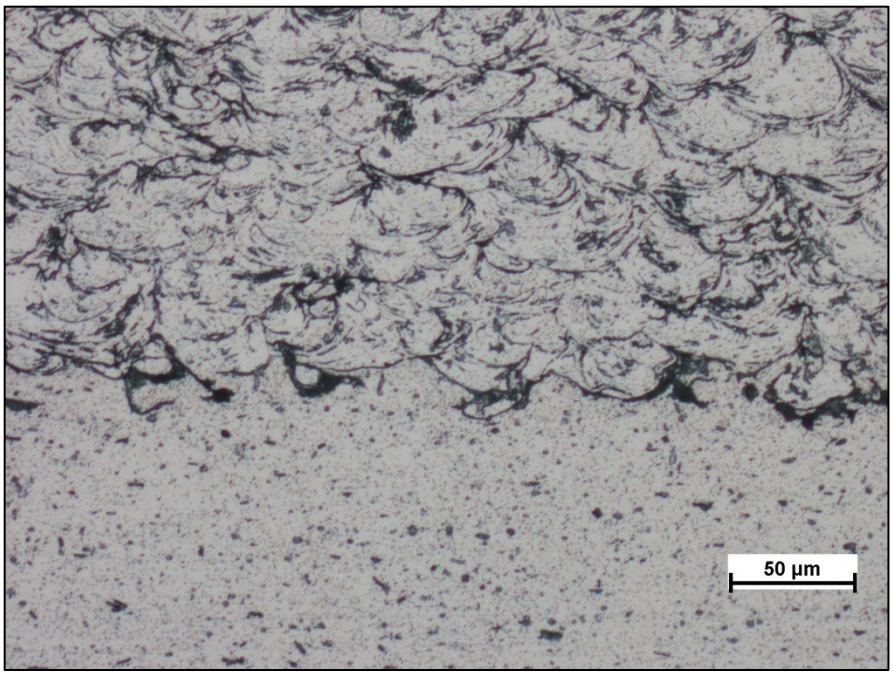


Optical Microscopy of Composition A-CN-M at Condition 3

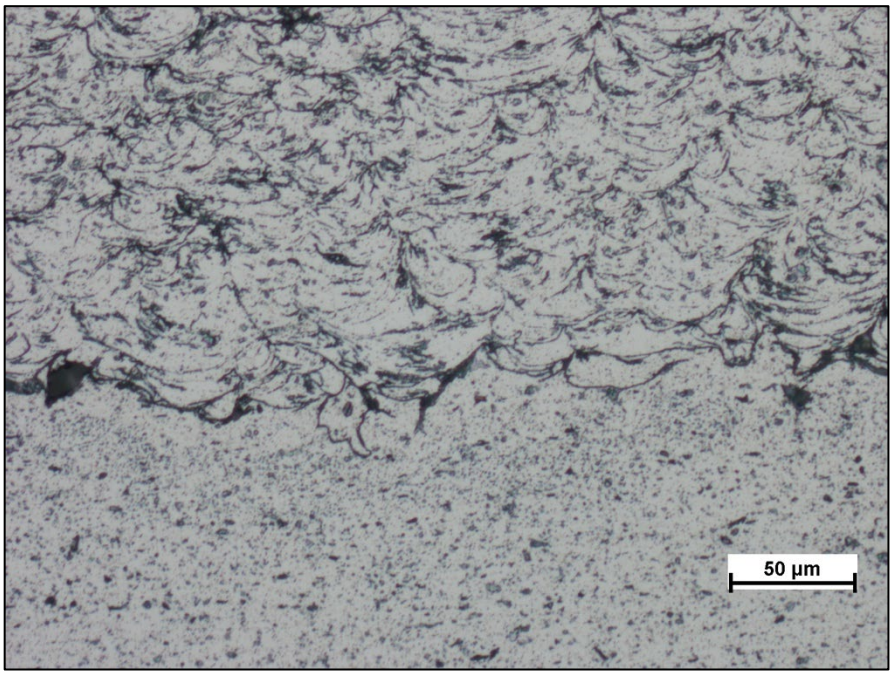


Optical Microscopy of Composition A-CN-M at Condition 4

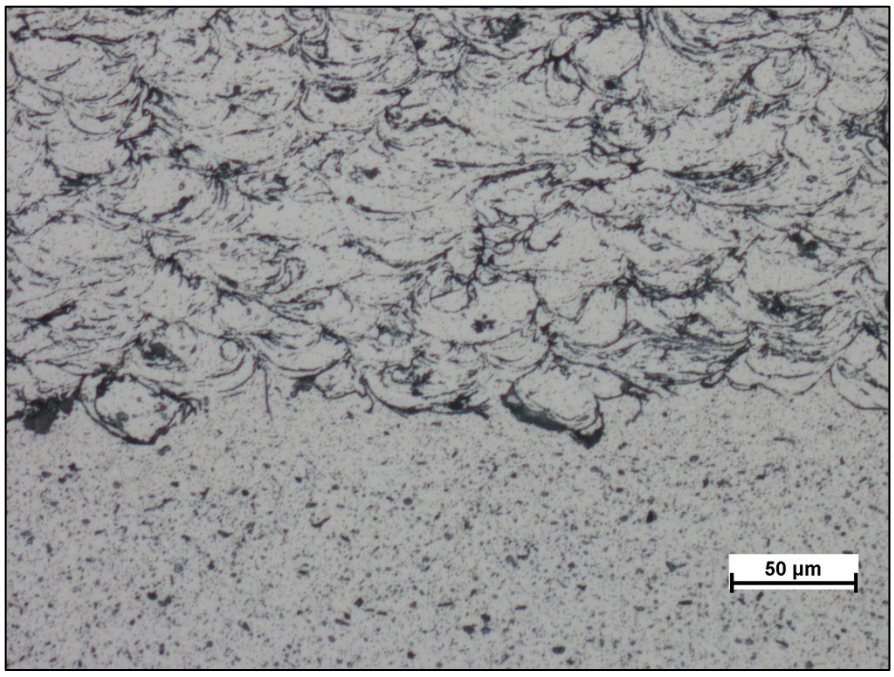


Optical Microscopy of Composition A-CN-M at Condition 5

THIS PAGE INTENTIONALLY LEFT BLANK

# APPENDIX B. NANOHARDNESS RESULTS

Nanohardness Results (GPa)

| | Heat Treatment | Condition 1 | Condition 2 | Condition 3 | Condition 4 | Condition 5 |
|---|---|---|---|---|---|---|
| **Compos-ition** | Details | As Received | Annealed at 300°C for 1 hour | Annealed at 300°C for 4 hours | Annealed at 500°C for 1 hour | Annealed at 500°C for 4 hours |
| **A** | 100% Al | 0.8962 ± 0.2283 | 1.0072 ± 0.2555 | 0.9278 ± 0.1570 | 0.6707 ± 0.1784 | 0.7449 ± 0.1177 |
| **A-C** | 98 vol % Al + 2 vol % n-$B_4C$ | 1.0258 ± 0.2462 | 0.8080 ± 0.2197 | 0.9181 ± 0.2786 | 0.7685 ± 0.2051 | 0.6962 ± 0.1766 |
| **A-N** | 98 vol % Al + 2 vol % BNNP | 0.8612 ± 0.3171 | 0.9224 ± 0.1856 | 0.8289 ± 0.1591 | 0.6272 ± 0.2118 | 0.5581 ± 0.1360 |
| **A-CN** | 98 vol % Al + 1 vol % n-$B_4C$ + 1 vol % BNNP | 0.9824 ± 0.2390 | 0.8715 ± 0.2264 | 0.9179 ± 0.1818 | 0.7565 ± 0.1625 | 0.7774 ± 0.2450 |
| **A-CN-M** | 98 vol % Al + 1 vol % n-$B_4C$ + 1 vol % BNNP | 0.9631 ± 0.2339 | 0.9193 ± 0.2194 | 0.8039 ± 0.1519 | 0.6842 ± 0.1486 | 0.7826 ± 0.1400 |

THIS PAGE INTENTIONALLY LEFT BLANK

# APPENDIX C. ELASTIC MODULUS BY NANOINDENTATION RESULTS

Elastic Modulus Results by Nanoindentation (GPa)

| | Heat Treatment | Condition 1 | Condition 2 | Condition 3 | Condition 4 | Condition 5 |
|---|---|---|---|---|---|---|
| **Compos-ition** | Details | As Received | Annealed at 300°C for 1 hour | Annealed at 300°C for 4 hours | Annealed at 500°C for 1 hour | Annealed at 500°C for 4 hours |
| **A** | 100% Al | 70.7310 ± 12.7430 | 82.3987 ± 9.4577 | 81.1634 ± 6.5222 | 66.7142 ± 11.7938 | 72.7735 ± 9.6952 |
| **A-C** | 98 vol % Al + 2 vol % n-$B_4C$ | 78.5389 ± 19.9869 | 70.6897 ± 11.2764 | 78.3539 ± 14.2403 | 70.8595 ± 9.2958 | 63.8943 ± 13.0824 |
| **A-N** | 98 vol % Al + 2 vol % BNNP | 74.5457 ± 17.7070 | 75.2547 ± 9.6862 | 61.2562 ± 9.4356 | 59.6760 ± 12.1200 | 42.0073 ± 7.8640 |
| **A-CN** | 98 vol % Al + 1 vol % n-$B_4C$ + 1 vol % BNNP | 55.2432 ± 12.4623 | 75.0492 ± 12.2793 | 69.5326 ± 8.4675 | 63.8569 ± 8.0297 | 65.5182 ± 13.1276 |
| **A-CN-M** | 98 vol % Al + 1 vol % n-$B_4C$ + 1 vol % BNNP | 77.4795 ± 14.6491 | 64.8792 ± 8.7648 | 67.6908 ± 9.7588 | 67.9983 ± 13.8801 | 66.7457 ± 11.3351 |

THIS PAGE INTENTIONALLY LEFT BLANK

# APPENDIX D. WORK OF INDENTATION BY NANOINDENTATION RESULTS

Load-Displacement Curve and Average Work of Indentation Results for each Composition / Heat Treatment

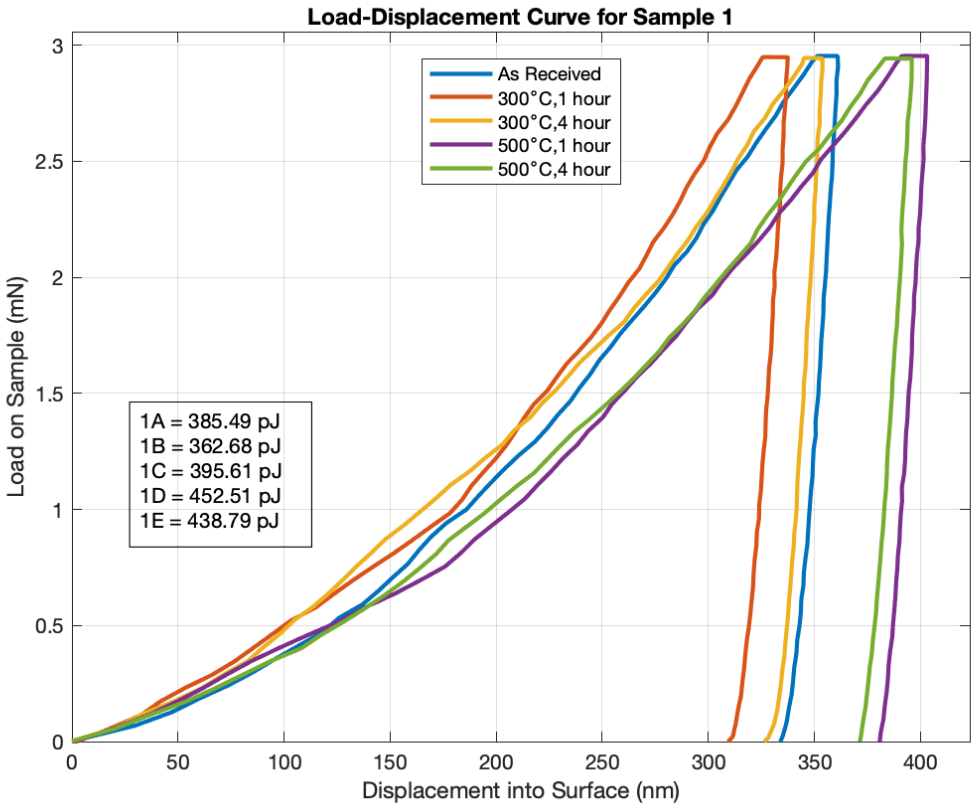


Composition A

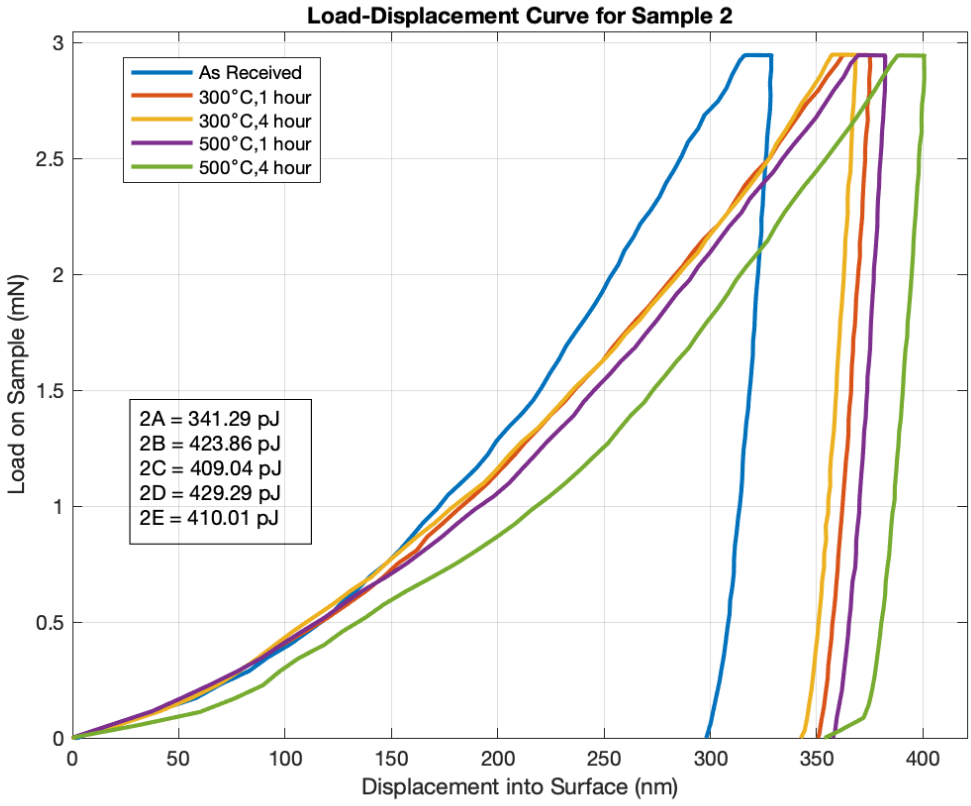


Composition A-C

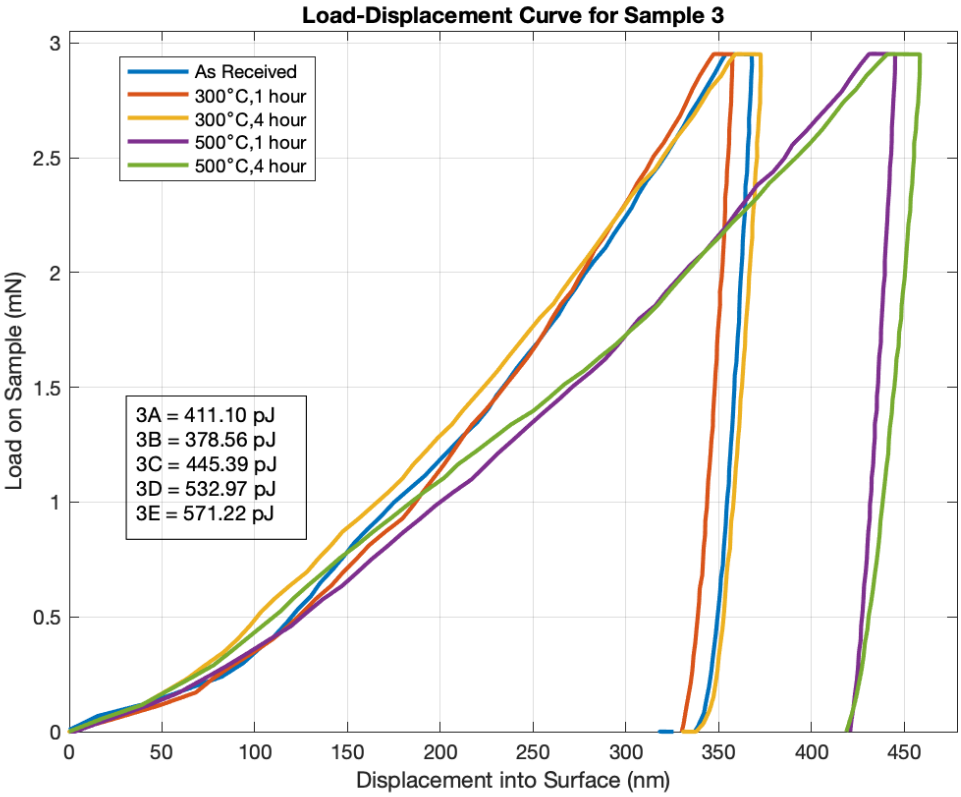


Composition A-N

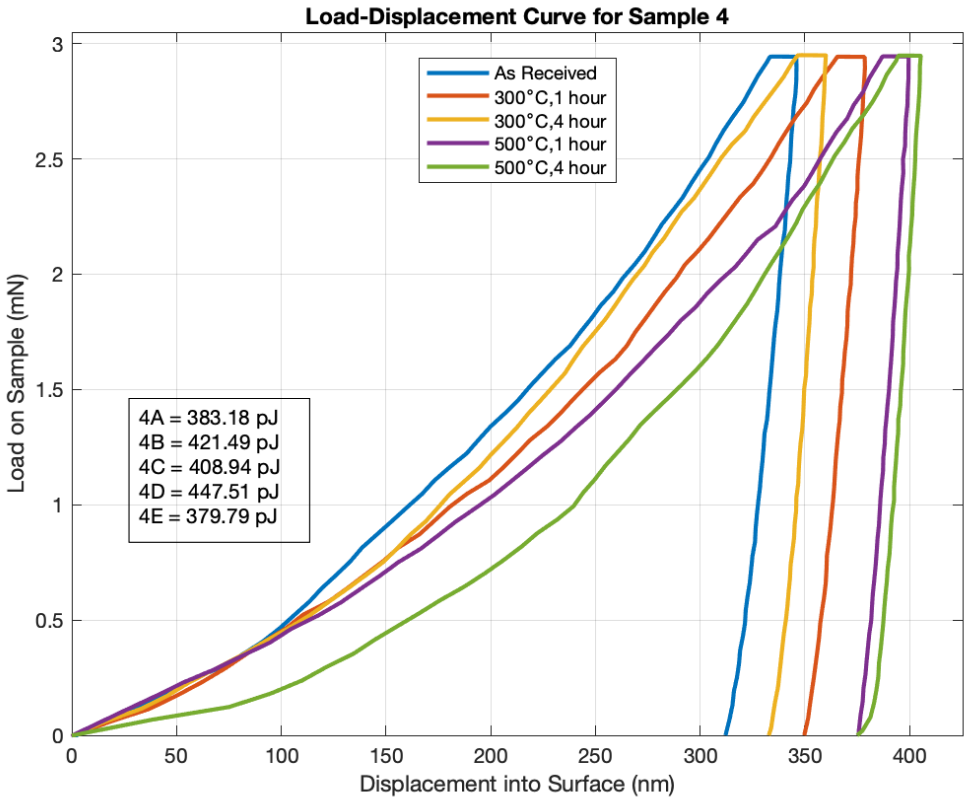


Composition A-CN

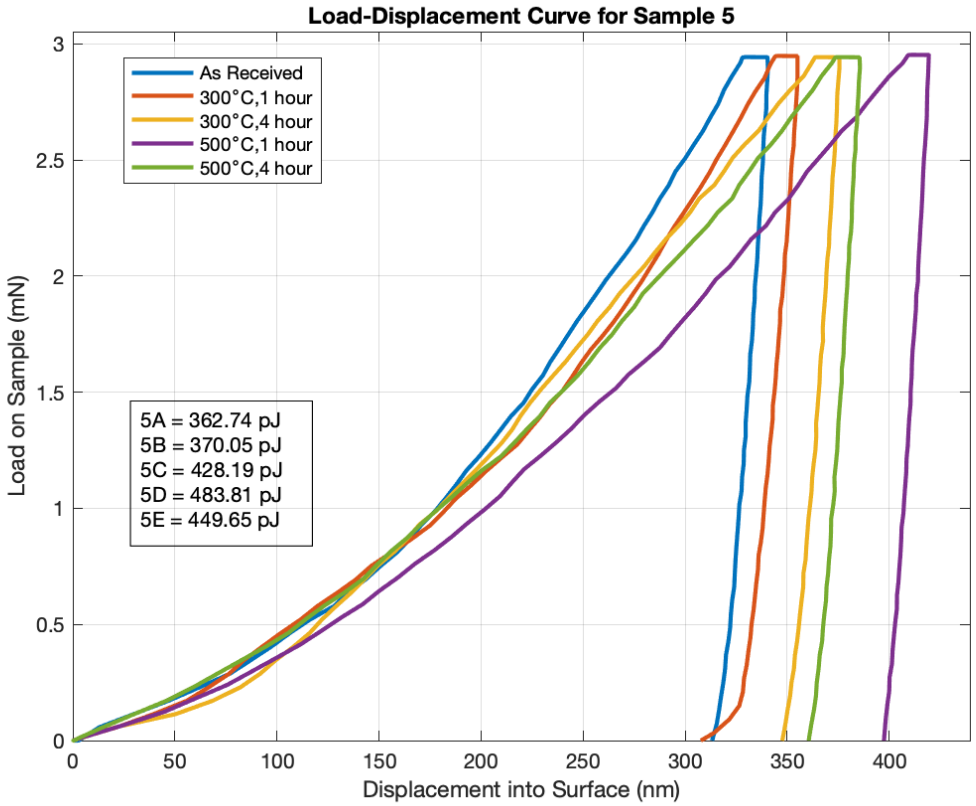


Composition A-CN-M

Summary of Work of Indentation for all Compositions and Heat Treatment Conditions

| | Work of Indentation (pJ) | | | | |
|---|---|---|---|---|---|
| **Composition** | **Condition 1** | **Condition 2** | **Condition 3** | **Condition 4** | **Condition 5** |
| A | 385.49 | 362.68 | 395.61 | 452.51 | 438.79 |
| A-C | 341.29 | 423.86 | 409.04 | 429.29 | 410.01 |
| A-N | 411.10 | 378.56 | 445.39 | 532.97 | 571.22 |
| A-CN | 383.18 | 421.49 | 408.94 | 447.51 | 379.79 |
| A-CN-M | 362.74 | 370.05 | 428.19 | 483.81 | 449.65 |

THIS PAGE INTENTIONALLY LEFT BLANK

# APPENDIX E. MICROHARDNESS RESULTS

Microhardness Results (HV0.05, 10 sec dwell time)

| | Heat Treatment | Condition 1 | Condition 2 | Condition 3 | Condition 4 | Condition 5 |
|---|---|---|---|---|---|---|
| **Compos-ition** | Details | As Received | Annealed at 300°C for 1 hour | Annealed at 300°C for 4 hours | Annealed at 500°C for 1 hour | Annealed at 500°C for 4 hours |
| **A** | 100% Al | 62.47 ± 2.77 | 58.99 ± 2.49 | 60.37 ± 1.82 | 37.2 ± 1.88 | 38.26 ± 1.5 |
| **A-C** | 98 vol % Al + 2 vol % n-$B_4C$ | 65.35 ± 3.49 | 59.5 ± 2.78 | 57.77 ± 2.39 | 42.1 ± 2.06 | 41.8 ± 1.77 |
| **A-N** | 98 vol % Al + 2 vol % BNNP | 63.01 ± 2.71 | 59.28 ± 3.03 | 58.69 ± 1.4 | 40.31 ± 2.39 | 39.17 ± 1.54 |
| **A-CN** | 98 vol % Al + 1 vol % n-$B_4C$ + 1 vol % BNNP | 63.61 ± 2.88 | 58.28 ± 2.92 | 59.31 ± 1.67 | 42.33 ± 0.98 | 42.1 ± 1.84 |
| **A-CN-M** | 98 vol % Al + 1 vol % n-$B_4C$ + 1 vol % BNNP | 62.08 ± 1.95 | 59.13 ± 2.61 | 59.41 ± 1.88 | 38.67 ± 2.24 | 39.24 ± 1.32 |

THIS PAGE INTENTIONALLY LEFT BLANK

# APPENDIX F. COEFFICIENT OF FRICTION AND MASS LOSS RESULTS

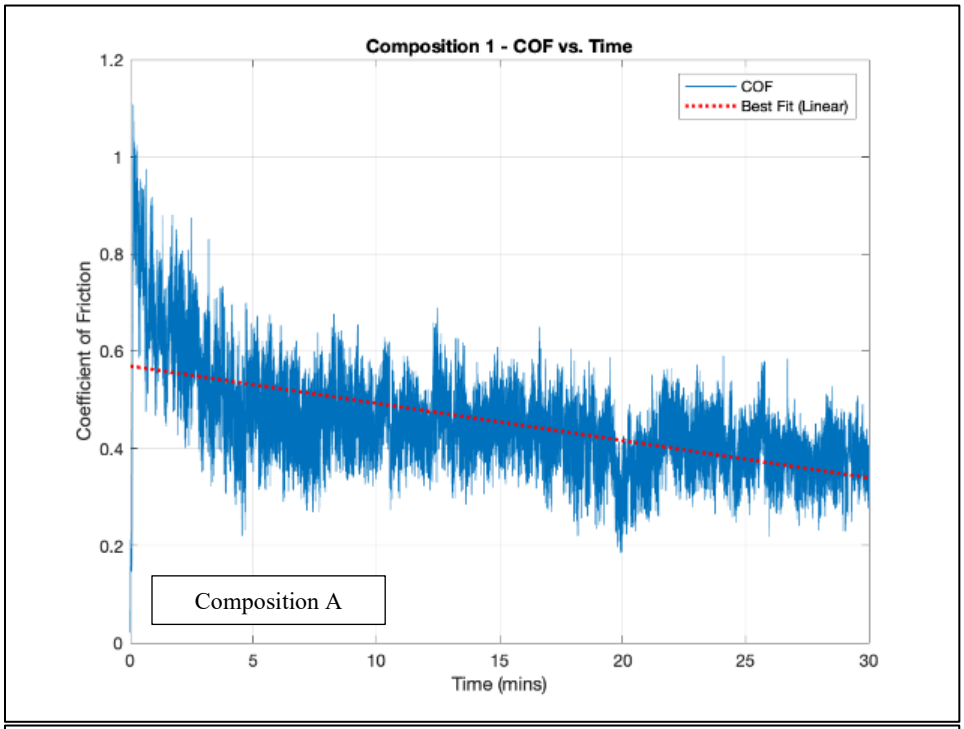


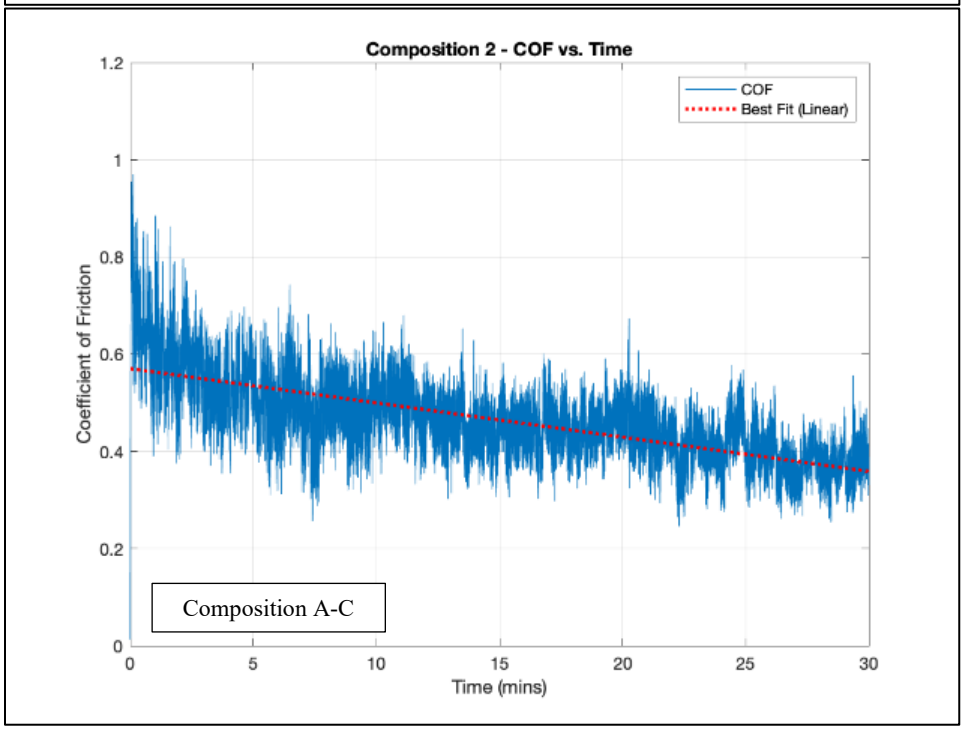

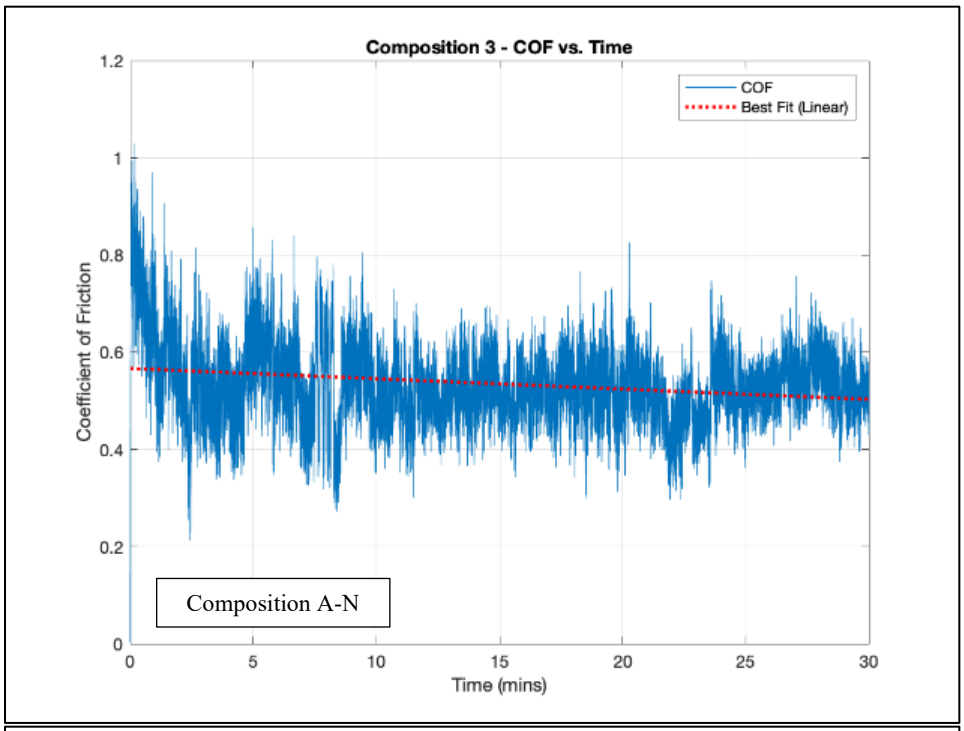
Composition 3 - COF vs. Time
COF
Best Fit (Linear)
Coefficient of Friction
Time (mins)
Composition A-N

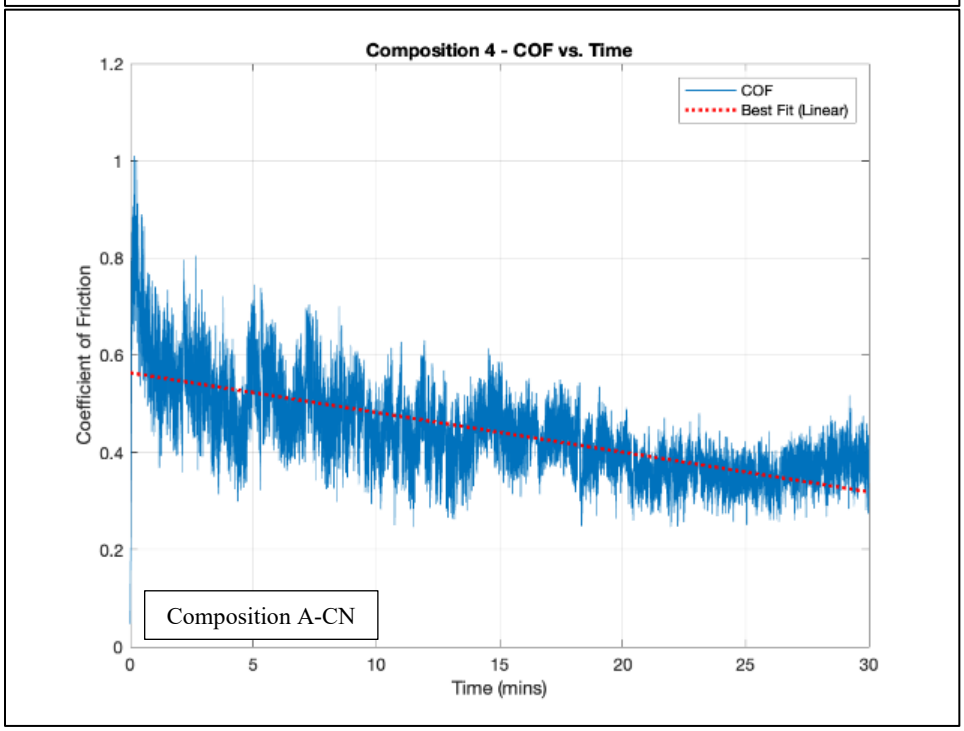
Composition 4 - COF vs. Time
COF
Best Fit (Linear)
Coefficient of Friction
Time (mins)
Composition A-CN

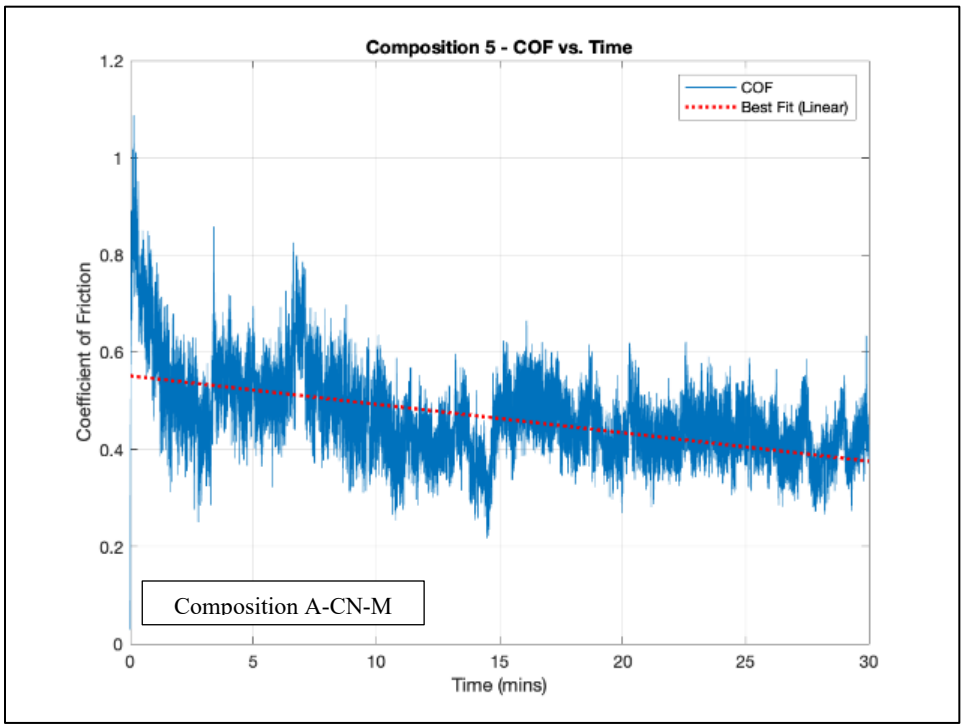


Mass Loss (g) for all Compositions after Condition 4 Heat Treatment

| | Mass Loss (g) | | | | |
|---|---|---|---|---|---|
| | **Composition A** | **Composition A-C** | **Composition A-N** | **Composition A-CN** | **Composition A-CN-M** |
| **Test 1** | 0.0009 | 0.0016 | 0.0024 | 0.0015 | 0.0016 |
| **Test 2** | 0.0014 | 0.0011 | 0.0032 | 0.0016 | 0.0017 |
| **Test 3** | 0.0012 | 0.0016 | 0.0021 | 0.0014 | 0.0018 |
| **Test 4** | 0.0015 | 0.0018 | 0.0025 | 0.0011 | 0.0013 |
| **Test 5** | 0.0012 | 0.0016 | 0.0025 | 0.0019 | 0.0014 |
| **Average** | 0.0012 | 0.0015 | 0.0025 | 0.0015 | 0.0016 |
| **Std. Dev** | 0.0002 | 0.0003 | 0.0004 | 0.0003 | 0.0002 |

THIS PAGE INTENTIONALLY LEFT BLANK

# APPENDIX G. DEPTH PROFILE AND WEAR DEBRIS SIZE FOR WEAR TESTS

| | Heat Treatment Condition 4 | | | | |
|---|---|---|---|---|---|
| **Composition** | Composition Details | Depth (μm) | Width (mm) | Average Depth (μm) | Average Width (mm) |
| **A** | 100% Al | 76.348 | 0.9837 | 78.964 | 0.9794 |
| | | 92.981 | 1.0085 | | |
| | | 96.575 | 1.0790 | | |
| | | 89.801 | 1.0451 | | |
| | | 72.631 | 0.9722 | | |
| | | 52.2747 | 0.8978 | | |
| | | 102.130 | 1.0888 | | |
| | | 67.1871 | 0.9585 | | |
| | | 76.5066 | 0.831 | | |
| | | 54.4155 | 0.9291 | | |
| **A-C** | 98 vol % Al + 2 vol % n-$B_4C$ | 112.744 | 1.0792 | 101.592 | 1.0888 |
| | | 100.523 | 1.05788 | | |
| | | 98.054 | 1.0739 | | |
| | | 100.552 | 1.1262 | | |
| | | 96.5313 | 1.0144 | | |
| | | 94.0852 | 1.052 | | |
| | | 107.439 | 1.0616 | | |
| | | 75.776 | 0.9779 | | |
| | | 121.197 | 1.1900 | | |
| | | 109.021 | 1.2548 | | |
| **A-N** | 98 vol % Al + 2 vol % BNNP | 113.799 | 1.1401 | 103.541 | 1.0989 |
| | | 106.379 | 1.0925 | | |
| | | 103.889 | 1.0989 | | |
| | | 81.855 | 1.0165 | | |
| | | 106.56 | 1.0874 | | |
| | | 115.946 | 1.0833 | | |
| | | 111.267 | 1.1703 | | |
| | | 114.383 | 1.2594 | | |
| | | 102.174 | 1.0618 | | |
| | | 79.1536 | 0.9783 | | |

| | | | | | |
|---|---|---|---|---|---|
| **A-CN** | 98 vol % Al + 1 vol % n-$B_4C$ + 1 vol % BNNP | 77.8769 | 1.0362 | 76.447 | 0.977 |
| | | 53.5639 | 0.8284 | | |
| | | 49.4319 | 0.757 | | |
| | | 84.5152 | 0.9699 | | |
| | | 90.7533 | 0.9962 | | |
| | | 88.8436 | 1.0798 | | |
| | | 112.05 | 1.1253 | | |
| | | 61.1569 | 0.9291 | | |
| | | 29.7277 | 0.8861 | | |
| | | 116.548 | 1.1584 | | |

| | | | | | |
|---|---|---|---|---|---|
| **A-CN-M** | 98 vol % Al + 1 vol % n-$B_4C$ + 1 vol % BNNP | 77.0135 | 0.9437 | 83.94616 | 0.9484 |
| | | 83.916 | 0.9700 | | |
| | | 110.372 | 0.9600 | | |
| | | 87.8063 | 1.0003 | | |
| | | 81.7734 | 1.0114 | | |
| | | 77.6095 | 0.9707 | | |
| | | 72.6695 | 0.7688 | | |
| | | 73.1235 | 0.8994 | | |
| | | 88.3769 | 1.0201 | | |
| | | 86.801 | 0.9396 | | |

Average Wear Debris Size for Each Composition

| | **Composition A** | **Composition A-C** | **Composition A-N** | **Composition A-CN** | **Composition A-CN-M** |
|---|---|---|---|---|---|
| Average Wear Debris Size (μm) | 106.764 | 49.489 | 78.735 | 68.923 | 137.819 |
| Std Dev (μm) | 63.071 | 31.120 | 47.904 | 99.730 | 109.401 |
| Max (μm) | 594.439 | 840.321 | 555.514 | 1202.157 | 669.122 |
| Min (μm) | 2.108 | 6.392 | 2.299 | 6.734 | 13.557 |

# APPENDIX H. PERCENTAGE CHANGE IN MECHANICAL AND TRIBOLOGICAL PROPERTIES FOR ALL COMPOSITIONS AND HEAT TREATMENT CONDITIONS

Mechanical Properties: Compared Composition A with no Heat Treatment

| Conditon 1: No Heat Treatment | | | | | | |
|---|---|---|---|---|---|---|
| Properties \ Composition | | Composition A | Composition A-C | Composition A-N | Composition A-CN | Composition A-CN-M |
| | | Average | Average | Average | Average | Average |
| Mechanical Properties | Nanohardness (GPa) | **0.896** | 14.46% | -3.91% | 9.62% | 7.46% |
| | Microhardness (HV0.05) | **62.470** | 4.61% | 0.86% | 1.82% | -0.62% |
| | Elastic Modulus (GPa) | **70.731** | 11.04% | 5.39% | -21.90% | 9.54% |
| | Work of Indentation (pJ) | **385.490** | -11.47% | 6.64% | -0.60% | -5.90% |

| Condition 2: 300°C, 1hr | | | | | | |
|---|---|---|---|---|---|---|
| Properties \ Composition | | Composition A | Composition A-C | Composition A-N | Composition A-CN | Composition A-CN-M |
| | | Average | Average | Average | Average | Average |
| Mechanical Properties | Nanohardness (GPa) | 12.39% | -9.84% | 2.92% | -2.76% | 2.58% |
| | Microhardness (HV0.05) | -5.57% | -4.75% | -5.11% | -6.71% | -5.35% |
| | Elastic Modulus (GPa) | 16.50% | -0.06% | 6.40% | 6.11% | -8.27% |
| | Work of Indentation (pJ) | -5.92% | 9.95% | -1.80% | 9.34% | -4.01% |

| Condition 3: 300°C, 4hr | | | | | | |
|---|---|---|---|---|---|---|
| Properties \ Composition | | Composition A | Composition A-C | Composition A-N | Composition A-CN | Composition A-CN-M |
| | | Average | Average | Average | Average | Average |
| Mechanical Properties | Nanohardness (GPa) | 3.53% | 2.44% | -7.51% | 2.42% | -10.30% |
| | Microhardness (HV0.05) | -3.36% | -7.52% | -6.05% | -5.06% | -4.90% |
| | Elastic Modulus (GPa) | 14.75% | 10.78% | -13.40% | -1.69% | -4.30% |
| | Work of Indentation (pJ) | 2.63% | 6.11% | 15.54% | 6.08% | 11.08% |

| Condition 4: 500°C, 1hr | | | | | | |
|---|---|---|---|---|---|---|
| Properties \ Composition | | Composition A | Composition A-C | Composition A-N | Composition A-CN | Composition A-CN-M |
| | | Average | Average | Average | Average | Average |
| Mechanical Properties | Nanohardness (GPa) | -25.16% | -14.25% | -30.02% | -15.59% | -23.66% |
| | Microhardness (HV0.05) | -40.45% | -32.61% | -35.47% | -32.24% | -38.10% |
| | Elastic Modulus (GPa) | -5.68% | 0.18% | -15.63% | -9.72% | -3.86% |
| | Work of Indentation (pJ) | 17.39% | 11.36% | 38.26% | 16.09% | 25.51% |

| Condition 5: 500°C, 4hr | | | | | | |
|---|---|---|---|---|---|---|
| Properties \ Composition | | Composition A | Composition A-C | Composition A-N | Composition A-CN | Composition A-CN-M |
| | | Average | Average | Average | Average | Average |

| | | | | | | |
|---|---|---|---|---|---|---|
| **Mechanical Properties** | **Nanohardness (GPa)** | -16.88% | -22.32% | -37.73% | -13.26% | -12.68% |
| | **Microhardness (HV0.05)** | -38.75% | -33.09% | -37.30% | -32.61% | -37.19% |
| | **Elastic Modulus (GPa)** | 2.89% | -9.67% | -40.61% | -7.37% | -5.63% |
| | **Work of Indentation (pJ)** | 13.83% | 6.36% | 48.18% | -1.48% | 16.64% |

| | | | | | | | | | | |
|---|---|---|---|---|---|---|---|---|---|---|
| -40.001 to -50% | -30.001 to -40% | -20.001 to -30% | -10.001 to -20% | -0.001 to -10% | Same as Al CS Coating (No Heat Treatmt) | 0.001 to 10% | 10.001 to 20% | 20.001 to 30% | 30.001 to 40% | 40.001 to 50% |

## Tribological Properties: Compared to Composition A, Heat Treated at Condition 4

| **Condition 4: 500°C, 1hr** | | | | | | |
|---|---|---|---|---|---|---|
| **Properties \ Composition** | | **Composition A** | **Composition A-C** | **Composition A-N** | **Composition A-CN** | **Composition A-CN-M** |
| | | **Average** | **Average** | **Average** | **Average** | **Average** |
| **Tribological** | **CoF** | - | -1.89% | 6.86% | -3.03% | 0.17% |
| | **Specific Wear Rate ($m^3$/Nm)** | - | -43.02% | -47.11% | 3.46% | -2.93% |
| | **Average Debris Size** | - | -53.56% | -26.11% | -30.85% | -35.32% |

| | | | | | | | | | | |
|---|---|---|---|---|---|---|---|---|---|---|
| -40.001 to -50%+ | -30.001 to -40% | -20.001 to -30% | -10.001 to -20% | -0.001 to -10% | Same as Al CS Coating Baseline | 0.001 to 10% | 10.001 to 20% | 20.001 to 30% | 30.001 to 40% | 40.001 to 50% |

THIS PAGE INTENTIONALLY LEFT BLANK

# LIST OF REFERENCES


[1] Office of the Under Secretary of Defense, "Military equipment useful life study - Phase II, OTEMPO studies," 2008. [Online]. Available: https://www.acq.osd.mil/ pepolicy/pdfs/OPTEMPO/OPTEMPO%20Phase%20II% 20Final%20Report.pdf.

[2] J. Freeman and G. Paoli, "Additive manufacturing and obsolescence management in the defence context, RAND Corp. (Europe)," 2015. [Online]. Available: https://www.rand.org/pubs/perspectives/PE171.html.

[3] K. Sertoglu, "Australian Army pushes spee3d 3D printer to the limit with latest field test," 3D Printing Industry, Nov. 1, 2021. [Online]. Available: https://3dprintingindustry.com/news/australian-army-pushes-spee3d-3d-printer-to-thelimit- with-latest-field-test-19.

[4] T. Husseini, "US NAVSEA develops cold spray technique for ship maintenance," Naval Technology, Jan. 25, 2019. [Online]. Available: https://www.naval-technology.com/news/us-navsea-cold-spray-naval/.

[5] D. Heyer, "Cold spray technology enhances Army depot's capabilities," U.S. Army, Mar. 31, 2022. [Online]. Available: https://www.army.mil/article/255245/cold_ spray_technology_enhances_army_depots_capabilities.

[6] X. Xie, S. Yin, R. N. Raoelison, C. Chen, C. Verdy, W. Li, G. Ji, Z. Ren and H. Liao, "Al matrix composites fabricated by solid-state cold spray deposition: A critical review," *Journal of Material Science & Technology,* vol. 86, pp. 20–55, Sep. 30, 2021.

[7] V. K. Champagne and D. Helfritch, "The unique abilities of cold spray deposition," *International Materials Review,* vol. 61, no. 7, pp. 437–455, Jul. 5, 2016.

[8] E. Irissou, J. G. Legoux, A. Ryabinin and B. Jodoin, "Review on cold spray process and technology: Part I - Intellectual property," *Journal of Thermal Spray Technology,* vol. 17, Dec. 17, 2008.

[9] W. Li, K. Yang, S. Yin, X. Yang, Y. Xu and R. Lupoi, "Solid-state additive manufacturing and repairing by cold spraying: A review," *Journal of Materials Science & Technology,* vol. 34, no. 3, pp. 440–457, Sep. 21, 2018.

[10] R. N. Raoelison, Y. Xie, T. Sapanathan, M. Planche, R. Kromer, S. Costil and C. Langlade, “Cold gas dynamic spray technology: A comprehensive review of processing conditions for various technological developments till to date,” *Additive Manufacturing,* vol. 19, pp. 134–159, Jan. 1, 2018.

[11] H. Assadi, H. Kreye, F. Gärtner and T. Klassen, “Cold spraying – A materials perspective,” *Acta Materialia,* vol. 116, pp. 382–407, Sep. 1, 2016.

[12] R. N. Raoelison, C. Verdy and H. Liao, “Cold gas dynamic spray additive manufacturing today: Deposit possibilities, technological solutions and viable applications,” *Materials & Design,* vol. 133, pp. 266–287, Nov. 5, 2017.

[13] M. R. Rokni, C. A. Widener, V. K. Champagne and G. A. Crawford, “Microstructure and mechanical properties of cold sprayed 7075 deposition during non-isothermal annealing,” *Surface & Coatings Technology,* vol. 276, pp. 305–315, Jul. 15, 2015.

[14] Y. Zou, W. Qin, E. Irissou, J. G. Legoux, S. Yue and J. A. Szpunar, “Dynamic recrystallization in the particle/particle interfacial region of cold-sprayed nickel coating: Electron backscatter diffraction characterization,” *Scripta Materialia,* vol. 61, no. 9, pp. 899–902, Nov. 1, 2009.

[15] V. K. Champagne, D. Helfritch and P. Grend, “Interface material mixing formed by the deposition of copper on aluminum by means of the cold spray process,” *Journal of Thermal Spray Technology,* vol. 14, no. 3, pp. 330–334, Sep. 2005.

[16] D. Seo, M. Sayar and K. Ogawa, “SiO2 and MoSi2 formation on Inconel 625 surface via SiC coating deposited by cold spray,” *Surface and Coatings Technology,* vol. 206, no. 11–12, pp. 2851–2858, Feb. 15, 2012.

[17] X. L. Zhou, A. F. Chen, J. C. Liu, X. K. Wu and J. S. Zhang, “Preparation of metallic coatings on polymer matrix composites by cold spray,” *Surface and Coatings Technology,* vol. 206, no. 1, pp. 132–136, Oct. 15, 2011.

[18] K. Spencer, D. Fabijanic and M.-X. Zhang, “The influence of Al2O3 reinforcement on the properties of stainless steel cold spray coatings,” *Surface and Coatings Technology,* vol. 206, no. 14, pp. 3275–3282, Mar. 15, 2012.

[19] A. Nieto, A. Bisht, D. Lahiri, C. Zhang and A. Agarwal, “Graphene reinforced metal and ceramic matrix composites: A review,” *International Materials Reviews,* vol. 62, no. 5, pp. 241–302, Jul. 4, 2017.

[20] S. P. Rawal, “Metal-matrix composites for space applications.,” *JOM,* vol. 53, no. 4, pp. 14–17, Apr., 2001.

[21] M. O. Bodunrin, K. K. Alaneme and L. H. Chown, “Aluminium matrix hybrid composites: A review of reinforcement philosophies; mechanical, corrosion and tribological characteristics,” *Journal of Materials Research and Technology,* vol. 4, no. 4, pp. 434–445, Jun. 5, 2015.

[22] J. A. Hooker and P. J. Doorbar, “Metal matrix composites for aeroengines,” *Materials Science and Technology,* vol. 16, no. 7–8, pp. 725–731, Jul. 19, 2013.

[23] D. M. Shinde, P. Sahoo and J. P. Davim, “Tribological characterization of particulate-reinforced aluminum metal matrix nanocomposites: A Review,” *Advanced Composites Letters,* vol. 29, p. 2633366X20921403, Apr. 24, 2020.

[24] A. Moridi, S. M. Hassani-Gangaraj, M. Guagliano and M. Dao, “Cold spray coating: Review of material systems and future perspectives,” *Surface Engineering,* vol. 30, no. 6, pp. 369–395, Jun. 1, 2014.

[25] D. D. Kanta, M. P. Chandra, S. Saranjit and T. R. Kumar, “Properties of ceramic-reinforced aluminium matrix composites — A review,” *International Journal of Mechanical and Materials Engineering,* vol. 9, pp. 1–12, Dec., 2014.

[26] E. O. Hall, “The deformation and ageing of mild steel: III Discussion of results,” *Proceedings of the Physical Society. Section B,* vol. 64, no. 9, p. 747, 1951.

[27] R. Huang, M. Sone, W. Ma and H. Fukanuma, “The effects of heat treatment on the mechanical properties of cold-sprayed coatings,” *Surface and Coatings Technology,* vol. 261, pp. 278–288, Jan. 15, 2015.

[28] M. R. Rokni, C. A. Widener, V. K. Champagne and G. A. Crawford, “Microstructure and mechanical properties of cold sprayed 7075 deposition during non-isothermal annealing,” *Surface & Coatings Technology,* vol. 276, pp. 305–315, Jul. 15, 2015.

[29] C. Zener, “Theory of growth of spherical precipitates from solid solution,” *Journal of Applied Physics,* vol. 20, no. 10, pp. 950–953, Oct. 20, 1949.

[30] A. Agnoli, M. Bernacki, R. E. Logé, J.-M. Franchet, J. Laigo and N. Bozzolo, “Understanding and modeling of grain boundary pinning in Inconel718,” in *Superalloys 2012: The 12th International Symposium on Superalloys*, Pennsylvannia, USA, 2012.

[31] R. W. Hertzberg, R. P. Vinci and J. L. Hertzberg, “Deformation and fracture mechanics of engineering materials (5th. Ed.),” Hoboken, NJ, John Wiley & Sons, 2012, p. 169.

[32] V. C. Nardone and K. M. Prewo, “On the strength of discontinous silicone carbide reinforced aluminum composite,” *Scripta Metallurgica,* vol. 20, no. 1, pp. 43–48, Jan. 1, 1986.

[33] Z. Zhang, X. Sun, S. Huang, X. Han, P. Zhu, C. Shi and T. Zhang, “Microstructure, mechanical properties and corrosion behavior of the aluminum alloy components repaired by cold spray with Al-based powders,” *Metals,* vol. 10, no. 11, p. 1633, Oct. 14, 2021.

[34] T. Norell, G. Ferguson, T. Ansell, T. Saladin, A. Nardi and A. Nieto, “Synthesis and corrosion behavior of cold sprayed dual nanoparticle reinforced Al coatings,” *Surface & Coating Technology,* vol. 401, p. 126280, Nov. 15, 2020.

[35] W. C. Oliver and G. M. Pharr, “An improved technique for determining hardness and elastic modulus using load and displacement sensing indentation experiments,” *Journal of Materials Research,* vol. 7, no. 6, pp. 1564–1583, Jun. 7, 1992.

[36] A. C. Hall, D. J. Cook, R. A. Neiser, T. J. Roemer and D. A. Hirschfeld, “The effect of a simple annealing heat treatment on the mechanical properties of cold-sprayed aluminum,” *Journal of Thermal Spray Technology,* vol. 15, no. 2, pp. 233–238, Jun. 15, 2006.

[37] T. Paul, C. Zhang, N. Denis, B. Boesl and A. Agarwal, “Role of ultrasonic treatment on microstructure, mechanical and tribological behavior of 2D boron nitride reinforced aluminum composites,” *Materials Science & Engineering A,* vol. 809, p. 140970, Feb. 24, 2021.

[38] A. Moridi, S. M. Hassani-Gangaraj, M. Guagliano and M. Dao, “Cold spray coating: Review of material systems and future perspectives,” *Surface Engineering,* vol. 30, no. 6, pp. 369–395, Jun. 1, 2014.

# INITIAL DISTRIBUTION LIST

1. Defense Technical Information Center
   Ft. Belvoir, Virginia

2. Dudley Knox Library
   Naval Postgraduate School
   Monterey, California